UNIVERSITY
OF OSLO

Master thesis

New Insights into Adolescent 15q11.2 CNVs

A Dual Approach Using Normative Modelling and Raw Metrics

Victor-José Aravena Lande

Cognitive Neuroscience
Spring 2025 [125 credits]

Submitted as Master's Thesis at the Department of Psychology
University of Oslo

Table of Contents

Acknowledgements

Firstly, I would like to give a big thank you to my two supervisors, Ida Elken Sønderby and Rune Bøen, for the positive guidance, acceptance and patience throughout this thesis project. Even across language barriers, the Atlantic Ocean, and periods of no communication from my side, we you made it work with smile. You have both been nothing but great supervisors.

Additionally, thank you to the Centre for Precision Psychiatry (NORMENT) for taking me in and welcoming me as one of your own.

Also, thank you to the University of Oslo for the interesting degree, but also for the people I got to meet and keep.

Most importantly, thank you to every single member of my family, who all know what they have done for me. I would not be where I am today if it weren't for you, and I hope I get the chance to do as much back.

Lastly, many thanks to my friends for being supportive throughout a hard academic period. Hopefully it will end.

Abstract

The 15q11.2 BP1-BP2 copy number variant (CNV) is associated with atypical neurodevelopment, increased risk of developmental neuropsychiatric disorders and cognitive deficits. Previous studies have found higher cortical thickness and lower cortical surface area in deletion carriers and lower cortical thickness in duplication carriers. However, these studies have mainly focused on adult carriers. At the same time, there is a lack of studies on children and adolescents with the 15q11.2 BP1-BP2 CNV, a period where most developmental neuropsychiatric disorders typically emerge. The rare occurrence of 15q11.2 BP1-BP2 CNVs and their subtle effect on structural development demands the adoption of normative modelling, a tool potentially more sensitive to age-related changes. Using normative modelling, the current thesis explores whether brain structural differences emerge during or are already present in adolescents carrying a 15q11.2 BP1-BP2 variant. Leveraging mixed cross-sectional and longitudinal neuroimaging data from the ABCD dataset, 45 15q11.2 BP1-BP2 deletion carriers (mean age = 11.22, 51% males, n scans = 93) and 53 duplication carriers (mean age = 10.76, 51% males, n scans = 107) were compared to control participants (mean age = 11, 523, 52% males, n scans = 22 315). The mixed cross-sectional group comparison analysis showed that carriers of the 15q11.2 BP1-BP2 deletion had widespread but regionally higher cortical thickness, lower cortical surface area, lower subcortical and cerebellar volume, and ventricular enlargement compared to controls. The duplication carriers showed lower cortical surface area and lower subcortical and cerebellar volume in 15q11.2 BP1-BP2 duplication carriers compared to controls. The normative modelling longitudinal analysis confirmed the initial group differences across age, showing cortical thickening, decreased surface area and increased ventricle volume for deletion carriers compared to controls, while duplication carriers showed cortical thinning, volume decrease and effects in both directions for surface area compared to controls. The results indicate that brain structural alterations in 15q11.2 BP1-BP2 carriers are detectable in adolescence, indicating an altered neurodevelopment that emerges earlier than the adolescent period in both carriers. These brain structural differences, also found in adult samples, show divergent and convergent effects with those observed in idiopathic developmental neuropsychiatric disorders, potentially contributing to the neuroanatomical heterogeneity observed in these disorders and associated cognitive deficits. The current study design

demonstrated how normative modelling can provide CNV researchers with a nuanced understanding of the deviations found in the developmental trajectories of CNV carriers.

Introduction

Psychiatric and neurodevelopmental research has increasingly recognized the deep challenge of clinical and biological heterogeneity, which complicates the discovery of reliable biomarkers and the development of effective interventions (Insel et al., 2010; Wolfers et al., 2018; Parkes et al., 2020). A most common example are individuals diagnosed with psychiatric disorders, such as schizophrenia, who differ vastly in their response to treatment and prognosis (Malhotra, 2015; Huber, 1997) and neuroanatomical differences (Alnæs et al., 2019). For instance, individuals diagnosed with schizophrenia have been found to show widespread lower cortical thickness compared to controls (Van Erp et al., 2018) but are also characterized by substantial within-group variability in cortical thickness potentially reflecting subgroups of individuals with lower and higher cortical thickness (Alnæs et al., 2019). Rare genetic variant carriers such as copy number variants (CNVs) carriers might contribute to some of this heterogeneity. CNVs are regions of the genome either deleted or duplicated, and certain rare CNVs have been associated with an increased risk of developmental neuropsychiatric disorders (Calle Sánchez et al., 2022). The recurrent 15q11.2 break point (BP)1 – BP2 CNV illustrates the point: both the deletion and its reciprocal duplication are found in roughly 0.5–1 % of the population and confer heightened liability for autism, schizophrenia, learning difficulties, and other cognitive or behavioural difficulties, yet penetrance is low and clinical expressivity ranges from unaffected to severely impaired (Rafi & Butler, 2020; Jonsson et al., 2023). In CNV research focusing on the 15q11.2 CNV, group average MRI studies report thicker cortex and reduced surface area in deletion carriers, most prominently in frontal, cingulate, and parietal regions (van der Meer et al., 2020). Precision psychiatry has emphasized the need for methods that can dissect person-specific markers as a discipline focused on tailoring diagnosis, prognosis, and treatment to the unique biological and environmental profiles of individuals (Collins & Varmus, 2015; Insel & Cuthbert, 2015). In this context, normative modelling meets the need for individual level inference by learning age dependent population trajectories for each brain metric and expressing every participant as a deviation (z-score) from that norm. Applied to 15q11.2 CNVs, this framework quantifies person specific impact, probes gene dosage gradients, and remains compatible with

conventional case–control statistics (Marquand et al., 2016; Wolfers et al., 2018; van der Meer et al., 2020; Rutherford et al., 2023).

The present thesis pairs classic group contrasts with normative model deviation maps to test how adolescent 15q11.2 BP1–BP2 carriers depart from typical cortical and subcortical maturation, directly advancing the aims of precision psychiatry by characterizing the neuroanatomical deviations in a genetic subgroup that may contribute to the heterogeneity in developmental neuropsychiatric disorders.

Case-control neuroimaging

Historically, clinical and neuroimaging research has relied on case-control designs that compare patient groups to healthy controls in search of average group differences. Neuroimaging are non-invasive methods used to visualize the structure and function of the brain, providing critical insights into neural architecture and its alterations in psychiatric and neurodevelopmental disorders (Insel & Cuthbert, 2015). Among these, structural MRI has been central in finding and investigating structural biomarkers, with key modalities including cortical thickness (CT), cortical surface area (SA), and subcortical volume (SV) and cerebellar volume metrics that reflect distinct aspects of brain morphology and maturation (Hagler et al., 2019). Following normal expectations, CT reaches its peak at approximately 1.7 years where widespread cortical thinning continues throughout late adulthood, however, accelerates during mid to late adolescence during the most active period of synaptic pruning and myelination. Diversly, SA peaks around 11 years of age, with the orbitofrontal and frontal-pole regions being the last to plateau and declines gradually across the rest of the lifespan (Tamnes et al., 2017; Bethlehem et al., 2022). The subcortical volume trajectory is, however, non-linear and structure specific. Basal ganglia nuclei (caudate, putamen, nucleus accumbens) generally peak in late childhood/early adolescence and shrink thereafter, whereas the hippocampus and amygdala continue to enlarge well into the teens (Herting et al., 2018). Finally, the cerebellar volume shows a U-inverted trajectory reaching its peak at approximately 12-16 years, with the posterior lobules maturing last (Tiemeier et al., 2010). These modalities are recognized as potential psychopathological diagnostic biomarkers to use in a case-control paradigm, as large-scale meta-analyses show structural deviations in disorders like schizophrenia, major depression disorder, bipolar disorder and autism spectrum disorder (Van Erp et al., 2018; Matsumoto et al., 2023; Okada et al., 2023).

The case-control paradigm has been the go-to in the understanding of psychiatric disorders. Its enticement lies in its intuitive interpretation, and well-established statistical tools such as t-tests, general linear models, and mass-univariate analyses. Case-control studies have yielded foundational insights, identifying, for instance, reduced cortical thickness in schizophrenia and altered subcortical volumes in mood disorders (Wolfers et al., 2018).

However, while case-control neuroimaging has produced important insights, it is increasingly recognized as insufficient for precision applications. These methods assume that individuals within diagnostic groups are biologically homogeneous, yet extensive evidence shows that this is rarely the case (Rutherford et al., 2023; Wolfers et al., 2018). A seminal *JAMA Psychiatry* study on individuals at clinically high risk for psychosis revealed that although group-level structural differences were detectable, most high-risk individuals exhibited brain metrics nested well within normative ranges, highlighting the disconnect between group findings and individual clinical reality (Wolfers et al., 2018). Similarly, Zabihi et al. (2019) showed that autism spectrum disorder is associated with significant group-level differences in cortical structure, and the effects are primarily driven by a minority of cases, highlighting the challenge of translating group findings into actionable biomarkers.

Copy number variants and risk for developmental neuropsychiatric disorders

In recent years, specific rare copy number variants, segments of the DNA spanning over 1000 base pairs that are either deleted or duplicated. Although CNVs create normal and expected variation in the population, some rare variations have been found to yield an increased risk for developmental neuropsychiatric disorders (Rees & Kirov, 2021). CNVs alter the copy number of genes within a genomic region; losing one copy (haploinsufficiency) typically reduces expression, whereas gaining a third copy (triplosensitivity) usually increases expression (Hastings et al., 2009; Quigley et al., 2025). These imbalances can be particularly disruptive in genes critical to neurodevelopment, as precise regulation of gene expression is essential for processes such as neuronal differentiation, synapse formation, and brain circuit maturation (Toro et al., 2010; Javed et al., 2020; Rees & Kirov, 2021). For example, Domínguez-Iturza et al. (2019) describe the mechanisms of the haploinsufficiency for the 15q11.2 CNV-related gene CYFIP1 and neighbouring genes in mice, where the authors conclude that this haploinsufficiency disrupts brain function and connectivity most likely caused by irregular myelin maturation and synaptic pruning, specifically in association and motor-callosal fibres. A critical driver of CNV

formation is the presence of low-copy repeats (LCRs). These are highly similar DNA sequences on both sides of specific genomic regions. During cell division, particularly during meiosis (which generates eggs and sperm) or mitosis (regular cell division for growth and repair), these LCRs can misalign and mistakenly pair with a similar sequence at a different location instead of their correct partner. When recombination occurs between these misaligned, non-allelic (i.e., non-identical but similar) regions, it can result in deletions, duplications, or more complex rearrangements: a process known as non-allelic homologous recombination (NAHR) (Hastings et al., 2009; Sønderby et al., 2020). These recurrent CNVs appear at the same loci across unrelated individuals, explaining why specific pathogenic CNVs are seen repeatedly in human populations. Beyond direct effects, CNVs can also disturb the expression of genes outside the CNV region, likely by disrupting regulatory elements or the 3D organization of the genome, compounding their impact on neurodevelopment (Spielmann et al., 2018; Sønderby et al., 2022. This also ties directly into rarity and recurrence: while CNVs overall are rare, those mediated by LCRs are more likely to recur at specific hotspots, making them "rare but recurrent," which is why they can be systematically studied across different cohorts despite their low individual prevalence (Redon et al., 2006; Sønderby et al., 2020, 2022) The clinical significance of CNVs is typically assessed through effect size metrics, with high-penetrance CNVs, such as 22q11.2 deletions, displaying strong phenotypic effects, while others like 15q11.2 BP1–BP2 deletions exhibit milder but still measurable impacts on neurodevelopment (van der Meer al. 2020, Sønderby et al., 2022.

The 15q11.2 BP1-BP2 deletion involves four genes (i.e. TUBGCP5, CYFIP1, NIPA1, NIPA2). It has been found to yield an increased risk for developmental neuropsychiatric disorders such as schizophrenia (Stefansson et al., 2008), ADHD (Vaez et al., 2024), cognitive deficits (van der Meer al., 2020), autism spectrum disorder, developmental delay, motor and language delays, and behavioural problems (Burnside et al., 2011; Cox & Butler, 2015). Moreover, the 15q11.2 BP1–BP2 deletion has been associated with increased cortical thickness and reduced cortical surface area in deletion carriers. In contrast, duplication carriers exhibit the opposite pattern (thinner cortex and larger surface area) with approximately half the effect size of deletions (Van der Meer et al., 2020; Boen et al., 2024). Despite these robust group-level findings from primarily adult carriers, it remains unclear when these alterations occur. Previous results have suggested that these are unlikely to stem from altered neurodegenerative processes, which may indicate that

these morphological changes stem from altered neurodevelopmental trajectories (Boen et al., 2023). Still, there is a lack of studies examining the neurodevelopmental trajectories of neuroimaging-derived features in children and adolescents carrying a 15q11.2 deletion or duplication.

Normative modelling

Considering the limitations of traditional case–control designs, assumes group homogeneity and often overlook individual neuroanatomical variability, normative modelling represents a paradigm shift in neuroimaging research. Rather than comparing average morphometric differences between cases and controls, normative models establish statistical mappings of brain structure as a function of age, sex, and other covariates, enabling the computation of individualized deviation scores (z-scores) that reflect how much an individual diverges from expected population norms (Marquand et al., 2016; Rutherford et al., 2023). This approach is conceptually akin to paediatric growth charts (Bethlehem et al., 2022), and its major advantage lies in reframing neurodevelopment as a continuum, allowing nuanced detection of atypical brain development across individuals rather than binary groupings.

Leveraging advanced statistical methods such as Gaussian Process Regression and Generalized Additive Models for Location, Scale, and Shape (GAMLSS), it flexibly models non-linear brain development trajectories and provides individualized deviation scores across the full brain (Marquand et al., 2016; Rutherford et al., 2023). Toolkits like PCNtoolkit have further democratized access to these models, enabling researchers to apply normative frameworks trained on large, harmonized reference datasets, such as the Adolescent Brain Cognitive Development (ABCD) study and UK Biobank to new cohorts with minimal computational overhead (Rutherford et al., 2023). Importantly, Rutherford and colleagues have publicly released a suite of pre-trained lifespan normative models as part of the PCNtoolkit “braincharts” framework, which allows users to derive normative z-scores for cortical thickness, surface area, and subcortical volumes across development and aging without needing to train models locally (Rutherford et al., 2023). These models, hosted on GitHub (Barkema et al., 2023; Rutherford & Marquand, 2023), have been rigorously validated across diverse datasets and are designed for easy application, lowering the barrier to replication and comparing new samples to a global reference. This scalability and adaptability make normative modelling exceptionally well-suited

for rare variant research where sample sizes are often limited (Wolfers et al., 2018; Rutherford et al., 2023).

While the traditional strength of normative modelling is in mapping heterogeneity, its utility in longitudinal designs deserves critical attention. Because normative z-scores are standardized against developmental trajectories, they inherently control for age-related effects, making them well-suited to detect deviations from typical brain maturation over time (Wolfers et al., 2018). In theory, if 15q11.2 B1-B2 CNV carriers exhibit increased cortical thickness at baseline but maintain a stable developmental trajectory thereafter, longitudinal z-score analyses may not reveal additional divergence over time; the deviation would remain static, reflecting a persistent early deviation rather than progressive change. Conversely, if CNV carriers show dynamic changes, either worsening or normalizing brain morphology relative to peers, this would emerge as a significant trajectory shift in their deviation scores.

This sensitivity to both static and dynamic neurodevelopment was recently demonstrated by Berthet et al. (2024), who applied normative modelling in a 10-year longitudinal schizophrenia cohort. They found that while certain cortical regions showed consistent deviations at both baseline and follow-up, other regions showed changes in the trajectory shifts parallel with symptom changes. This example underscores that normative modelling not only quantifies baseline atypicality but also captures whether clinical populations remain on a stable developmental path or diverge further over time. This is an essential consideration when investigating neurodevelopmental conditions like 15q11.2 BP1-BP2 CNV.

One way to assess whether 15q11.2 BP1-BP2 CNV carriers simply manifest an early static deviation or whether their brain development diverges progressively from normative trajectories would be to integrate normative z-scores with repeated measures. Most important, this tool complements case–control analysis by testing both the presence of early group differences and the potential for ongoing divergence, thus maximizing sensitivity to subtle and maybe clinically meaningful changes. Another consideration is that its full potential relies on access to large, high-quality datasets that provide both the normative training base and the longitudinal depth necessary for developmental tracking. To meet this need, ABCD study offers a uniquely positioned resource.

The ABCD Study

The ABCD Study is the largest longitudinal neurodevelopmental cohort in the United States, enrolling nearly 11,900 participants approximately aged 9 to 10 years at baseline across 22 research sites (Casey et al., 2018; Garavan et al., 2018; Volkow et al., 2018). Its mission is to examine how genetic, environmental, and social factors shape brain development and mental health through adolescence. The ABCD Study provides a state of the art dataset, offering integrating multi-modal MRI together with genomic data (including CNV profiling), cognitive assessments, and detailed environmental measures.

Most notably is its rigorously harmonized imaging and genotyping protocols, which ensure that all samples and sites are comparable. Its large, demographically diverse cohort mirrors the U.S. youth population, boosting external validity (Heeringa & Berglund, 2020). With baseline imaging and biennial follow-ups, the study captures detailed neurodevelopmental trajectories, critical for understanding age-related brain deviations in CNV carriers (Hagler et al., 2019). ABCD's neuroimaging and genetic data undergo stringent preprocessing and quality control, including bias and gradient correction, FreeSurfer segmentation, and multi-level Quality Control (QC; Hagler et al., 2019). Genotyping via the Affymetrix NIDA SmokeScreen Array ensures reliable CNV detection through robust metrics like Log R Ratio (LRR) and B Allele Frequency (BAF) (Uban et al., 2018).

Crucially, the ABCD dataset not only offers a large, demographically diverse sample with harmonised imaging protocols but also serves as a core component of the normative baseline in existing normative modelling frameworks. As forementioned, the pre-trained models developed by Rutherford et al. (2023) are trained in part on ABCD data, ensuring that derived z-scores for brain measures (such as cortical thickness, surface area, and subcortical volumes) are calibrated against a reference that includes the very population under study. This alignment is especially critical when investigating rare CNVs like 15q11.2 BP1-BP2, where small sample sizes increase the need for robust, externally validated normative baselines, as well as the ABCD study's longitudinal depth offers sufficient statistical power and the ability to track within-subject developmental changes (Saragosa-Harris et al., 2022). In sum, the ABCD Study's size, diversity, and methodological rigor provide the ideal foundation for normative modeling in 15q11.2 BP1-

BP2 CNV research, offering both the population-wide training base and longitudinal follow-up critical for robust developmental analysis.

Analytical Strategy and Its Justification

To rigorously assess the neuroanatomical impact of 15q11.2 BP1-BP2 CNVs, this study employed a dual-analytical framework combining (1) a repeated-measures group comparisons analysis and (2) a longitudinal trajectory analysis. Each model offers complementary strengths that together provide a comprehensive view of CNV-related brain differences. The repeated-measures group comparison used all available timepoints to find group differences between CNV carriers and controls. It enhanced statistical power by pooling repeated measures per participant. This strategy is particularly critical in rare CNV research, where small sample sizes make traditional baseline-only designs underpowered and vulnerable to false negatives (Boen et al., 2024; Sønderby et al., 2020; Rutherford et al., 2023). In parallel, the longitudinal trajectory model explicitly modelled group by age interactions to probe dynamic neurodevelopmental changes. Unlike cross-sectional designs, this design might have enough leverage to reveal whether CNV-related structural differences diverge over time as well as its direction. This insight offers a developmental understanding of both CNV risk and resilience.

To date, no study has systematically combined lifespan normative models with longitudinal MRI data to map neurodevelopmental trajectories in adolescent 15q11.2 BP1-BP2 CNV carriers. Addressing this gap, the present thesis leverages the ABCD study to derive z-score trajectories and provide the first detailed map of developmental neuroanatomical deviations across adolescence which is a critical window of brain maturation marked by cortical thinning, surface area reorganization, and subcortical restructuring (Bethlehem et al., 2022; Rutherford et al., 2023).

Research Questions, Aims, and Hypotheses

It is evident that, while raw models (e.g., cortical thickness in millimetres) are commonly used in neuroimaging, they require complex adjustments for confounders like age, sex, and scanner site and are sensitive to covariate misspecification (Rutherford et al., 2023). It is also evident that normative z-scores being pre-adjusted for these confounders and quantify deviations relative to a population norm, offer potentially greater sensitivity to detect subtle neuroanatomical effects (Marquand et al., 2016; Rutherford et al., 2023). A direct comparison of these approaches would

allow us to assess whether normative modelling increases sensitivity to neuroanatomical differences and altered trajectories, with potential benefits for precision neuroimaging. Thus, the thesis' dual-analytical framework, combining repeated-measures group comparisons analysis and longitudinal trajectory modelling, has been designed to capture both static group differences and dynamic neurodevelopmental changes, offering a dynamic evaluation of 15q11.2 BP1-BP2 CNV effects on brain structure. This CNV has great potential in showcasing whether normative modelling offers a valuable perspective to heterogeneity with its balance between population frequency and morphological effects in the population.

Large-scale ENIGMA-CNV analyses (van der Meer et al., 2020), first established that adults with the 15q11.2 BP1-BP2 deletion exhibit a globally thicker cortex which is most pronounced in dorsolateral/medial pre-frontal, anterior cingulate and pre-/post-central cortices, accompanied by smaller total surface area and a selectively reduced nucleus accumbens, while the reciprocal duplication presents a weaker mirror pattern of cortical thinning and slight surface area expansion with minimal subcortical change. Follow up work in the UK Biobank shows these morphometric signatures persist into late adulthood without evidence of accelerated brain ageing, implying a developmental rather than degenerative origin (Boen et al., 2023). Using an intraindividual normative metric, Boen et al. (2024) demonstrated that deletion carriers display disproportionate positive deviation z scores in association cortex, whereas duplication carriers show few extreme deviations. Normative frameworks such as the lifespan 'brain charts' (Bethlehem et al., 2022) and high-resolution deviation models (Rutherford et al., 2023) corroborate that normative modelling is more sensitive than raw morphometry for detecting region specific effects.

Critically, almost all evidence to date comes from adult cohorts. Yet, 15q11.2 BP1-BP2 CNVs are present from conception, and cortical as well as subcortical architecture is profoundly remodelled during childhood and adolescence (Burnside et al., 2011; Mills & Tamnes, 2014). By applying normative models to an adolescent sample, the present thesis asks whether the adult patterns are already evident during early brain maturation and quantifies individual departures from typical trajectories. This thesis therefore integrates normative modelling with longitudinal measures to map brain structure deviations in adolescent 15q11.2 BP1–BP2 CNV carriers from

the ABCD cohort. This approach is powerful but usually not feasible given the rarity of CNVs and previously limited sample sizes.

In sum, normative modeling offers a powerful framework to disentangle whether group differences in 15q11.2 BP1-BP2 CNV carriers reflect static early-life effects or dynamic neurodevelopmental shifts, providing a more granular and developmentally contextualized understanding of CNV-related brain differences. By utilising the case–control comparisons with individualized developmental benchmarking, this thesis has the potential to clarify both the grade and trajectory of atypical brain development in this higher-risk adolescent cohort.

Aims:

1. Apply normative modelling to assess brain development in 15q11.2 BP1-BP2 CNV carriers (deletion and duplication), quantifying individual deviations from typical neurodevelopmental trajectories.
2. Compare group differences between CNV carriers and controls using both raw morphometric measures and normative z-scores to evaluate whether z-scores enhance sensitivity and interpretability.
3. Model longitudinal z-score trajectories to determine whether 15q11.2 BP1-BP2 CNV carriers exhibit atypical age-related changes across childhood and adolescence.

Primary Research Question: Do 15q11.2 BP1-BP2 CNV adolescent carriers exhibit regionally specific and developmentally dynamic brain structure deviations, and are these more sensitively detected using normative modelling compared to traditional raw morphometric analyses?

Hypotheses:

- **H1:** 15q11.2 BP1-BP2 deletion carriers will show thicker cortices, particularly in frontal and motor regions, and less SA, especially in the frontal pole and orbitofrontal cortices.
- **H2:** Less SV in deletion carriers, and this effect will be localised, notably in the caudate, nucleus accumbens and pallidum.
- **H3:** Duplication carriers will exhibit milder and partly opposing effects, consistent with dosage sensitivity (i.e. thinner cortices).

- **H4:** Normative z-score models will demonstrate greater sensitivity than raw morphometric models in detecting group differences and will more effectively capture developmental trajectories, particularly in association cortices.

Methods and materials

The ABCD Study Sample

Sample Recruitment

Participants were drawn from the ABCD Study, which enrolled 11,868 children approximately aged 8.5–10 years across 22 U.S. research sites (Garavan et al., 2018). Recruitment was conducted through school-based outreach using stratified probability sampling, targeting a cohort broadly representative of the U.S. population by age, sex, race/ethnicity, socioeconomic status, and geographic region (Heeringa & Berglund, 2020). Detailed sampling procedures are documented in Garavan et al. (2018)

Eligibility criteria were intentionally broad to maximize generalizability. Children were included if they could complete study assessments and MRI procedures, with sufficient English proficiency and no contraindications for scanning (e.g., non-removable metal, severe claustrophobia). Individuals with common clinical diagnoses such as ADHD or learning disabilities were not excluded. Exclusion criteria were limited to conditions that could interfere with protocol compliance or participant safety (Volkow et al., 2018).

Written informed consent was obtained from guardians or parents. This inclusive sampling strategy aimed to ensure demographic diversity while supporting high retention and compliance across longitudinal follow-up assessments.

Participant demographics

The analytical sample for this thesis was drawn from the ABCD Study, comprising baseline and follow-up datapoints. After QC procedures, the baseline sample included 11,621 participants (5,527 females), aged 8.92 to 15.75 years (M = 11.44, SD = 1.27). Of these, 11,523 participants had no detectable 15q11.2 BP1-BP2 CNVs and were classified as controls, while 45 participants carried a 15q11.2 BP1–BP2 deletion and 53 carried a duplication. At follow-up, 68% of control participants (n = 7,824), 69% of deletion carriers (n = 31), and 75% of duplication carriers (n =

40) completed the 2-year timepoint. Retention at the 4-year follow-up was lower across groups, with 26% of controls (n = 2,968), 38% of deletion carriers (n = 17), and 26% of duplication carriers (n = 14) participating. Baseline demographics showed balanced sex distributions across groups, with approximately 51% males in the deletion and duplication cohorts, comparable to 52% in controls. A Kruskal-Wallis test revealed a significant difference in age across groups, $H(2) = 21.39$, $p < .001$, though absolute differences were minor (Control: M = 11.44, SD = 1.27; Deletion: M = 11.22, SD = 1.67; Duplication: M = 10.76, SD = 1.23). Sex distributions did not differ significantly ($\chi^2(2) = 0.04$, $p = .98$). Participation rates over time also differed across groups ($\chi^2(4) = 78.79$, $p < .001$), reflecting expected patterns of attrition (see Supplementary Table 2).

Participants originated from 21 ABCD research sites across the US. Site 22 was excluded from the present analysis (see *Dataset Quality Control*)**.** CNV carrier distribution varied across sampling sites, with higher concentrations at sites: ABCD_04, ABCD_06, ABCD_10, ABCD_12, ABCD_16, and ABCD_17, while no CNV carriers were enrolled at ABCD_01, ABCD_07, and ABCD_08 (see Supplementary Table 1). The CNV analysed in this thesis encompassed the 15q11.2 BP1–BP2 region (chr15:22,805,313–23,094,530, hg19). Full details regarding MRI and genetic data acquisition, processing, and quality control are provided in subsequent sections.

Table 1

Demographic Statistics Across Sample Timepoint by CNV group.

Demographic characteristics of 15q11.2 BP1–BP2 CNV carriers (deletion and duplication) and matched controls at baseline and follow-up. The table summarizes group sizes, mean age (M ± SD), age range, sex distribution (n, %), and participant retention at the 2nd-year and 4th-year follow-ups.

CNV Group	Baseline (1st year)		Age (M +/- SD)	Age Range	2nd year (n)	4th year (n)
	n	%				
Control	11523	99.2	11.44 +/- 1.27	8.92 -15.75	7824	2968

Deletion	45	0.4	11.22 +/- 1.67	9 - 15.33	31	17
Duplication	53	0.5	10.76 +/- 1.23	9 - 15.08	40	14

Note. CNV carrier groups were markedly smaller than the control group, reflecting the rarity of 15q11.2 BP1-BP2 CNVs in the ABCD dataset. Sex distribution was balanced across groups, and follow-up attrition was similar between carriers and controls.

MRI acquisition.

The ABCD Study implemented a rigorously harmonised imaging protocol across the research sites using 3T scanners from Siemens (Prisma), GE (750), and Philips (Achieva), with acquisition protocols designed to maximize cross-site comparability while accommodating minor vendor-specific differences (Casey et al., 2018; Hagler et al., 2019). T1-weighted structural images were acquired using a 3D magnetisation-prepared rapid gradient echo (MPRAGE) or equivalent SPGR sequence tailored to each scanner platform. Across sites, image acquisition was standardised to achieve 1 mm isotropic resomaximiselution with a 256 × 256 mm field of view and 176–225 slices per scan. Specific acquisition parameters varied slightly by scanner vendor but were harmonised using the consensus parameters outlined in Hagler et al. (2019). (see Supplementary Figure 2 for Neuroimaging Parameters). Parameters for Siemens Prisma, for example, included a TR of 2500 ms, TE of 2.88 ms, TI of 1060 ms, and flip angle of 8°, whereas GE and Philips had corresponding but calibrated parameter sets to yield comparable image contrast and signal-to-noise profiles. Follow-up MRI sessions are conducted approximately every two years, employing the same scanner-specific acquisition protocols and processing pipelines as baseline to ensure comparability over time (Casey et al., 2018). Longitudinal image processing utilises intra-subject registration to align timepoints for assessing developmental trajectories in cortical and subcortical features.

Each T1-weighted acquisition sequence had a duration of approximately 7 minutes. Including additional sequences (diffusion-weighted imaging, resting-state fMRI, task-based fMRI), the core scanning protocol lasted approximately 26–30 minutes per participant when considering only the in-scanner sequence time (Casey et al., 2018). However, the total time participants spent engaged in the neuroimaging protocol per visit could span approximately 2.5 to 3 hours. Participants typically underwent 25–45 minutes of prescan procedures (including re-screening, mock scanner training, and practice fMRI tasks), followed by 90–120 minutes of actual scanning in either a single or two-session format. This was concluded with 15–20 minutes of post-scan

assessments, such as recognition memory tasks and post-task questionnaires (see Supplementary Figure 1; Casey et al., 2018)

MRI Quality control and preprocessing

Importantly, ABCD implemented prospective motion correction (PMC) for Siemens and GE platforms, leveraging embedded navigators (vNavs) during acquisition to correct head motion in real time. Participants were also trained before scanning using mock scanner protocols to reduce in-scanner movement. Additional documentation of ABCD's motion correction approach and compliance rates is provided in the ABCD Supplementary Materials of Hagler et al. (2019). The ABCD image quality control (QC) process followed a multi-tiered framework. First, raw DICOM images were subjected to visual inspection for motion artefacts, truncation, and field-of-view errors. Second, FreeSurfer outputs were subjected to both automated and manual QC procedures. These included assessments such as the Euler number, which quantifies surface reconstruction quality. While technical thresholds for exclusion were based on empirical Euler number distributions, the specific cutoff criteria are documented in the ABCD Release 5.1 QC Manual, which can be found on the ABCD Wiki together with other acquisition and processing-related information (Haist & Jernigan, 2025). The ABCD Data Analysis and Informatics Center (DAIRC) conducted post-acquisition image processing centrally using the Multi-Modal Processing Stream (MMPS). This pipeline includes gradient nonlinearity correction, bias field correction, and intensity normalization to a white matter reference value of 110, followed by spatial registration to a study-specific standard template. To address spatial intensity inhomogeneities, particularly problematic in frontal and temporal regions, ABCD implemented a B1-bias field correction strategy using sparse spatial smoothing and white matter segmentation, which ensures normalized white matter intensity across scans. For Siemens scanners, which generate both raw and bias-corrected DICOMs (e.g., T1 and T1_NORM), only the normalized volumes (T1_NORM, T2_NORM) were used in ABCD's processing pipeline (Hagler et al., 2019).

Derivation of dependent variables

Cortical reconstruction and segmentation were performed using FreeSurfer version 5.3.0, and regional morphometric features were extracted based on the Desikan-Killiany atlas (Desikan et al., 2006; Fischl et al., 2002). Processed morphometric metrics used in the current thesis

included cortical thickness, surface area, and subcortical and cerebellar volumes. The morphometric outputs were organized into participant-level summary tables, provided by ABCD as tabulated imaging-derived measures, which served as the basis for all downstream structural analyses in this project.

Genetic Data and Initial Quality Control

Genetic data in the ABCD Study were acquired using the Affymetrix NIDA SmokeScreen Array, a genotyping platform developed explicitly by BioRealm for high-throughput genetic screening, including the detection of CNVs (Uban et al., 2018). This microarray platform assesses genome-wide signal intensities through the fragmentation of genomic DNA, hybridization to a comprehensive set of single-stranded DNA probes, and fluorescent labelling of bound sequences. Each probe targets a defined region of the human genome, allowing for precise identification of structural variation. The resulting fluorescence intensities were captured and quantified to derive key metrics indicative of genomic alterations. Two principal metrics, Log R Ratio (LRR) and B Allele Frequency (BAF), were used to detect CNVs: LRR reflects deviations in signal intensity relative to a normative reference, identifying gains or losses in genomic content, while BAF provides allele-specific information to distinguish between heterozygous and homozygous genomic states, improving CNV detection accuracy (Heeringa & Berglund, 2020). Integrating LRR and BAF metrics across the array enables high-resolution identification of genome deletions and duplications. The ABCD Study's primary QC protocols included excluding samples and loci exhibiting excessive noise, technical artefacts, or missingness beyond predefined thresholds and standardization of genotyping procedures across collection sites to minimize batch effects (Uban et al., 2018). This initial processing provided a robust foundation for subsequent CNV analyses.

Ethical Approvals

All study procedures in the ABCD project were conducted by ethical standards for research involving human participants. The ABCD protocol was approved by a centralized Institutional Review Board (IRB) at the University of California, San Diego, which served as the single IRB for all 22 data collection sites in compliance with NIH policy on multi-site research (Casey et al., 2018). Additionally, local IRB oversight was maintained at each site as needed for institutional

compliance. Written informed consent was obtained from each participant's parent or legal guardian, and child assent was required for enrolment. Age-appropriate materials and procedures were used to ensure that participants fully understood the voluntary nature of the study and their right to withdraw at any time without penalty. To further protect participant privacy and data confidentiality, the study was granted a Certificate of Confidentiality by the National Institutes of Health (Volkow et al., 2018), and strict protocols were implemented to de-identify all research data before public sharing or analysis.

Data processing and statistical modelling were conducted on the TSD secure server at the University of Oslo, in compliance with GDPR, under ethical approvals REK 2009/2485 and REK 2018/1061.

Study Specific Quality Control

CNV identification and Quality Control

Array-based platforms have reduced sensitivity for detecting small CNVs (<10 kb) and complex structural rearrangements, particularly in repetitive genomic regions. We conducted CNV identification and QC pipeline to ensure only well-validated CNV calls were retained for downstream analyses. The initial dataset contained 11,088 individuals with genotypes across five different genotyping batches (one obtained from blood, four from saliva). Briefly, we used the lrr.txt & baf-txt files released from ABCD release 3.0 and compiled lrr-baf files for each individual to use in calling autosomal (chromosomes 1-22) CNVs with PennCNV v1.0.5 (Wang et al., 2007). We used Affy6.0.hmm and the PFB-file (ABCD_allChrs.pfb') and its corresponding GCmodel-file, kindly provided by the lab of Sebastien Jacquemont (compiled by Zohra Saci). In the generation of the PFB-file, all individuals were used, SNPs that were not genotyped in at least 95% of samples were filtered out using the plink files given by ABCD (using this command line:

plink2 --bfile ABCD_release_3.0_QCed --missing --out test). Duplicate SNPs were filtered out. No hardy weinberg equilibrium (HWE) cut-off was applied because the samples are multiethnic.

Sample Exclusion Criteria: After CNV calling, samples were excluded if they met any of the following thresholds:

- Log R Ratio (LRR) standard deviation > 0.50.

- B Allele Frequency (BAF) drift > 0.02.
- Wave factor below –0.05 or above 0.05.
- CNVs covering fewer than 15 probes.
- CNVs overlapping more than 50% with problematic genomic regions (centromeres, telomeres, segmental duplications or immunoglobulin regions).

After applying these thresholds, 225 individuals were removed, leaving 10,863 participants for downstream analysis.

CNV Identification and Curation: Specific deletions and duplications were identified by extracting them from the raw CNV calling dataset based on overlap with a list of known pathogenic CNVs (Kendall et al., 2017; overlap threshold = 0.3) using the iPsychCNV R package. Initially, 375 CNV carriers were identified. After manual, visual curation of LRR-BAF plots, 315 high-confidence pathogenic CNVs across 312 individuals remained. Three participants carried two CNVs each, where only one of these were a carrier of the 15q11.2 BP1-BP2 CNV in addition to another CNV.

Final sample exclusion criteria: Based on observations in the visual inspection and additional QC plots, we finally applied an additional overall QC filter, removing samples with LRR_BAF>0.35, number of CNVs identified (NumCNV >225).

The final sample included 10,118 individuals with sufficient genetic data quality. In this sample, there were 45 15q11.2 BP1–BP2 deletions (copy number = 1) and 53 15q11.2 BP1-BP2 duplications (copy number = 3).

All QC procedures were conducted with PennCNV and in R version 3.4.2 on the TSD (Services for Sensitive Data) platform to ensure reproducibility and data security.

Dataset Quality Control

Following initial recruitment, eligibility screening, processing and QC by the ABCD Study, we applied additional QC procedures to derive the final analytic sample for the present thesis using in R (R-bundle-CRAN/2024.06-foss-2023b):

1. Participants who met the quality control thresholds (MR_QC = 1) predefined and recommended by the ABCD study were retained. These thresholds included adequate neuroimaging data quality, no significant protocol deviations, and availability of core

demographic, cognitive, and phenotypic variables, yielding a subsample of 11,639 participants (Hagler et al., 2019).

2. All participants from site 22 were excluded due to its small sample size (n = 15), which contrasts sharply with the ≥300 participants per site typical of the remaining 21 ABCD sites. This limited sample size substantially reduces the reliability of site-level estimates and can introduce instability when modelling site effects (Casey et al., 2018). In addition, the normative model used in this thesis was not trained on site 22 data, precluding effective harmonization of its scanner-related variance within the multi-site framework (Rutherford et al., 2022). Including such a small site risks overfitting and inflating model uncertainty, as normative modelling is sensitive to sample size heterogeneity, which can impair the generalizability of deviation estimates (Rutherford et al., 2022). Therefore, excluding site 22 was necessary to maintain model stability, ensure site-effect robustness, and preserve the validity of individual deviation scores.

3. The normative model implemented in this thesis was calibrated using a binary sex variable (male = 1, female = 0) as a key covariate to account for well-documented sex differences in brain development during adolescence (Lenroot & Giedd, 2010; Casey et al., 2018). Participants with demographic covariates that the normative model did not support were excluded (n = 3).

Statistical Analysis

Normative Modelling

We applied a normative modelling framework using pre-trained models to quantify individual deviations in brain structure relative to age-normed trajectories (Rutherford & Marquand, 2023). These normative models were trained on large datasets (n ≈ 46,000–59,000) spanning 59–82 imaging sites worldwide, with robust representation of the ABCD cohort (excluding site 22; see section *Dataset Quality Control*). This ensured direct data compatibility with the normative framework, reducing the risk of site-related bias. Using standardized pipelines, ABCD-derived morphometric data (parcellated using the Desikan-Killiany atlas) were processed through the normative models. For each participant and ROI, the models returned predicted means ($\hat{\mu}$) and

standard deviations (σ), accounting for individual-specific covariates. Regional z-scores were calculated as follows:

$$Deviation\ score_{i,r} = \frac{x_{i,r} - \hat{\mu}_{i,r}}{\sigma_{i,r}}$$

Where $x_{i,r}$ is the observed ROI value for participant i and region r. These z-scores quantify individual-level deviations from expected normative values, centred on zero with unit variance, facilitating sensitive detection of atypical developmental patterns (Rutherford et al., 2022).
No additional adaptation or re-calibration was required, as ABCD data were embedded within the normative model's training distribution. This direct model application reduces the risk of data leakage or overfitting, in line with best practices in normative modelling (Rutherford et al., 2023).
The final output comprised three z-score datasets (CT, SA, SV), mirroring the structure of the raw data and serving as inputs for all downstream analyses. These z-scores allowed robust group-level comparisons while controlling for age, sex, and site effects implicitly through the model structure, aligning with recent recommendations for best practices in neurodevelopmental MRI research (Rutherford et al., 2023)

Repeated measures Group comparison Analysis: Raw vs. Z-score

Group differences in brain morphology between 15q11.2 BP1–BP2 CNV carriers (deletion and duplication) and controls were assessed using linear mixed-effects models applied across all available timepoints. Analyses were conducted separately for CT, SA and SV.

For each modality, two parallel modeling strategies were implemented: (1) models using raw morphometric data and (2) models using normative deviation scores (z-scores). This dual approach enabled direct comparison of traditional covariate-adjusted models with deviation-based models derived from normative modeling.

Model specifications were:

- *Raw data models:* ROI ~ Group + Age (centered) + Sex + Site + (1 | ID).
- *Z-score models:* Z-score ~ Group + (1 | ID)

The inclusion of a random intercept for participant ID accounted for repeated measurements over time. Raw data models included age, sex, and scanner site as fixed effects; in contrast, z-score models excluded these covariates because the normative framework had already adjusted for them. If convergence issues arose in raw models, covariates would be sequentially removed (site, then sex, then age). If mixed models failed entirely, fallback fixed-effects models would be applied. The estimated group effect, 95% confidence intervals, and p-values were obtained for each ROI and CNV group comparison (Deletion vs. Control, Duplication vs. Control).

False discovery rate (FDR) correction (Benjamini–Hochberg, q < .05) was applied separately by CNV group and model type to account for multiple comparisons across ROIs. This approach is consistent with methods used in recent large-scale CNV studies (e.g., Boen et al., 2024; Sønderby et al., 2022, where p-value correction was applied within modality-specific ROI sets. This correction strategy ensures appropriate control of Type I errors across the high-dimensional ROI data typically analysed in CNV studies. Both raw and FDR-adjusted p-values are reported, in addition to the number and percentage of significant ROIs (uncorrected and FDR-corrected), Analyses were conducted in R (R-bundle-CRAN/2024.06-foss-2023b) using the nlme package (Pinheiro et al., 2025).

Longitudinal Group Difference Analysis: Z-scores

To assess whether 15q11.2 BP1-BP2 CNVs are associated with altered neurodevelopmental trajectories, we conducted longitudinal analyses using normative z-score datasets for CT, SA and SV. Analyses were performed separately for each modality, using all available timepoints from the ABCD dataset. Z-score datasets were loaded, reshaped into long format (participant × timepoint × ROI), and CNV status was recoded as a categorical factor (Control, Deletion, Duplication). Age at scan was mean-centred to improve interpretability of main effects and interactions in the mixed-effects models.

For each ROI, a linear mixed-effects model was fitted:

- *Model:* Z-score ~ Group × Age (centered) + (1 | Participant ID).
- *Fixed effects:* CNV Group, centered Age, and their interaction.
- *Random effects:* Random intercepts by participant (no random slopes).
- *Estimator:* Restricted Maximum Likelihood (REML).

- *Optimizer:* Optim optimizer with extended iterations (maxIter = 1e5) to improve convergence.

The primary effect of interest was the Group × Age interaction, capturing differential developmental trajectories across CNV groups. Benjamini–Hochberg FDR correction ($q < .05$) was applied within each modality to control for multiple comparisons (CT: 69 ROIs; SA: 68 ROIs; SV: 31 ROIs). We report nominal and FDR-corrected p-values; B refers to unstandardized effect estimates from the raw models, whereas β refers to standardized estimates from the z-score models. All models were fitted using the *nlme* package in R.

Results

A full overview of the group comparison and longitudinal results is presented in Supplementary Table 3 -Supplementary Table 14). Concordance between the effect sizes derived from raw values and z-score values are described in the supplementary materials (Repeated Measures Group Differences

Supplementary Notes **1** - Supplementary Notes 3). Group comparisons using mixed cross-sectional and longitudinal data revealed several significant differences between 15q11.2 BP1-BP2 deletions compared to controls and between 15q11.2 BP1-BP2 duplications and controls. The following results sections describe the significant group differences at nominal and FDR corrected thresholds.

Repeated Measures Group Differences in Deletion Carriers.

Cortical thickness. Group comparison models revealed several significantly increased ROIs for cortical thickness among 15q11.2 BP1–BP2 deletion carriers compared to noncarriers. Both raw estimates (B) and z-score estimates (β) are included in the 16 effects surviving FDR correction (see Table 2). The bilateral pars triangularis showed the largest effects (right: B = 0.064, β = 0.489; left: B = 0.049, β = 0.367). Pronounced increases were also observed in the para hippocampal gyrus (left: B = 0.110, β = 0.431; right: B = 0.061, β = 0.287) and the rostral middle frontal cortex (right: B = 0.041, β = 0.323; left: B = 0.030, β = 0.199). Additional ROIs showing increased cortical thickness was the left insula (B = 0.047, β = 0.321), right cuneus (B = 0.039, β = 0.285), and left postcentral gyrus (B = 0.036, β = 0.180).

Table 2

FDR-Significant Group Differences in Cortical Thickness Between 15q11.2 BP1–BP2 Deletion Carriers and Controls Across Raw and Z-Score Models.

Sorted by model and estimate. This table summarizes the results of 16 FDR-significant mixed-effects models comparing cortical thickness between 15q11.2 BP1–BP2 deletion carriers and controls in 9 ROIs. Regions that showed statistically significant group differences after FDR correction ($q < .05$) are listed. For each ROI and model type, the table includes the estimated effect (Estimate), standard error (SE), test statistic (statistic), 95% confidence interval (CI), and FDR-corrected p-value. All effects reflect increased cortical thickness in deletion carriers relative to controls. * $p < .001$.

ROI	Model	Estimate	*SE*	t	CI (95%)		FDR p-value
					LL	UL	
lh_parahippocampal	raw	0.110	0.025	4.458	0.061	0.158	.001*
rh_parstriangularis	raw	0.064	0.013	5.104	0.039	0.089	.001*
rh_parahippocampal	raw	0.061	0.021	2.978	0.021	0.101	.032
lh_parstriangularis	raw	0.049	0.013	3.811	0.024	0.074	.002
lh_insula	raw	0.047	0.014	3.381	0.020	0.074	.010
rh_rostralmiddlefrontal	raw	0.041	0.011	3.835	0.020	0.062	.002
rh_cuneus	raw	0.039	0.013	2.943	0.013	0.066	.032
lh_postcentral	raw	0.036	0.013	2.757	0.010	0.062	.045
lh_rostralmiddlefrontal	raw	0.030	0.011	2.849	0.009	0.051	.038
rh_parstriangularis	z-score	0.489	0.098	4.994	0.297	0.681	.001*
lh_parahippocampal	z-score	0.431	0.102	4.202	0.230	0.631	.001*
lh_parstriangularis	z-score	0.367	0.099	3.702	0.173	0.561	.005
rh_rostralmiddlefrontal	z-score	0.323	0.095	3.408	0.137	0.508	.011
lh_insula	z-score	0.321	0.101	3.179	0.123	0.519	.020
rh_parahippocampal	z-score	0.287	0.101	2.835	0.089	0.485	.045
rh_cuneus	z-score	0.285	0.098	2.912	0.093	0.478	.041

Cortical Surface area. Group comparison models revealed significantly lower cortical SA in 15q11.2 BP1–BP2 deletion carriers, with eight z-score and raw effects surviving FDR correction (see Table 3). The left inferior parietal cortex showed the lowest score (B = –254.855, β = –0.318), followed by the left fusiform gyrus (B = –126.437, β = –0.287) and the left banks of the superior temporal sulcus (B = –58.691, β = –0.289). Further smaller SA estimates were observed in the left caudal anterior cingulate (B = –48.939, β = –0.294) and left parahippocampal gyrus (B = –28.818, β = –0.316), with a comparable effect in the right parahippocampal gyrus (B = –31.384, β = –0.343). Significantly lower cortical SA were also detected only in the z-score models for the right inferior parietal cortex (β = –0.348) and the left supramarginal gyrus (β = –0.277).

Table 3

FDR-Significant Group Differences in Cortical Surface Area Between 15q11.2 BP1–BP2 Deletion Carriers and Controls Across Raw and Z-Score Models.

Sorted by model and estimate. This table summarizes the results of a subset of 14 FDR-significant mixed-effects models comparing SA between 15q11.2 BP1–BP2 deletion carriers and controls in eight ROIs. Regions that showed statistically significant group differences after FDR correction ($q < .05$) are listed. For each ROI and model type, the table includes the estimated effect (Estimate), standard error (SE), test statistic (t), 95% confidence interval (CI) and FDR-corrected p-value.

ROI	Model	Estimate	*SE*	t	CI (95%)		FDR p-value
					LL	UL	
lh_inferiorparietal	raw	-254.855	74.463	-3.423	-400.807	-108.9	.014
lh_fusiform	raw	-126.437	39.580	-3.195	-204.016	-48.858	.020
lh_bankssts	raw	-58.691	20.236	-2.900	-98.36	-19.03	.036
lh_caudalanteriorcingulate	raw	-48.939	16.489	-2.968	-81.258	-16.62	.034
rh_parahippocampal	raw	-31.384	8.906	-3.524	-48.84	-13.928	.014

lh_parahippocampal	raw	-28.818	9.076	-3.175	-46.607	-11.029	.020
rh_inferiorparietal	z-score	-0.348	0.090	-3.853	-0.525	-0.171	.008
rh_parahippocampal	z-score	-0.343	0.096	-3.568	-0.532	-0.155	.012
lh_inferiorparietal	z-score	-0.318	0.096	-3.321	-0.505	-0.13	.017
lh_parahippocampal	z-score	-0.316	0.098	-3.219	-0.509	-0.124	.017
lh_caudalanteriorcingulate	z-score	-0.294	0.102	-2.880	-0.494	-0.094	.034
lh_bankssts	z-score	-0.289	0.098	-2.941	-0.48	-0.10	.032
lh_fusiform	z-score	-0.287	0.088	-3.244	-0.46	-0.114	.017
lh_supramarginal	z-score	-0.277	0.092	-3.012	-0.457	-0.097	.029

Cerebellar and subcortical volume. Group comparison models identified significant volume differences between 15q11.2 BP1–BP2 deletion carriers and controls, with nine regions surviving FDR correction (see Table 4). Ventricular spaces were larger in deletion carriers, most notably the right lateral ventricle (B = 782.180, β = 0.331), the third ventricle (B = 67.297, β = 0.286), and total CSF (B = 64.533, β = 0.316). In contrast, cerebellar tissues were smaller, particularly the left cerebellar cortex (B = –1 417.702, β = –0.272), right cerebellar cortex (B = –1 617.405, β = –0.272), and left cerebellar white matter (B = –211.131, β = –0.236). Subcortically, the putamen showed the most pronounced bilateral differences (left: B = –211.131, β = –0.378; right: B = –213.922, β = –0.385), with the right hippocampus also smaller (B = –113.291, β = –0.265).

Table 4

FDR-Significant Group Differences in Subcortical and Cerebellar Volume Between 15q11.2 BP1–BP2 Deletion Carriers and Controls Across Raw and Z-Score Models.

Sorted by model and estimate. This table summarizes the results of a subset of 16 FDR-significant mixed-effects models comparing SV between 15q11.2 BP1–BP2 deletion carriers and controls in nine ROIs. Regions that showed statistically significant group differences after FDR correction ($q < .05$) are listed. For each ROI and model type, the table includes the estimated

effect (estimate), standard error (SE), test statistic (t), 95% confidence interval (CI), and FDR-corrected p-value.

ROI	Model	Estimate	*SE*	t	CI (95%)		FDR p-value
					LL	UL	
Right.Lateral.Ventricle	raw	782.180	294.344	2.657	205.244	1359.116	.035
X3rd.Ventricle	raw	67.297	22.787	2.953	22.632	111.962	.020
CSF	raw	64.533	21.370	3.020	22.647	106.419	.020
Right.Hippocampus	raw	-113.291	41.442	-2.734	-194.521	-32.061	.032
Left.Putamen	raw	-211.131	56.364	-3.746	-321.609	-100.652	.003
Right.Putamen	raw	-213.922	55.889	-3.828	-323.468	-104.376	.003
Right.Cerebellum.Cortex	raw	-1417.702	556.944	-2.546	-2509.352	-326.051	.042
Left.Cerebellum.Cortex	raw	-1617.405	546.470	-2.960	-2688.525	-546.285	.020
Right.Lateral.Ventricle	z-score	0.331	0.095	3.482	0.145	0.518	.004
CSF	z-score	0.316	0.108	2.937	0.105	0.526	.021
X3rd.Ventricle	z-score	0.286	0.083	3.452	0.124	0.449	.004
Left.Cerebellum.White.Matter	z-score	-0.236	0.092	-2.551	-0.417	-0.055	.042
Right.Hippocampus	z-score	-0.265	0.103	-2.569	-0.468	-0.063	.042
Left.Cerebellum.Cortex	z-score	-0.272	0.103	-2.649	-0.473	-0.071	.042
Left.Putamen	z-score	-0.378	0.100	-3.765	-0.574	-0.181	.003
Right.Putamen	z-score	-0.385	0.098	-3.920	-0.578	-0.193	.003

Repeated Measures Group Differences in Duplication Carriers.

Cortical thickness. Group comparison models revealed no statistically significant differences in cortical thickness between 15q11.2 BP1–BP2 duplication carriers and controls after FDR correction. However, the top nominal effects (uncorrected p-values) are shown to provide an overview of the strongest trends observed with estimates for models on both raw or z-scores. (see Table 5**).** Overall, duplication carriers showed regionally less cortical thickness than control. The left entorhinal cortex exhibited the largest estimate for thinner cortex (B = –0.084, β = –0.312), followed by the right banks of the superior temporal sulcus (B = –0.046, β = –0.288) and

the left rostral middle frontal cortex (B = –0.029, β = –0.255). Additional regions with nominally thinner cortex included the left pars triangularis (B = –0.031, β = –0.246), left fusiform gyrus (B = –0.024, β = –0.224), left isthmus cingulate (B = –0.030, β = –0.224), left postcentral gyrus (B = –0.028, β = –0.207), and left precuneus (B = –0.022, β = –0.203). Smaller nominal deviations appeared only in the z-score estimates for the left caudal anterior cingulate (β = –0.194) and left lateral orbitofrontal cortex (β = –0.181).

Table 5

Nominally Significant Group Differences in Cortical Thickness Between 15q11.2 BP1–BP2 Duplication Carriers and Controls Across Raw and Z-Score Models.

Sorted by model and estimate. This table summarizes the results of non-significant mixed-effects models after FDR-correction, comparing cortical thickness between 15q11.2 BP1–BP2 duplication carriers and controls. Regions of interest (ROIs) that showed nominally significant group differences ($p < .05$, uncorrected) are listed. For each ROI and data type, the table reports the estimated effect (estimate), standard error (SE), test statistic (t), 95% confidence interval (CI), and nominal *p*-value. Only 10 unique ROIs (18 total model effects) are displayed here, out of 29 total nominally significant models for the duplication group (see Supplementary Table 9)

ROI	Model	Estimate	*SE*	t	CI (95%)		Nominal p-value
					LL	UL	
lh_precuneus	raw	-0.022	0.010	-2.243	-0.041	-0.003	.025
lh_fusiform	raw	-0.024	0.010	-2.288	-0.044	-0.003	.022
lh_postcentral	raw	-0.028	0.012	-2.256	-0.051	-0.004	.024
lh_rostralmiddlefrontal	raw	-0.029	0.010	-2.885	-0.048	-0.009	.004
lh_isthmuscingulate	raw	-0.030	0.013	-2.231	-0.056	-0.004	.026
lh_parstriangularis	raw	-0.031	0.012	-2.608	-0.055	-0.008	.009
rh_bankssts	raw	-0.046	0.015	-3.052	-0.076	-0.016	.002
lh_entorhinal	raw	-0.084	0.025	-3.358	-0.134	-0.035	.001*
lh_lateralorbitofrontal	z-score	-0.181	0.091	-1.989	-0.36	-0.003	.047

lh_caudalanteriorcingulate	z-score	-0.194	0.095	-2.042	-0.380	-0.008	.041
lh_precuneus	z-score	-0.203	0.087	-2.325	-0.373	-0.032	.020
lh_postcentral	z-score	-0.207	0.093	-2.218	-0.39	-0.024	.027
lh_isthmuscingulate	z-score	-0.224	0.095	-2.355	-0.41	-0.038	.019
lh_fusiform	z-score	-0.224	0.094	-2.381	-0.408	-0.04	.017
lh_parstriangularis	z-score	-0.246	0.092	-2.671	-0.427	-0.066	.008
lh_rostralmiddlefrontal	z-score	-0.255	0.090	-2.836	-0.432	-0.079	.005
rh_bankssts	z-score	-0.288	0.095	-3.047	-0.474	-0.103	.002
lh_entorhinal	z-score	-0.312	0.098	-3.188	-0.503	-0.12	.001

Cortical Surface area. Group comparison models revealed 26 significant effect of regionally lower cortical SA among 15q11.2 BP1–BP2 duplication carriers compared to noncarriers, with all presented effects surviving FDR correction (see Table 6). These effects are reported with estimates from raw models (B) and z-score model (β). The rostral middle frontal cortex showed the strongest effects (right: B = –219.352; left: B = –214.996), suggesting a bilateral frontal pattern. Additional less SA appeared in the right middle temporal gyrus (B = –150.610), right postcentral gyrus (B = –143.549), and right lingual gyrus (B = –137.934, β = –0.299). The largest standardized deviation was found in the left caudal anterior cingulate (β = –0.401, B = –63.766), with lower SA in the left rostral anterior cingulate (β = –0.318), left insula (B = –86.613, β = –0.290), right banks of the superior temporal sulcus (B = –46.172, β = –0.283), and left pars triangularis (B = –84.777, β = –0.271). Moderate negative effects were also present across the superior and middle temporal gyri and in the parietal cortex (e.g., left postcentral gyrus, β = –0.235). In contrast to this overall pattern, the left entorhinal cortex displayed a larger

surface area in duplication carriers (B = 40.655, β = 0.408).

Table 6

Group Differences in Cortical Surface Area Between 15q11.2 BP1–BP2 Duplication Carriers and Controls Across Raw and Z-Score Models.

Sorted by model and estimate This table summarizes the results of a subset of 26 FDR-significant mixed-effects models comparing cortical surface area between 15q11.2 BP1–BP2 duplication carriers and controls in 13 ROIs. For each ROI and model type, the table includes the estimated effect (estimate), standard error (SE), test statistic (t), 95% confidence interval (CI), and FDR-corrected p-value. * $p < .001$.

ROI	Model	Estimate	*SE*	t	CI (95%)		FDR
					LL	UL	p-value
lh_entorhinal	raw	40.655	9.302	4.371	22.422	58.888	.001*
rh_bankssts	raw	-46.172	14.839	-3.112	-75.258	-17.087	.016
lh_rostralanteriorcingulate	raw	-57.474	15.795	-3.639	-88.434	-26.514	.006
lh_caudalanteriorcingulate	raw	-63.766	15.365	-4.150	-93.882	-33.649	.001
rh_parstriangularis	raw	-84.777	26.963	-3.144	-137.627	-31.928	.016
lh_insula	raw	-86.613	24.792	-3.494	-135.207	-38.019	.008
lh_middletemporal	raw	-113.778	43.292	-2.628	-198.635	-28.922	.041
lh_superiortemporal	raw	-127.211	49.535	-2.568	-224.304	-30.118	.043
rh_lingual	raw	-137.934	43.124	-3.199	-222.461	-53.408	.016
rh_postcentral	raw	-143.549	49.756	-2.885	-241.075	-46.023	.027
rh_middletemporal	raw	-150.610	45.491	-3.311	-239.775	-61.445	.013
lh_rostralmiddlefrontal	raw	-214.996	75.935	-2.831	-363.833	-66.158	.029
rh_rostralmiddlefrontal	raw	-219.352	82.708	-2.652	-381.466	-57.238	.041
lh_entorhinal	z-score	0.408	0.093	4.397	0.226	0.59	.001*
rh_rostralmiddlefrontal	z-score	-0.213	0.084	-2.549	-0.377	-0.049	.049
lh_superiortemporal	z-score	-0.217	0.083	-2.610	-0.38	-0.054	.046
lh_middletemporal	z-score	-0.220	0.085	-2.596	-0.386	-0.054	.046

lh_rostralmiddlefrontal	z-score	-0.225	0.083	-2.724	-0.387	-0.063	.040
rh_postcentral	z-score	-0.235	0.086	-2.729	-0.404	-0.066	.040
rh_parstriangularis	z-score	-0.271	0.089	-3.046	-0.445	-0.097	.020
rh_bankssts	z-score	-0.283	0.091	-3.093	-0.462	-0.104	.019
rh_middletemporal	z-score	-0.284	0.084	-3.372	-0.449	-0.119	.010
lh_insula	z-score	-0.290	0.084	-3.442	-0.455	-0.125	.010
rh_lingual	z-score	-0.299	0.092	-3.250	-0.479	-0.119	.013
lh_rostralanteriorcingulate	z-score	-0.318	0.088	-3.616	-0.49	-0.146	.007
lh_caudalanteriorcingulate	z-score	-0.401	0.095	-4.222	-0.587	-0.215	.001*

Subcortical and cerebellar volume. Group comparison models, including raw estimates and z-score estimates, showed seven effects of the duplication carriers having regionally smaller volumes than control, with robust effects in both cerebellar and subcortical regions (Table 7). The cerebellar cortex displayed the largest differences (right: B = –1 636.414, β = –0.325; left: B = –1 592.905, β = –0.316). Subcortically, the right accumbens area also differed markedly (B = –28.880, β = –0.357), and the left accumbens was likewise smaller (B = –26.913).

Table 7

Group Differences in Subcortical and Cerebellar Volume Between 15q11.2 BP1–BP2 Duplication Carriers and Controls Across Raw and Z-Score Models.

Sorted by model and estimate. This table summarizes the results of all seven FDR-significant mixed-effects models comparing volume between 15q11.2 BP1–BP2 duplication carriers and controls in three ROIs. For each ROI and model type, the table includes the estimated effect (estimate), standard error (SE), test statistic (t), 95% confidence interval (CI), and FDR-corrected *p*-value.

ROI	Model	Estimate	*SE*	t	CI (95%)		FDR p-value
					LL	UL	
Left.Accumbens.area	raw	-26.913	9.842	-2.735	-46.204	-7.622	.048

Right.Accumbens.area	raw	-28.880	9.094	-3.176	-46.704	-11.056	.018
Left.Cerebellum.Cortex	raw	-1592.905	509.395	-3.127	-2591.356	-594.454	.018
Right.Cerebellum.Cortex	raw	-1636.414	519.150	-3.152	-2653.986	-618.843	.018
Left.Cerebellum.Cortex	z-score	-0.316	0.095	-3.313	-0.504	-0.129	.010
Right.Cerebellum.Cortex	z-score	-0.325	0.096	-3.390	-0.512	-0.137	.010
Right.Accumbens.area	z-score	-0.357	0.098	-3.658	-0.549	-0.166	.008

Developmental trajectories.

Cortical thickness. The longitudinal analyses of CT z-scores identified 14 ROIs demonstrating nominally significant CNV Group × Age interactions ($p < .05$); however, none survived FDR correction. Effects were evenly distributed between carrier types, with seven ROIs driven by duplication carriers and seven driven by deletion carriers. Significant regions were primarily localized to frontal cortices, with additional involvement observed in occipital, motor (precentral gyrus), cingulate, and insular regions. Specifically, among duplication carriers, all seven ROIs exhibited cortical thinning with age, while deletion carriers showed cortical thickening across all seven significant regions. Significant regions were primarily localized to frontal cortices (8 ROIs; 4 deletion, 4 duplication), with additional involvement observed in occipital (2 ROIs; 1 deletion, 1 duplication), motor (precentral gyrus; 1 ROI, deletion), cingulate (2 ROIs; 1 deletion, 1 duplication), and insular regions (1 ROI, duplication; see Supplementary Table 6)

Cortical surface area. The longitudinal analyses of SA z-scores identified three ROIs with nominally significant CNV Group × Age interactions ($p < .05$); however, these interactions did not survive FDR correction. The identified significant ROIs were driven by one deletion carrier exhibiting a surface area decrease in the left lateral orbitofrontal, and two duplication carrier models with effects in both directions: decreased left superior frontal and increased left insula (3 ROIs, all frontal; see Supplementary Table 7).

Subcortical and cerebellar volume. The longitudinal analyses of subcortical and cerebellar volume z-scores identified seven ROIs with nominally significant CNV Group × Age interactions ($p < .05$); however, none survived FDR correction. Significant ROIs included ventricular structures (Right Lateral Ventricle, Left Lateral Ventricle, 4th Ventricle, CSF), basal

ganglia regions (Right Pallidum, Left Caudate), and the Left Hippocampus. More specifically, effects were predominantly driven by deletion carriers (5 ROIs) compared to duplication carriers (2 ROIs). Deletion carriers exhibited progressive volume increase with age across all significant regions, while duplication carriers showed volume decrease. Significant ROIs included 4 ventricular structures dominated by deletion models showing an increase in volume (lateral ventricles, 4th ventricle and CSF volume), and 2 duplication models with a volume decrease in the right pallidum and left caudate. Notably, there was an increase in the left hippocampus for the last significant deletion model (see Supplementary Table 8).

Discussion

The current thesis examined brain structural group differences and longitudinal trajectories in 15q11.2 BP1-BP2 CNV carriers and controls on large samples of children and adolescents. This is the first longitudinal study of 15q11.2 BP1-BP2 CNV carriers.

Tackling our first hypothesis, our results are consistent with the adult ENIGMACNV megaanalysis (van der Meer et al., 2020) and its UK Biobank replication (Boen et al., 2023). We show that children and adolescents carrying the 15q11.2 BP1-BP2 deletion already have a thicker cortex in the same prefrontal and sensorimotor regions, but reduced SA in only frontal area. In addition, the longitudinal analyses indicated the same subtle effect reflected in the age-related modulation.

Deletion carriers exhibited the expected thicker cortex, with 9 FDR-significant regions clustering in dorsolateral/medial prefrontal, and post-central cortices. This pattern replicates adult findings and supports the hypothesis that *CYFIP1* haploinsufficiency *interrupts* cortical thinning in late-maturing association regions, although we found no motor area effects (Domínguez-Iturza et al., 2019). *Duplication carriers*, for comparison, indicates a dosage-dependent acceleration of normative neurodevelopmental processes (van der Meer et al., 2020; Boen et al., 2023).

For surface area, deletion carriers showed FDR-significant reductions in left inferior parietal, fusiform, and banks of the STS regions. Duplication carriers diverged from adult patterns, displaying widespread smaller surface area, consistent with normative growth curves where SA peaks around ages 10-12 and then declines (Tamnes et al., 2017). Longitudinal models suggested

possible attenuation of SA deficits in deletion carriers during adolescence, though this preliminary finding requires confirmation in independent samples.
Developmentally, CT deletion effects seem evident by late childhood, whereas duplication effects emerge gradually and reach statistical visibility only after adolescence, mirroring dosage-dependent modulation of the cortex's protracted thinning trajectory. For our SA results (the effect of less SA in duplications are even stronger in in deletion carriers), and prior research, deletion-related deficits are seemingly established by late childhood and persist as a stable offset throughout development, whereas duplication effects emerge later and become significant only in early adulthood, reflecting differential impact on the normative SA trajectory that peaks around age 11 and subsequently declines (van der Meer et al., 2020; Boen et al., 2023).

H2 anticipated that 15q11.2 BP1–BP2 deletion carriers would show a focal reduction in ventral striatum and most clearly the nucleus accumbens, with subtler reduction in the caudate and pallidum, mirroring adult patterns from prior research. Our findings partially support this hypothesis. Deletion carriers showed bilateral putamen reduction but no significant differences in nucleus accumbens. Instead, duplication carriers were the ones to show significant bilateral nucleus accumbens reduction. This ventral-to-dorsal shift accords with normative striatal maturation, whereby reward-related ventral circuits (nucleus accumbens) stabilise by early adolescence, while dorsal sensorimotor territories (putamen) continue to remodel into the late teens (Raznahan et al., 2014; Narvacan et al., 2017; Goddings & Giedd, 2014). Also, regarding the nucleus accumbens, van der Meer et al. (2020) showed that total cortical surface area and volume jointly mediated lower cognitive performance in adult 15q11.2 BP1-BP2 deletion carriers. Although our adolescent data revealed a nucleus accumbens reduction in duplication rather than deletion carriers, the adult mediation result underscores that striatal and areal alterations in either dosage direction may have downstream cognitive consequences that evolve with age.
Furthermore, longitudinal analyses revealed nominal age interactions, with deletion carriers showing progressive volume increase in basal ganglia regions while duplication carriers exhibited volume decrease. These developmental trajectories suggest haploinsufficiency perturbs developmental trajectories rather than producing static ventral-striatal signatures (Bethlehem et al., 2022).

Beyond the basal ganglia effects, we also detected smaller cerebellar cortex volumes and enlarged lateral/third ventricles in deletion carriers. Both alterations are well established in schizophrenia: meta-analysis of >2000 patients show cerebellar volume loss (Haijma et al., 2013), and ventricular enlargement is one of the most robust neuroimaging signals in the disorder (Svancer & Španiel, 2021). Mechanistically, the cerebellum has been implicated both in psychosis via disrupted predictive processing (Moberget & Ivry, 2019) and in higher cognition more broadly (Schmahmann, 2019). Together, these results strengthen the idea that CNV alters brain development along pathways that overlap genetically with schizophrenia, however, the direction and clinical impact of those alterations are complex and still not strictly linear (van der Meer et al., 2020; Rees & Kirov, 2021; Frei et al., 2022).

H3 assumed that duplication carriers would exhibit milder and partly opposing effects, consistent with dosage sensitivity (i.e. thinner cortices). In partial support, duplication carriers display nominally thinner cortex in multiple regions, most pronounced in the left entorhinal cortex and right banks of the superior temporal sulcus. This pattern opposes the significant cortical thickening observed in deletion carriers, but its effect is notably milder than the robust thickening in deletion carriers, and no duplication effects survived FDR correction.
Longitudinally, duplication carriers had steeper cortical thinning slopes across frontal regions, contrasting with deletion carriers who exhibited cortical thickening in our results. Previous large studies have not found these slope differences (van der Meer et al., 2020; Boen et al., 2023). While our findings suggest that having too many or too few copies of the 15q11.2 BP1-BP2 region might affect brain development in opposite ways, this should be considered preliminary evidence that needs further confirmation.
For SA, duplication carriers showed widespread significant reductions, most prominently in bilateral rostral middle frontal cortex. This pattern was unexpected as it parallels rather than opposes the reductions seen in deletion carriers, with the lone exception of an enlarged left entorhinal parcel, representing a mirror effect consistent with dosage sensitivity.
These predominantly concordant surface area effects suggest certain neurodevelopmental processes may respond non-linearly to gene dosage, reflecting shared vulnerability regardless of copy number direction (van der Meer et al., 2020; Collins et al., 2022).

In subcortical regions, duplication carriers showed significant volume reductions in the nucleus accumbens, while deletion carriers exhibited reductions primarily in the putamen. This pattern is opposite to the results reported in adult cohort studies (van der Meer et al., 2020).
Our findings show that duplication carriers exhibit milder brain changes than deletion carriers, and these changes are only occasionally in the opposite direction. Interestingly, some modalities (e.g. SA) respond to gene dosage in complex ways that vary with age. These findings support recent research suggesting that brain structure changes continuously and non-linearly as gene copy numbers change and as the brain develops over time (Bethlehem et al., 2022; Boen et al., 2024).

In partial support of *H4*, the results demonstrate that using both conventional case-control analyses on raw neuroimaging derived metrics and Z-scores derived from normative modelling, the results suggest largely a convergence of group differences, but with subtle differences in significant ROIs. Thus, this may indicate that Z-scores can provide additional information about the neuroanatomical alterations in 15q11.2 BP1-BP2 CNV carriers (Marquand et al., 2016; Rutherford et al., 2023).
For the repeated-measures group-difference analyses, z-score and raw models mostly identified similar regions showing significant group differences. In deletion carriers, both approaches detected comparable patterns of increased cortical thickness in frontal, limbic and paralimbic regions. Where the approaches diverged was in subtle or region-specific findings. Normative z-scores revealed three effects that the raw model missed, reflecting evidence that normative frameworks boost sensitivity for smaller regional effects (Rutherford et al., 2023). In duplications, where alterations are inherently milder, z-scores produced larger but sub-threshold effect sizes in association cortices, consistent with the idea that normative modelling is most informative when group differences are small (Marquand et al., 2016).
The longitudinal trajectory analyses, conducted exclusively with z-score models, revealed nominal but informative CNV group by age interactions that provide valuable developmental insights despite not surviving strict FDR correction. Deletion carriers showed progressive cortical thickening in seven regions, SA increase in three left-hemispheric frontal regions and also a progressive volume increase in five subcortical and cerebellar regions. Moreover, duplication carriers showed increased thinning across similar regions, no difference in SA and a

progressive volume decrease in subcortical and cerebellar regions. Thus, the strongest z-score deviations clustered in late maturing association cortex (prefrontal, anterior cingulate, inferior parietal), exactly the regions where Boen et al. (2024) found disproportionate positive deviation scores in deletion carriers, and which the brainchart project pinpoints as having the greatest interindividual heterogeneity across adolescence (Bethlehem et al., 2022). Together, these results support H4 in showing that normative modelling provides incremental, regions-pecific sensitivity to heterogeneity beyond what raw group means can reveal. This advantage was anticipated by the normative modelling framework of Marquand et al. (2016), and most evident here for subtle duplication effects and for developmental trajectory analyses.

Strengths and limitations.

This thesis employs two complementary analytical strategies to investigate neurodevelopmental trajectories in 15q11.2 BP1-BP2 CNV carriers, following Bethlehem et al.'s (2022) recommendation for dual-analysis approaches in developmental neuroimaging. The repeated-measures group comparison leverages within-subject sensitivity across timepoints to enhance statistical power and minimize individual variability (Twisk, 2013), applying both raw MRI metrics and normative z-scores to capture absolute morphometric differences and deviations from age-typical trajectories (Rutherford et al., 2023). While this provides robust detection of group effects, it does not directly test developmental slopes. Conversely, the longitudinal group by age analysis explicitly models trajectory differences to assess whether carriers deviate from expected maturation curves (Bethlehem et al., 2022; Marquand et al., 2016), though this approach relies solely on z-scores and is more vulnerable to noise, dropout, and potential normative miscalibration, particularly at younger ages and in small ROIs (Bethlehem et al., 2022; Rutherford et al., 2023). Together, these methods offer complementary insights, stable group contrasts and developmental trajectory dynamics, while acknowledging the interpretive caution required for small samples typical in rare-CNV research (Boen et al., 2023; van der Meer et al., 2020). Both methods thus provide complementary strengths: repeated-measures models deliver stable group contrasts across time with more power from repeated measures, while group by age models probe the shape and directionality of developmental trajectories. This positions our work at the methodological intersection recommended by current best practices, enabling

robust CNV effect detection while directly evaluating developmental dynamics, all while transparently acknowledging the inherent limitations typically found in rare-CNV research (Boen et al., 2023; van der Meer et al., 2020).

Furthermore, there are several considerations worth noting regarding the strengths of this thesis, firstly related to the analysis. The implementation of brain-chart z-scores (Bethlehem et al., 2022) enabled detection of subtle regional brain differences that standard methods might have missed, particularly in duplication carriers. This methodological approach, which Marquand et al. (2016) had anticipated, and Rutherford et al. (2023) later validated, demonstrates robust technical reliability with median |z| values below 0.04 across ages 9–15. To improve reliability in the analysis, the ABCD study's sample site 22 (n = 33) was excluded. The sample size fell below the minimum threshold for stable normative modeling and its inclusion would have negatively effected the results. The exclusion ensures proper alignment with model assumptions while we balance between data integrity and analytical power.

Furthermore, the ABCD Study provides major strengths for this thesis through its large sample size, harmonized multi-site imaging and standardized protocols. Especially, the longitudinal data enables robust modelling of brain development and deviation tracking in 15q11.2 BP1-BP2 CNV carriers, with its normative framework supporting precise z-scoring adjusted for age, sex, and scanner site (Casey et al., 2018; Hagler et al., 2019; Rutherford et al., 2023). This framework effectively addresses critical gaps in prior CNV consortia research while inheriting their strengths. Also, with precisely the initial 11,868 baseline scans (post QC = 11,621), the ABCD study delivers unprecedented statistical power, yielding the largest adolescent 15q11.2 BP1-BP2 carrier sample to date, while maintaining raw metric compatibility with ENIGMA-CNV (van der Meer et al., 2020) and UK Biobank (Boen et al., 2023). Unlike previous cross-sectional designs with essentially null group by age interactions, ABCD's longitudinal sampling enables the first measured developmental slopes in youth carriers through z-score mixed-effects modelling, while its multi-ethnic cohort addresses the European bias of prior studies, with ancestry principal components, nested scanner-site effects, and ComBat-GAM harmonization mitigating potential confounds (Hagler et al., 2019; Pomponio et al., 2020).

Despite these advantages, there are also considerations to be taken regarding the weaknesses of the current study design and related articles. the current CNV carrier groups are small in size,

especially the duplication group. Thus, effect size estimates are less precise, and some true effects may have gone undetected (van der Meer et al., 2020; Boen et al., 2023). Thirdly, the normative model we used is tuned mainly to larger brain regions and older age ranges (Bethlehem et al., 2022); its accuracy is lower for adolescents and for smaller ROIs such as the entorhinal cortex. Therefore, duplication findings and any effects in small cortical areas should be viewed as provisional and interpreted with caution. Lastly, although longitudinal data significantly enhances the thesis's robustness, relatively high attrition rates at follow-up points (especially at 4-year follow-up) can potentially bias this longitudinal analyses and weaken the inferential strength for developmental trajectories.

Another key limitation of the normative-modelling approach used in this study is its dependence on the accuracy and calibration of the underlying reference models (Marquand et al., 2016). While z-scores offer a standardised metric of deviation from typical development, they are inherently constrained by the normative model's assumptions about age-related brain trajectories (Rutherford et al., 2023; Bethlehem et al., 2022; Kia & Marquand, 2018). If the true neurodevelopmental trajectory of 15q11.2 BP1-BP2 CNV carriers diverges substantially from these normative patterns, for example, exhibiting atypical growth curves not represented in the reference data, z-scores may mischaracterise the nature or magnitude of group differences (Wolfers et al., 2018; Zabihi et al., 2019). This risk is especially pertinent in rare-CNV research, where limited prior data exist to validate normative fits (Kia & Marquand, 2018). However, the integration of raw morphometric models alongside z-score analyses in repeated-measures designs ensures that observed group effects could be interpreted both in absolute and deviation-standardised terms. In contrast, the longitudinal mixed models relied solely on z-scores to leverage developmental benchmarking, results should therefore be interpreted cautiously, recognising that normative-based metrics complement rather than replace raw-data perspectives, particularly in genetically defined cohorts where atypical developmental patterns may fall outside normative expectations (Berthet et al., 2024; Rutherford et al., 2023).

These genetically defined cohorts are usually so rare in the field of rare-CNV research that it creates a practical challenge of independent replication. Pathogenic copy number variants such as 15q11.2 BP1-BP2 occur in well under 1 % of the population, so even large single cohorts seldom contain enough carriers for a standalone confirmatory sample. Recent reviews of the CNV field explicitly highlight this issue, noting that the low prevalence of high impact CNVs

makes independent replication difficult and necessitates international data sharing consortia to obtain adequate sample sizes for robust inference (Rees & Kirov, 2021; Sullivan & Owen, 2020). Our findings therefore require cautious interpretation until they can be reproduced in other datasets or within collaborative frameworks such as ENIGMA-CNV; future waves of ABCD and ongoing population biobanks will be essential for that next step.

Moreover, a common consideration in large neuroimaging datasets like the ABCD cohort, is the "healthy volunteer bias". Heeringa and Berglund (2020) demonstrated that the ABCD cohort had lower rates of poverty, parental smoking, and chronic medical conditions compared to a age-matched reference sample. This necessitates the development of population weights to address this misrepresentation. However, this selection bias is not unique to the ABCD study. Fry et al. (2017) documented similar skews toward healthier, better-educated participants in the UK Biobank. Such systematic over-representation of healthier individuals potentially attenuates associations linked to clinical burden, limiting the generalizability of findings to broader populations. Consequently, our results should be interpreted with appropriate consideration of this sampling limitation, ideally employing future weighting procedures or sensitivity analyses to account for this well-documented bias. However, some considerations still needs to be taken event though they are controlled for. For example, despite ABCD's harmonized pipeline, several scanner-level artefacts can still bias small genetic sub-samples. Persistent head motion in children degrades T1 quality and can inflate or mask CNV effects even after prospective correction (Fair et al., 2012; Power et al., 2012). In addition, vendor-specific gradients and subtle changes in head position create distortion and intensity drift that widen longitudinal variance (Reuter et al., 2015). Lastly, high-density phased-array coils introduce strong bias-fields; incomplete correction can mis-segment tissue and warp cortical metrics (Yendiki et al., 2013). Other sides of the ABCD protocol can lower power in an already low-power sample, like the binary quality control system for T1-weighted MRI that classifies scans as either acceptable or unacceptable (Hagler et al., 2019). The ABCD QC recommendations ensure data fidelity, but further decreases potential power in a sample where every CNV carrier is crucial for statistical rigor. The ABCD approach excludes potentially usable data from an already limited sample of approximately 45 deletions and 53 duplications pre-QC. This contrasts with the ENIGMA-CNV consortium's approach of incorporating continuous quality metrics into statistical models rather than excluding entire scans (van der Meer et al., 2020), highlighting how ABCD's rigorous QC

standards, while maximizing reliability, further restrict statistical power in rare variant research. Other mentions regarding the ABCD protocol is their demographic oversampling which ensures representation of the U.S population. However, rural populations remain underrepresented, limiting generalizability (Heeringa & Berglund, 2020). Although this is not considered in the current study, it should be considered. Lastly, familial clustering is flagged in the ABCD Family File, but this study did not exclude siblings, which may add dependency noise.

Conclusion

Overall, these results indicate that brain structural alterations in 15q11.2 BP1-BP2 carriers are detectable in adolescence, indicating an altered neurodevelopment that emerges earlier than the adolescent period in both carriers. These brain structural differences, also found in adult samples, show divergent and convergent effects with those observed in idiopathic developmental neuropsychiatric disorders, potentially contributing to the neuroanatomical heterogeneity observed in these disorders and associated cognitive deficits. To answer the initial research question, 15q11.2 BP1-BP2 CNV adolescent carriers do exhibit regionally specific and developmentally dynamic brain structure deviations, depending on the CNV group and ROI. Furthermore, this thesis has complimented prior studies in demonstrating how normative modelling can provide CNV researchers with a nuanced understanding of the structural deviations found in the developmental trajectories of 15q11.2 BP1-BP2 CNV adolescent carriers. The normative model did find more subtle effect and is seemingly more sensitive to region-specific findings compared to the use of raw metrics alone. However, the power of this thesis lies in the dual-faceted approach.

Ethical considerations

Due to the continuing research and evidence arising regarding CNV's effect on neurodevelopmental disorders, CNV research and neuroimaging for predictive diagnostics present intricate dilemmas. In the future, the application of genetic testing to predict disease risk based on CNV status could enhance clinical preparedness and intervention strategies, it simultaneously creates an ethical risk which includes psychological distress, stigmatisation, and potential discrimination for the potential CNV carrier. Particularly delicate is the question of initiating such testing during adolescence, a critical developmental period where labelling or predicting neuropsychiatric outcomes may profoundly affect identity formation and mental

health trajectories (Singh, 2013; Sabatello & Appelbaum, 2017). In addition, the enormous volume of genetic data produced by CNV analysis highlights the significance of informed consent and reducing the possibility of privacy abuse. Given the nature of CNV analysis, informed consent may be more difficult to obtain than for the testing of a single gene (Coughlin et al., 2012). The predictive capability of normative modelling approaches, though robust and innovative, still inherently carries uncertainty. The ability to accurately forecast individual outcomes from generalised brain measures is not absolute, and false predictions could lead to unnecessary anxiety or self-fulfilling negative expectations. Additionally, providing neuroimaging diagnostics to asymptomatic people, particularly adolescents, requires strict ethical management, that guaranties an informed consent and suitable counselling if required. It is important to understand that while abnormalities are shown to have a higher risk of mental disorders and that some can be detected by brain imaging, their predictive ability for clinical outcomes are not absolute. Therefore, to provide social integrity, mental health, and individual autonomy must be considered at the use of these technologies thorough communication tactics that express the probabilistic character of predictions. In the end, even though genetic testing and normative modelling have potential for personalized medicine, their ethical application necessitates careful evaluation of the psychosocial ramifications, consent procedures, and predictive validity to make sure the advantages greatly exceed any potential drawbacks.

Future challenges:

To further our understanding of 15q11.2 BP1-BP2 CNV effects, future research should integrate multimodal neuroimaging (e.g. combining structural, functional, and diffusion MRI) to elucidate how morphometric alterations translate into network-level dysfunction and behavioural phenotypes (Moberget & Ivry, 2019; Schmahmann, 2019). Specifically, linking cortical and subcortical deviations to cognitive performance and psychiatric outcomes will clarify the clinical relevance of observed structural differences (van der Meer et al., 2020; Boen et al., 2023). Also, expanding normative models to incorporate functional metrics and longitudinal cognitive data could enhance prediction accuracy and biological specificity (Bethlehem et al., 2022; Rutherford et al., 2023). Furthermore, larger, harmonized international cohorts will be essential to increase carrier sample sizes, enabling robust subgroup analyses (e.g., by sex, ancestry, or environmental exposures) and independent replication (Rees & Kirov, 2021; Sullivan & Owen, 2020). As current normative models perform best in adult cohorts and for larger regions, future model

refinements should improve precision in very young cohorts and in small regions like the entorhinal cortex (Bethlehem et al., 2022; Rutherford et al., 2023). Finally, ethical frameworks must evolve alongside technical advances to ensure responsible use of predictive neuroimaging and genetic data, balancing early intervention opportunities with risks of overdiagnosis and psychosocial harm (Sullivan & Owen, 2020).

Data Acknowledgement

In regard to the data used in the preparation of this article, which were obtained from the Adolescent Brain Cognitive DevelopmentSM (ABCD) Study (https://abcdstudy.org), held in the NIMH Data Archive (NDA). This is a multisite, longitudinal study designed to recruit more than 10,000 children age 9-10 and follow them over 10 years into early adulthood. The ABCD Study® is supported by the National Institutes of Health and additional federal partners under award numbers U01DA041048, U01DA050989, U01DA051016, U01DA041022, U01DA051018, U01DA051037, U01DA050987, U01DA041174, U01DA041106, U01DA041117, U01DA041028, U01DA041134, U01DA050988, U01DA051039, U01DA041156, U01DA041025, U01DA041120, U01DA051038, U01DA041148, U01DA041093, U01DA041089, U24DA041123, U24DA041147. A full list of supporters is available at https://abcdstudy.org/federal-partners.html. A listing of participating sites and a complete listing of the study investigators can be found at https://abcdstudy.org/consortium_members/. ABCD consortium investigators designed and implemented the study and/or provided data but did not necessarily participate in the analysis or writing of this report. This manuscript reflects the views of the authors and may not reflect the opinions or views of the NIH or ABCD consortium investigators. The ABCD data repository grows and changes over time. The ABCD data used in this report came from annual release 3.0 and 5.1 (DOI: 10.15154/z563-zd24) This work was performed on the TSD (Tjenester for Sensitive Data) facilities, owned by the University of Oslo, operated and developed by the TSD service group at the University of Oslo, IT-Department (USIT). (tsd-drift@usit.uio.no)

References

Alnæs, D., Kaufmann, T., Van Der Meer, D., Córdova-Palomera, A., Rokicki, J., Moberget, T., Bettella, F., Agartz, I., Barch, D. M., Bertolino, A., Brandt, C. L., Cervenka, S., Djurovic, S., Doan, N. T., Eisenacher, S., Fatouros-Bergman, H., Flyckt, L., Di Giorgio, A., Haatveit, B., … for the Karolinska Schizophrenia Project Consortium. (2019). Brain Heterogeneity in Schizophrenia and Its Association With Polygenic Risk. *JAMA Psychiatry*, *76*(7), 739. https://doi.org/10.1001/jamapsychiatry.2019.0257

Barkema, P., Rutherford, S., Lee, H.-C., Kia, S. M., Savage, H., Beckmann, C., & Marquand, A. (2023). Predictive Clinical Neuroscience Portal (PCNportal): Instant online access to research-grade normative models for clinical neuroscientists. *Wellcome Open Research*, *8*, 326. https://doi.org/10.12688/wellcomeopenres.19591.1

Bethlehem et al., 2022

Berthet, P., Haatveit, B. C., Kjelkenes, R., Worker, A., Kia, S. M., Wolfers, T., Rutherford, S., Alnaes, D., Dinga, R., Pedersen, M. L., Dahl, A., Fernandez-Cabello, S., Dazzan, P., Agartz, I., Nesvåg, R., Ueland, T., Andreassen, O. A., Simonsen, C., Westlye, L. T., … Marquand, A. (2024). A 10-Year Longitudinal Study of Brain Cortical Thickness in People with First-Episode Psychosis Using Normative Models. *Schizophrenia Bulletin*, *51*(1), 95–107. https://doi.org/10.1093/schbul/sbae107

Boen, R., Kaufmann, T., Frei, O., Van Der Meer, D., Djurovic, S., Andreassen, O. A., Selmer, K. K., Alnæs, D., & Sønderby, I. E. (2023). No signs of neurodegenerative effects in 15q11.2 BP1-BP2 copy number variant carriers in the UK Biobank. *Translational Psychiatry*, *13*(1), 61. https://doi.org/10.1038/s41398-023-02358-w

Boen, R., Kaufmann, T., Van Der Meer, D., Frei, O., Agartz, I., Ames, D., Andersson, M., Armstrong, N. J., Artiges, E., Atkins, J. R., Bauer, J., Benedetti, F., Boomsma, D. I., Brodaty, H., Brosch, K., Buckner, R. L., Cairns, M. J., Calhoun, V., Caspers, S., … Sønderby, I. E. (2024). Beyond the Global Brain Differences: Intraindividual Variability Differences in 1q21.1 Distal and 15q11.2 BP1-BP2 Deletion Carriers. *Biological Psychiatry*, *95*(2), 147–160. https://doi.org/10.1016/j.biopsych.2023.08.018

Burnside, R. D., Pasion, R., Mikhail, F. M., Carroll, A. J., Robin, N. H., Youngs, E. L., Gadi, I. K., Keitges, E., Jaswaney, V. L., Papenhausen, P. R., Potluri, V. R., Risheg, H., Rush, B., Smith, J. L., Schwartz, S., Tepperberg, J. H., & Butler, M. G. (2011). Microdeletion/microduplication of proximal 15q11.2 between BP1 and BP2: A susceptibility region for neurological dysfunction including developmental and language delay. *Human Genetics*, *130*(4), 517–528. https://doi.org/10.1007/s00439-011-0970-4

Calle Sánchez, X., Helenius, D., Bybjerg-Grauholm, J., Pedersen, C., Hougaard, D. M., Børglum, A. D., Nordentoft, M., Mors, O., Mortensen, P. B., Geschwind, D. H., Montalbano, S., Raznahan, A., Thompson, W. K., Ingason, A., & Werge, T. (2022). Comparing Copy Number Variations in a Danish Case Cohort of Individuals With Psychiatric Disorders. *JAMA Psychiatry*, *79*(1), 59. https://doi.org/10.1001/jamapsychiatry.2021.3392

Casey, B. J., Cannonier, T., Conley, M. I., Cohen, A. O., Barch, D. M., Heitzeg, M. M., Soules, M. E., Teslovich, T., Dellarco, D. V., Garavan, H., Orr, C. A., Wager, T. D., Banich, M. T., Speer, N. K., Sutherland, M. T., Riedel, M. C., Dick, A. S., Bjork, J. M., Thomas, K. M., … Dale, A. M. (2018). The Adolescent Brain Cognitive Development (ABCD) study: Imaging acquisition across 21 sites. *Developmental Cognitive Neuroscience*, *32*, 43–54. https://doi.org/10.1016/j.dcn.2018.03.001

Collins, F. S., & Varmus, H. (2015). A New Initiative on Precision Medicine. *New England Journal of Medicine*, *372*(9), 793–795. https://doi.org/10.1056/NEJMp1500523

Collins, R. L., Glessner, J. T., Porcu, E., Lepamets, M., Brandon, R., Lauricella, C., Han, L., Morley, T., Niestroj, L.-M., Ulirsch, J., Everett, S., Howrigan, D. P., Boone, P. M., Fu, J., Karczewski, K. J., Kellaris, G., Lowther, C., Lucente, D., Mohajeri, K., … Esko, T. (2022). A cross-disorder dosage sensitivity map of the human genome. *Cell*, *185*(16), 3041-3055.e25. https://doi.org/10.1016/j.cell.2022.06.036

Coughlin, C. R., Scharer, G. H., & Shaikh, T. H. (2012). Clinical impact of copy number variation analysis using high-resolution microarray technologies: Advantages, limitations and concerns. *Genome Medicine*, *4*(10), 80. https://doi.org/10.1186/gm381

Cox, D., & Butler, M. (2015). The 15q11.2 BP1–BP2 Microdeletion Syndrome: A Review. *International Journal of Molecular Sciences*, *16*(2), 4068–4082. https://doi.org/10.3390/ijms16024068

Desikan, R. S., Ségonne, F., Fischl, B., Quinn, B. T., Dickerson, B. C., Blacker, D., Buckner, R. L., Dale, A. M., Maguire, R. P., Hyman, B. T., Albert, M. S., & Killiany, R. J. (2006). An automated labeling system for subdividing the human cerebral cortex on MRI scans into gyral based regions of interest. *NeuroImage*, *31*(3), 968–980. https://doi.org/10.1016/j.neuroimage.2006.01.021

Domínguez-Iturza, N., Lo, A. C., Shah, D., Armendáriz, M., Vannelli, A., Mercaldo, V., Trusel, M., Li, K. W., Gastaldo, D., Santos, A. R., Callaerts-Vegh, Z., D'Hooge, R., Mameli, M., Van Der Linden, A., Smit, A. B., Achsel, T., & Bagni, C. (2019). The autism- and schizophrenia-associated protein CYFIP1 regulates bilateral brain connectivity and behaviour. *Nature Communications*, *10*(1), 3454. https://doi.org/10.1038/s41467-019-11203-y

Fair, D. A., Bathula, D., Nikolas, M. A., & Nigg, J. T. (2012). Distinct neuropsychological subgroups in typically developing youth inform heterogeneity in children with ADHD. *Proceedings of the National Academy of Sciences*, *109*(17), 6769–6774. https://doi.org/10.1073/pnas.1115365109

Fischl, B., Salat, D. H., Busa, E., Albert, M., Dieterich, M., Haselgrove, C., Van Der Kouwe, A., Killiany, R., Kennedy, D., Klaveness, S., Montillo, A., Makris, N., Rosen, B., & Dale, A. M. (2002). Whole Brain Segmentation. *Neuron*, *33*(3), 341–355. https://doi.org/10.1016/S0896-6273(02)00569-X

Fraza, C., Sønderby, I. E., Boen, R., Shi, Y., Beckmann, C. F., & Marquand, A. F. (2023). *Unraveling the Link between CNVs, General Cognition, and Individual Neuroimaging Deviation Scores from a Reference Cohort*. https://doi.org/10.1101/2023.11.29.23298954

Frei, S., Chatterji, N. S., & Bartlett, P. L. (2023). *Benign Overfitting without Linearity: Neural Network Classifiers Trained by Gradient Descent for Noisy Linear Data* (No. arXiv:2202.05928). arXiv. https://doi.org/10.48550/arXiv.2202.05928

Fry, A., Littlejohns, T. J., Sudlow, C., Doherty, N., Adamska, L., Sprosen, T., Collins, R., & Allen, N. E. (2017). Comparison of Sociodemographic and Health-Related Characteristics of UK Biobank Participants With Those of the General Population. *American Journal of Epidemiology*, *186*(9), 1026–1034. https://doi.org/10.1093/aje/kwx246

Garavan, H., Bartsch, H., Conway, K., Decastro, A., Goldstein, R. Z., Heeringa, S., Jernigan, T., Potter, A., Thompson, W., & Zahs, D. (2018). Recruiting the ABCD sample: Design

considerations and procedures. *Developmental Cognitive Neuroscience*, *32*, 16–22. https://doi.org/10.1016/j.dcn.2018.04.004

Gilmore, J. H., Schmitt, J. E., Knickmeyer, R. C., Smith, J. K., Lin, W., Styner, M., Gerig, G., & Neale, M. C. (2010). Genetic and environmental contributions to neonatal brain structure: A twin study. *Human Brain Mapping*, *31*(8), 1174–1182. https://doi.org/10.1002/hbm.20926

Goddings, A.-L., & Giedd, J. N. (2014). Structural Brain Development During Childhood and Adolescence. In M. S. Gazzaniga & G. R. Mangun (Eds.), *The Cognitive Neurosciences* (5th ed.). The MIT Press. https://doi.org/10.7551/mitpress/9504.003.0006

Hagler, D. J., Hatton, SeanN., Cornejo, M. D., Makowski, C., Fair, D. A., Dick, A. S., Sutherland, M. T., Casey, B. J., Barch, D. M., Harms, M. P., Watts, R., Bjork, J. M., Garavan, H. P., Hilmer, L., Pung, C. J., Sicat, C. S., Kuperman, J., Bartsch, H., Xue, F., … Dale, A. M. (2019). Image processing and analysis methods for the Adolescent Brain Cognitive Development Study. *NeuroImage*, *202*, 116091. https://doi.org/10.1016/j.neuroimage.2019.116091

Haijma, S. V., Van Haren, N., Cahn, W., Koolschijn, P. C. M. P., Hulshoff Pol, H. E., & Kahn, R. S. (2013). Brain Volumes in Schizophrenia: A Meta-Analysis in Over 18 000 Subjects. *Schizophrenia Bulletin*, *39*(5), 1129–1138. https://doi.org/10.1093/schbul/sbs118

Haist, F., & Jernigan, T. L. (n.d.). *Adolescent Brain Cognitive Development Study (ABCD)—Annual Release 5.1*. https://doi.org/10.15154/Z563-ZD24

Hastings et al., 2009

Heeringa, S. G., & Berglund, P. A. (2020). *A Guide for Population-based Analysis of the Adolescent Brain Cognitive Development (ABCD) Study Baseline Data*. Neuroscience. https://doi.org/10.1101/2020.02.10.942011

Herting, M. M., Johnson, C., Mills, K. L., Vijayakumar, N., Dennison, M., Liu, C., Goddings, A.-L., Dahl, R. E., Sowell, E. R., Whittle, S., Allen, N. B., & Tamnes, C. K. (2018). Development of subcortical volumes across adolescence in males and females: A multisample study of longitudinal changes. *NeuroImage*, *172*, 194–205. https://doi.org/10.1016/j.neuroimage.2018.01.020

Huber, G. (1997). The heterogeneous course of schizophrenia. *Schizophrenia Research*, *28*(2–3), 177–185. https://doi.org/10.1016/S0920-9964(97)00113-8

Insel, T., Cuthbert, B., Garvey, M., Heinssen, R., Pine, D. S., Quinn, K., Sanislow, C., & Wang, P. (2010). Research Domain Criteria (RDoC): Toward a New Classification Framework for Research on Mental Disorders. *American Journal of Psychiatry*, *167*(7), 748–751. https://doi.org/10.1176/appi.ajp.2010.09091379

Insel, T. R., & Cuthbert, B. N. (2015). Brain disorders? Precisely. *Science*, *348*(6234), 499–500. https://doi.org/10.1126/science.aab2358

Jansen, A. G., Mous, S. E., White, T., Posthuma, D., & Polderman, T. J. C. (2015). What twin studies tell us about the heritability of brain development, morphology, and function: A review. *Neuropsychology Review*, *25*(1), 27–46. https://doi.org/10.1007/s11065-015-9278-9

Jonsson, L., Martin, J., Lichtenstein, P., Magnusson, P. K. E., Lundström, S., Westberg, L., & Tammimies, K. (2023). Examining neurodevelopmental problems in 15q11.2 (BP1-BP2) copy number variation carriers at ages 9/12 and 18 in a Swedish twin sample. *Molecular Genetics & Genomic Medicine*, *11*(8), e2191. https://doi.org/10.1002/mgg3.2191

Kia, S. M., & Marquand, A. (2018). Normative Modeling of Neuroimaging Data Using Scalable Multi-task Gaussian Processes. In A. F. Frangi, J. A. Schnabel, C. Davatzikos, C. Alberola-López, & G. Fichtinger (Eds.), *Medical Image Computing and Computer Assisted Intervention – MICCAI 2018* (Vol. 11072, pp. 127–135). Springer International Publishing. https://doi.org/10.1007/978-3-030-00931-1_15

Lenroot, R. K., & Giedd, J. N. (2010). Sex differences in the adolescent brain. *Brain and Cognition*, *72*(1), 46–55. https://doi.org/10.1016/j.bandc.2009.10.008

Malhotra, A. K. (2015). Dissecting the Heterogeneity of Treatment Response in First-Episode Schizophrenia. *Schizophrenia Bulletin*, *41*(6), 1224–1226. https://doi.org/10.1093/schbul/sbv117

Marquand, A. F., Rezek, I., Buitelaar, J., & Beckmann, C. F. (2016). Understanding Heterogeneity in Clinical Cohorts Using Normative Models: Beyond Case-Control Studies. *Biological Psychiatry*, *80*(7), 552–561. https://doi.org/10.1016/j.biopsych.2015.12.023

Matsumoto, J., Fukunaga, M., Miura, K., Nemoto, K., Okada, N., Hashimoto, N., Morita, K., Koshiyama, D., Ohi, K., Takahashi, T., Koeda, M., Yamamori, H., Fujimoto, M., Yasuda, Y., Ito, S., Yamazaki, R., Hasegawa, N., Narita, H., Yokoyama, S., … Hashimoto, R. (2023). Cerebral cortical structural alteration patterns across four major psychiatric

disorders in 5549 individuals. *Molecular Psychiatry*, *28*(11), 4915–4923. https://doi.org/10.1038/s41380-023-02224-7

Mills, K. L., & Tamnes, C. K. (2014). Methods and considerations for longitudinal structural brain imaging analysis across development. *Developmental Cognitive Neuroscience*, *9*, 172–190. https://doi.org/10.1016/j.dcn.2014.04.004

Moberget, T., & Ivry, R. B. (2019). Prediction, Psychosis, and the Cerebellum. *Biological Psychiatry: Cognitive Neuroscience and Neuroimaging*, *4*(9), 820–831. https://doi.org/10.1016/j.bpsc.2019.06.001

Narvacan, K., Treit, S., Camicioli, R., Martin, W., & Beaulieu, C. (2017). Evolution of deep gray matter volume across the human lifespan. *Human Brain Mapping*, *38*(8), 3771–3790. https://doi.org/10.1002/hbm.23604

Okada, N., Fukunaga, M., Miura, K., Nemoto, K., Matsumoto, J., Hashimoto, N., Kiyota, M., Morita, K., Koshiyama, D., Ohi, K., Takahashi, T., Koeda, M., Yamamori, H., Fujimoto, M., Yasuda, Y., Hasegawa, N., Narita, H., Yokoyama, S., Mishima, R., … Hashimoto, R. (2023). Subcortical volumetric alterations in four major psychiatric disorders: A mega-analysis study of 5604 subjects and a volumetric data-driven approach for classification. *Molecular Psychiatry*, *28*(12), 5206–5216. https://doi.org/10.1038/s41380-023-02141-9

Parkes, L., Satterthwaite, T. D., & Bassett, D. S. (2020). *Towards precise resting-state fMRI biomarkers in psychiatry: Synthesizing developments in transdiagnostic research, dimensional models of psychopathology, and normative neurodevelopment* (No. arXiv:2006.04728). arXiv. https://doi.org/10.48550/arXiv.2006.04728

Pomponio, R., Erus, G., Habes, M., Doshi, J., Srinivasan, D., Mamourian, E., Bashyam, V., Nasrallah, I. M., Satterthwaite, T. D., Fan, Y., Launer, L. J., Masters, C. L., Maruff, P., Zhuo, C., Völzke, H., Johnson, S. C., Fripp, J., Koutsouleris, N., Wolf, D. H., … Davatzikos, C. (2020). Harmonization of large MRI datasets for the analysis of brain imaging patterns throughout the lifespan. *NeuroImage*, *208*, 116450. https://doi.org/10.1016/j.neuroimage.2019.116450

Power, J. D., Barnes, K. A., Snyder, A. Z., Schlaggar, B. L., & Petersen, S. E. (2013). Steps toward optimizing motion artifact removal in functional connectivity MRI; a reply to Carp. *NeuroImage*, *76*, 439–441. https://doi.org/10.1016/j.neuroimage.2012.03.017

Rafi, S. K., & Butler, M. G. (2020). The 15q11.2 BP1-BP2 Microdeletion (Burnside–Butler) Syndrome: In Silico Analyses of the Four Coding Genes Reveal Functional Associations with Neurodevelopmental Disorders. *International Journal of Molecular Sciences*, *21*(9), 3296. https://doi.org/10.3390/ijms21093296

Raznahan, A., Shaw, P. W., Lerch, J. P., Clasen, L. S., Greenstein, D., Berman, R., Pipitone, J., Chakravarty, M. M., & Giedd, J. N. (2014). Longitudinal four-dimensional mapping of subcortical anatomy in human development. *Proceedings of the National Academy of Sciences*, *111*(4), 1592–1597. https://doi.org/10.1073/pnas.1316911111

Redon, R., Ishikawa, S., Fitch, K. R., Feuk, L., Perry, G. H., Andrews, T. D., Fiegler, H., Shapero, M. H., Carson, A. R., Chen, W., Cho, E. K., Dallaire, S., Freeman, J. L., González, J. R., Gratacòs, M., Huang, J., Kalaitzopoulos, D., Komura, D., MacDonald, J. R., … Hurles, M. E. (2006). Global variation in copy number in the human genome. *Nature*, *444*(7118), 444–454. https://doi.org/10.1038/nature05329

Rees, E., & Kirov, G. (2021). Copy number variation and neuropsychiatric illness. *Current Opinion in Genetics & Development*, *68*, 57–63. https://doi.org/10.1016/j.gde.2021.02.014

Reuter, M., Tisdall, M. D., Qureshi, A., Buckner, R. L., Van Der Kouwe, A. J. W., & Fischl, B. (2015). Head motion during MRI acquisition reduces gray matter volume and thickness estimates. *NeuroImage*, *107*, 107–115. https://doi.org/10.1016/j.neuroimage.2014.12.006

Rutherford, S., Barkema, P., Tso, I. F., Sripada, C., Beckmann, C. F., Ruhe, H. G., & Marquand, A. F. (2023). Evidence for embracing normative modeling. *eLife*, *12*, e85082. https://doi.org/10.7554/eLife.85082

Rutherford, S., & Marquand, A. F. (2023). *Braincharts: Normative models for brain growth and againg* [Computer software]. https://github.com/predictive-clinical-neuroscience/braincharts

Sabatello, M., & Appelbaum, P. S. (2017). Behavioral Genetics in Criminal and Civil Courts. *Harvard Review of Psychiatry*, *25*(6), 289–301. https://doi.org/10.1097/HRP.0000000000000141

Saragosa-Harris, N. M., Chaku, N., MacSweeney, N., Guazzelli Williamson, V., Scheuplein, M., Feola, B., Cardenas-Iniguez, C., Demir-Lira, E., McNeilly, E. A., Huffman, L. G., Whitmore, L., Michalska, K. J., Damme, K. S., Rakesh, D., & Mills, K. L. (2022). A

practical guide for researchers and reviewers using the ABCD Study and other large longitudinal datasets. *Developmental Cognitive Neuroscience*, *55*, 101115. https://doi.org/10.1016/j.dcn.2022.101115

Schmahmann, J. D. (2019). The cerebellum and cognition. *Neuroscience Letters*, *688*, 62–75. https://doi.org/10.1016/j.neulet.2018.07.005

Singh, T., Walters, J. T. R., Johnstone, M., Curtis, D., Suvisaari, J., Torniainen, M., Rees, E., Iyegbe, C., Blackwood, D., McIntosh, A. M., Kirov, G., Geschwind, D., Murray, R. M., Di Forti, M., Bramon, E., Gandal, M., Hultman, C. M., Sklar, P., Palotie, A., … Barrett, J. C. (2017). The contribution of rare variants to risk of schizophrenia in individuals with and without intellectual disability. *Nature Genetics*, *49*(8), 1167–1173. https://doi.org/10.1038/ng.3903

Sønderby, I. E., Ching, C. R. K., Thomopoulos, S. I., Van Der Meer, D., Sun, D., Villalon-Reina, J. E., Agartz, I., Amunts, K., Arango, C., Armstrong, N. J., Ayesa-Arriola, R., Bakker, G., Bassett, A. S., Boomsma, D. I., Bülow, R., Butcher, N. J., Calhoun, V. D., Caspers, S., Chow, E. W. C., … Andreassen, O. A. (2022). Effects of copy number variations on brain structure and risk for psychiatric illness: Large-scale studies from the ENIGMA working groups on CNVs. *Human Brain Mapping*, *43*(1), 300–328. https://doi.org/10.1002/hbm.25354

Sønderby, I. E., Gústafsson, Ó., Doan, N. T., Hibar, D. P., Martin-Brevet, S., Abdellaoui, A., Ames, D., Amunts, K., Andersson, M., Armstrong, N. J., Bernard, M., Blackburn, N., Blangero, J., Boomsma, D. I., Bralten, J., Brattbak, H.-R., Brodaty, H., Brouwer, R. M., Bülow, R., … Andreassen, O. A. (2020). Dose response of the 16p11.2 distal copy number variant on intracranial volume and basal ganglia. *Molecular Psychiatry*, *25*(3), 584–602. https://doi.org/10.1038/s41380-018-0118-1

Spielmann, M., Lupiáñez, D. G., & Mundlos, S. (2018). Structural variation in the 3D genome. *Nature Reviews Genetics*, *19*(7), 453–467. https://doi.org/10.1038/s41576-018-0007-0

Stefansson, H., Rujescu, D., Cichon, S., Pietiläinen, O. P. H., Ingason, A., Steinberg, S., Fossdal, R., Sigurdsson, E., Sigmundsson, T., Buizer-Voskamp, J. E., Hansen, T., Jakobsen, K. D., Muglia, P., Francks, C., Matthews, P. M., Gylfason, A., Halldorsson, B. V., Gudbjartsson, D., Thorgeirsson, T. E., … Stefansson, K. (2008). Large recurrent microdeletions associated with schizophrenia. *Nature*, *455*(7210), 232–236. https://doi.org/10.1038/nature07229

Sullivan, P. F., & Owen, M. J. (2020). Increasing the Clinical Psychiatric Knowledge Base About Pathogenic Copy Number Variation. *American Journal of Psychiatry*, *177*(3), 204–209. https://doi.org/10.1176/appi.ajp.2019.19040335

Svancer, P., & Spaniel, F. (2021). Brain ventricular volume changes in schizophrenia. A narrative review. *Neuroscience Letters*, *759*, 136065. https://doi.org/10.1016/j.neulet.2021.136065

Tamnes, C. K., Herting, M. M., Goddings, A.-L., Meuwese, R., Blakemore, S.-J., Dahl, R. E., Güroğlu, B., Raznahan, A., Sowell, E. R., Crone, E. A., & Mills, K. L. (2017). Development of the Cerebral Cortex across Adolescence: A Multisample Study of Inter-Related Longitudinal Changes in Cortical Volume, Surface Area, and Thickness. *The Journal of Neuroscience*, *37*(12), 3402–3412. https://doi.org/10.1523/JNEUROSCI.3302-16.2017

Tiemeier et al., 2010

Twisk, J. W. R. (2013). *Applied longitudinal data analysis for epidemiology: A practical guide* (Second Edition). Cambridge University Press.

Uban, K. A., Horton, M. K., Jacobus, J., Heyser, C., Thompson, W. K., Tapert, S. F., Madden, P. A. F., & Sowell, E. R. (2018). Biospecimens and the ABCD study: Rationale, methods of collection, measurement and early data. *Developmental Cognitive Neuroscience*, *32*, 97–106. https://doi.org/10.1016/j.dcn.2018.03.005

Vaez, M., Montalbano, S., Calle Sánchez, X., Georgii Hellberg, K.-L., Dehkordi, S. R., Krebs, M. D., Meijsen, J., Shorter, J., Bybjerg-Grauholm, J., Mortensen, P. B., Børglum, A. D., Hougaard, D. M., Nordentoft, M., Geschwind, D. H., Buil, A., Schork, A. J., Helenius, D., Raznahan, A., Thompson, W. K., … Bækvad-Hansen, M. (2024). Population-Based Risk of Psychiatric Disorders Associated With Recurrent Copy Number Variants. *JAMA Psychiatry*, *81*(10), 957. https://doi.org/10.1001/jamapsychiatry.2024.1453

Van Der Meer, D., Sønderby, I. E., Kaufmann, T., Walters, G. B., Abdellaoui, A., Ames, D., Amunts, K., Andersson, M., Armstrong, N. J., Bernard, M., Blackburn, N. B., Blangero, J., Boomsma, D. I., Brodaty, H., Brouwer, R. M., Bülow, R., Cahn, W., Calhoun, V. D., Caspers, S., … Andreassen, O. A. (2020). Association of Copy Number Variation of the

15q11.2 BP1-BP2 Region With Cortical and Subcortical Morphology and Cognition. *JAMA Psychiatry*, *77*(4), 420. https://doi.org/10.1001/jamapsychiatry.2019.3779

Van Erp, T. G. M., Walton, E., Hibar, D. P., Schmaal, L., Jiang, W., Glahn, D. C., Pearlson, G. D., Yao, N., Fukunaga, M., Hashimoto, R., Okada, N., Yamamori, H., Bustillo, J. R., Clark, V. P., Agartz, I., Mueller, B. A., Cahn, W., De Zwarte, S. M. C., Hulshoff Pol, H. E., … Orhan, F. (2018). Cortical Brain Abnormalities in 4474 Individuals With Schizophrenia and 5098 Control Subjects via the Enhancing Neuro Imaging Genetics Through Meta Analysis (ENIGMA) Consortium. *Biological Psychiatry*, *84*(9), 644–654. https://doi.org/10.1016/j.biopsych.2018.04.023

Volkow, N. D., Koob, G. F., Croyle, R. T., Bianchi, D. W., Gordon, J. A., Koroshetz, W. J., Pérez-Stable, E. J., Riley, W. T., Bloch, M. H., Conway, K., Deeds, B. G., Dowling, G. J., Grant, S., Howlett, K. D., Matochik, J. A., Morgan, G. D., Murray, M. M., Noronha, A., Spong, C. Y., … Weiss, S. R. B. (2018). The conception of the ABCD study: From substance use to a broad NIH collaboration. *Developmental Cognitive Neuroscience*, *32*, 4–7. https://doi.org/10.1016/j.dcn.2017.10.002

Wolfers, T., Doan, N. T., Kaufmann, T., Alnæs, D., Moberget, T., Agartz, I., Buitelaar, J. K., Ueland, T., Melle, I., Franke, B., Andreassen, O. A., Beckmann, C. F., Westlye, L. T., & Marquand, A. F. (2018). Mapping the Heterogeneous Phenotype of Schizophrenia and Bipolar Disorder Using Normative Models. *JAMA Psychiatry*, *75*(11), 1146. https://doi.org/10.1001/jamapsychiatry.2018.2467

Yendiki, A., Koldewyn, K., Kakunoori, S., Kanwisher, N., & Fischl, B. (2014). Spurious group differences due to head motion in a diffusion MRI study. *NeuroImage*, *88*, 79–90. https://doi.org/10.1016/j.neuroimage.2013.11.027

Zabihi, M., Oldehinkel, M., Wolfers, T., Frouin, V., Goyard, D., Loth, E., Charman, T., Tillmann, J., Banaschewski, T., Dumas, G., Holt, R., Baron-Cohen, S., Durston, S., Bölte, S., Murphy, D., Ecker, C., Buitelaar, J. K., Beckmann, C. F., & Marquand, A. F. (2019). Dissecting the Heterogeneous Cortical Anatomy of Autism Spectrum Disorder Using Normative Models. *Biological Psychiatry: Cognitive Neuroscience and Neuroimaging*, *4*(6), 567–578. https://doi.org/10.1016/j.bpsc.2018.11.013

Supplementary materials

Supplementary Table 1

Distribution of Participant Groups Across Research Sites in the ABCD Study.

This table presents the distribution of three distinct participant groups (Control, Deletion, and Duplication) across 21 research sites (labeled as ABCD_01 through ABCD_21). Each row represents a unique research site, while the three columns display the number of participants (n) in each group category at that site. The table enables comparison of participant group distribution patterns across different research locations, with sites listed in numerical order by site ID rather than by participant count.

Site	Control (n)	Deletion (n)	Duplication (n)
ABCD_01	397	0	0
ABCD_02	559	3	2
ABCD_03	619	2	3
ABCD_04	714	6	3
ABCD_05	377	2	6
ABCD_06	577	3	7
ABCD_07	333	0	0
ABCD_08	336	0	0
ABCD_09	464	1	2
ABCD_10	718	4	1
ABCD_11	449	1	2
ABCD_12	588	4	4
ABCD_13	670	4	4
ABCD_14	590	2	3
ABCD_15	431	3	2

ABCD_16	993	3	6
ABCD_17	553	1	8
ABCD_18	372	1	1
ABCD_19	519	4	2
ABCD_20	697	2	1
ABCD_21	607	1	5

Supplementary Table 2

Longitudinal Participant Retention in the ABCD Study: Baseline to 4-Year Follow-up.
This table displays participant tracking data organized in a site-by-timepoint matrix format. The leftmost column identifies each research site (denoted as "ABCD" followed by a site number), with the first row showing aggregate totals. The three data columns represent different assessment timepoints: baseline enrollment, 2-year follow-up, and 4-year follow-up. Each cell contains the count of participants at the corresponding site and timepoint. The table allows for comparison of participant retention across sites and over time, with sites listed in descending order based on baseline enrollment numbers.

Site	Baseline	2-year follow-up	4-year follow-up
Total	11239	7895	2999
ABCD 16	1005	737	255
ABCD 10	690	561	218
ABCD 20	687	591	177
ABCD 04	654	602	284
ABCD 13	620	415	191
ABCD 03	605	347	220
ABCD 14	592	441	105
ABCD 21	585	405	194
ABCD 12	584	404	139
ABCD 06	579	392	177
ABCD 02	550	411	219

ABCD 17	548	377	68
ABCD 19	502	334	146
ABCD 11	446	275	59
ABCD 09	422	210	66
ABCD 15	420	246	80
ABCD 01	384	231	75
ABCD 05	376	260	115
ABCD 18	337	266	116
ABCD 07	332	214	14
ABCD 08	321	176	81

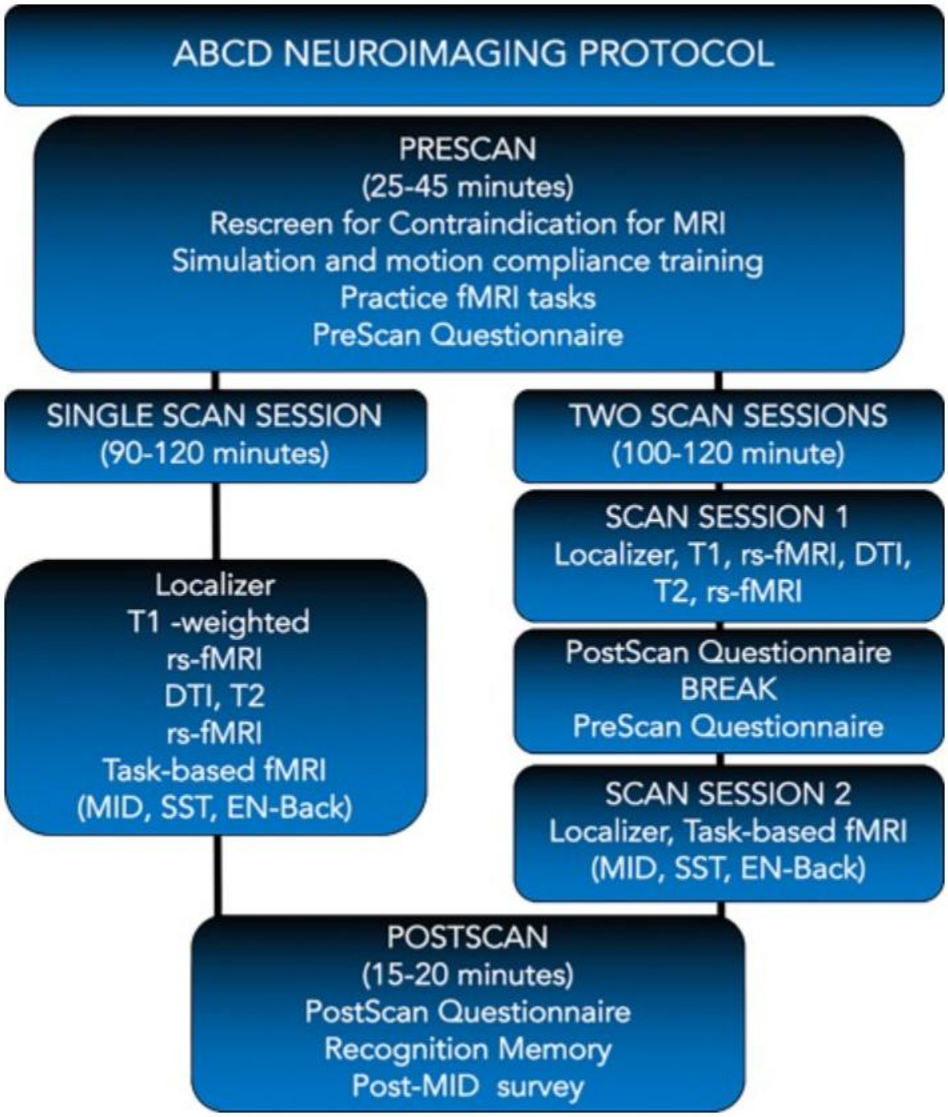

Supplementary Figure 1. ABCD Study Neuroimaging Protocol Workflow Diagram. From "ABCD Neuroimaging Protocol," by Adolescent Brain Cognitive Development Study, 2025. Retrieved from https://abcdstudy.org

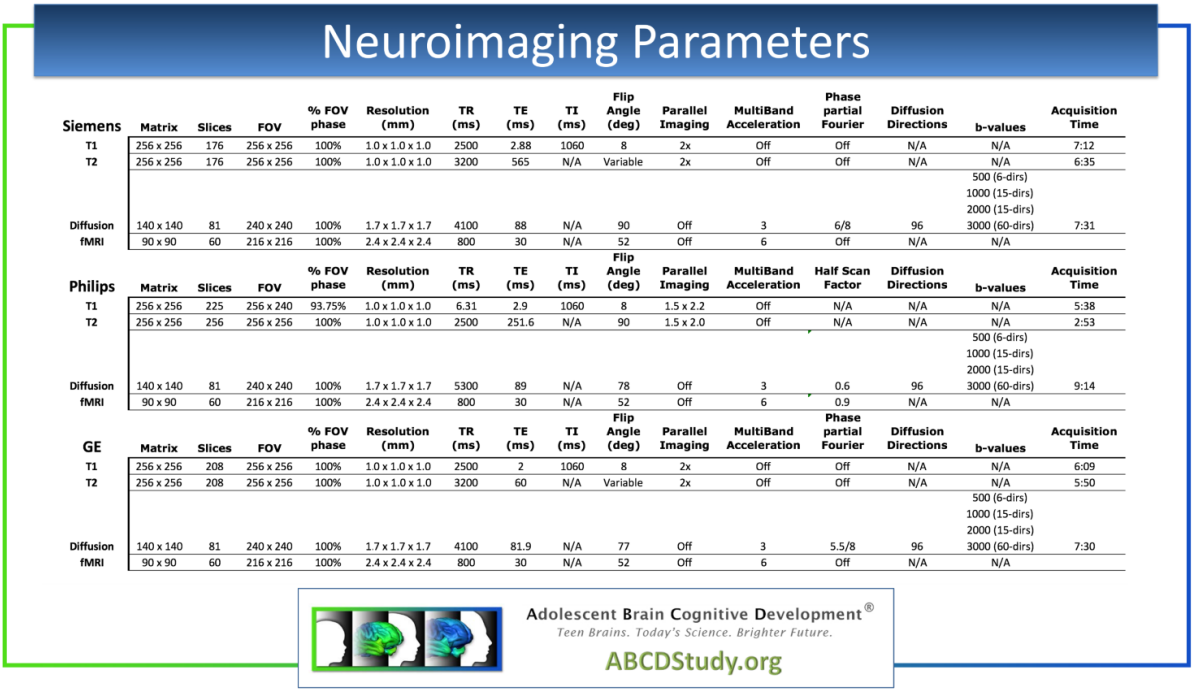

Supplementary Figure 2. Neuroimaging Parameters from the ABCD Study MRI Acquisition protocol describing how parameters vary by vendor. From "Neuroimaging Parameters," by Adolescent Brain Cognitive Development Study, 2025. Retrieved from https://abcdstudy.org

Repeated Measures Group Differences

Supplementary Notes 1

Cortical thickness. We examined CT differences between 15q11.2 BP1-BP2 CNV carriers and controls using both raw morphometric values and z-score standardized models. Analyses were conducted separately for deletion and duplication carriers across 68 cortical ROIs and mean cortical thickness. Deletion carriers showed widespread cortical thickening with a higher proportion of significant regions overall, while duplication carriers exhibited more subtle thinning effects. Group comparisons on raw values yielded 22 significant ROIs in the deletion group (9 FDR-corrected), and 13 in the duplication group (none when FDR-corrected). Group comparisons on Z-scores yielded 20 significant ROIs for deletion (7 FDR-corrected) and 16 for duplication (none FDR-corrected). Summary statistics are presented in **Table 2**, with group-level

significance and model sensitivity visualized in **Supplementary Table 3** and **Supplementary Figure 3**.

Supplementary Table 3

Summary of Group Differences in CT Across 15q11.2 BP1-BP2CNV Carriers.
Overview of significant regional effects observed in control vs. deletion and duplication comparisons, based on both raw morphometric measures and normative z-score–standardized data. Results include the number of significant ROIs (nominal and FDR-corrected).

Data Type	Comparison	Total ROIs	Sig ROIs	FDR Sig ROIs
raw	Control vs. Deletion	69	22	9
raw	Control vs. Duplication	69	13	0
z-score	Control vs. Deletion	69	20	7
z-score	Control vs. Duplication	69	16	0

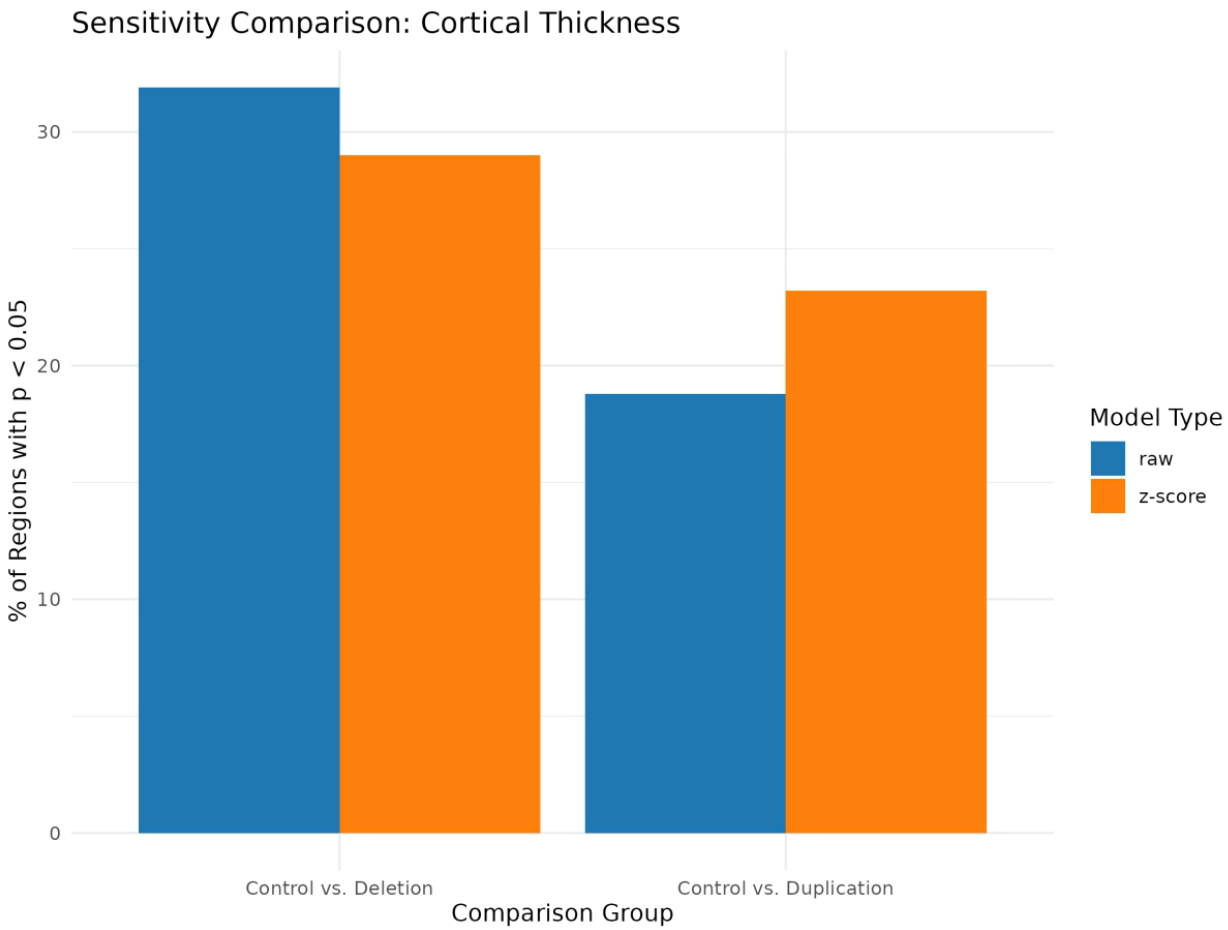

Supplementary Figure 3. *Proportion of Significant CT ROIs by CNV Group and Data Type.* Bar plot displaying the percentage of cortical ROIs with nominal significance ($p < 0.05$) across deletion and duplication comparisons. Raw morphometric values (blue) and z-score standardized models (orange) are shown separately.

Supplementary Notes 2

Subcortical and Cerebellar Volume. Subcortical and Cerebellar volume comparisons across 31 regions of interest revealed consistent and statistically significant deviations in both deletion and duplication carriers of the 15q11.2 BP1–BP2 CNV. Analyses were conducted using both raw

morphometric values and normative z-score standardized inputs to evaluate sensitivity across modeling strategies.

As summarized in **Supplementary Table 4** and visualized in **Supplementary Figure 4**, deletion carriers showed slightly improved detection of significant effects using z-score models (12 nominally significant ROIs, 8 FDR-corrected), relative to raw models (11 significant ROIs, 8 FDR-corrected). In duplication carriers, raw models identified seven significant ROIs (four FDR-corrected), while z-score models detected the same number of nominal effects but fewer survived FDR correction (three ROIs). Effect size estimates were highly consistent across methods, suggesting strong convergence of results. Nonetheless, z-score models demonstrated a marginal sensitivity advantage in deletion comparisons.

Supplementary Table 4

Summary of Group Differences in SV Across 15q11.2 BP1-BP2 CNV Carriers.
Overview of significant regional effects observed in control vs. deletion and duplication comparisons, based on both raw morphometric measures and normative z-score–standardized data. Results include the number of significant ROIs (nominal and FDR-corrected).

Data Type	Comparison	Total ROIs	Sig ROIs	FDR Sig ROIs
raw	Control vs. Deletion	31	11	8
raw	Control vs. Duplication	31	7	4
z-score	Control vs. Deletion	31	12	8
z-score	Control vs. Duplication	31	7	3

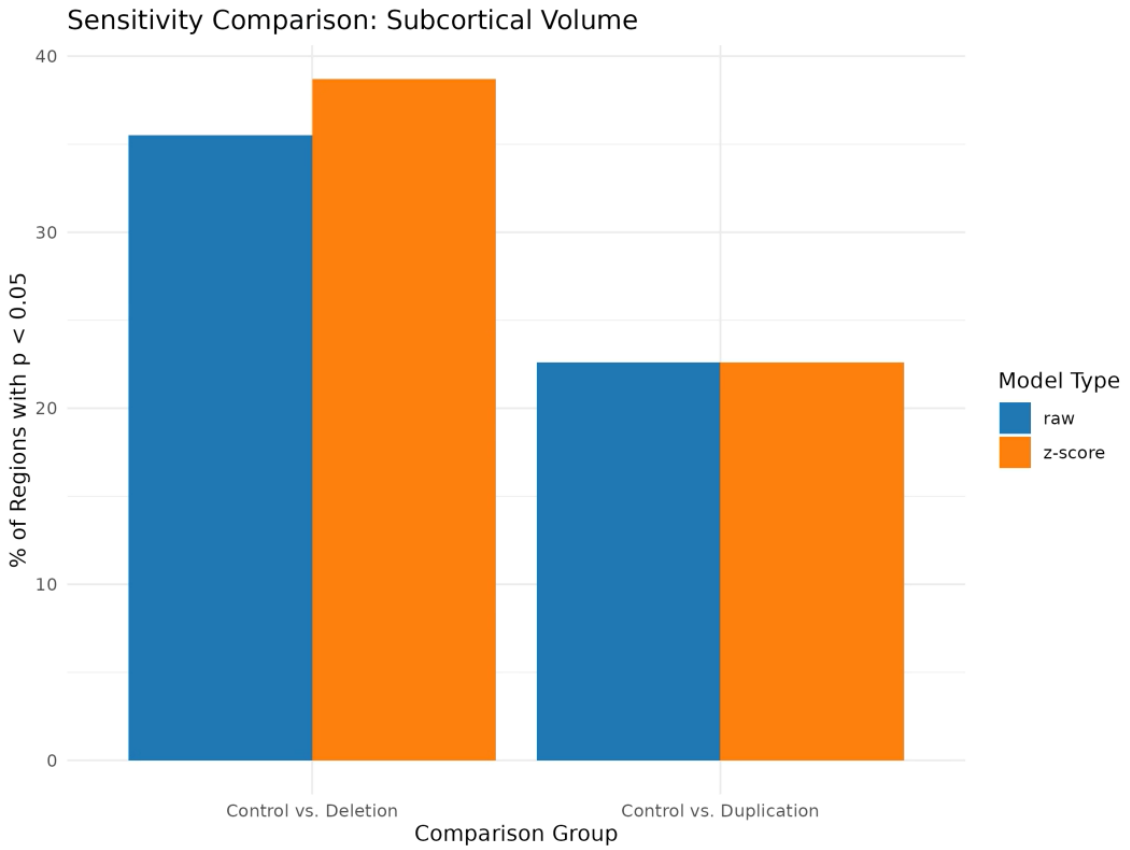

.

Supplementary Figure 4. *Proportion of Nominally Significant SV ROIs by CNV Group and Data Type.* Bar plot displaying the percentage of SV ROIs with nominal significance ($p < 0.05$) across deletion and duplication comparisons. Raw morphometric values (blue) and z-score standardized models (orange) are shown separately. Z-score models slightly outperformed raw models for deletions; no difference was observed in duplication models.

Supplementary Notes 3

Surface Area. Group comparisons of SA across 68 cortical regions revealed widespread and statistically significant alterations in both 15q11.2 BP1-BP2 deletion and duplication carriers. These effects were observed using both raw morphometric values and normative z-score standardized data.

As shown in **Supplementary Table 5** and **Supplementary Figure 5**, raw and z-score models identified comparable numbers of nominally significant ROIs for each CNV group. Among deletion carriers, z-score models identified 17 significant ROIs (8 FDR-corrected), slightly more than raw models (16 total; 7 FDR-corrected). In duplication carriers, raw and z-score models

yielded 26 and 25 significant ROIs, respectively, with nearly identical rates of FDR correction (16 and 15 ROIs). Mean and median effect sizes were also comparable across modeling strategies, showing high agreement between raw and z-score models in estimated effect sizes. Together, these findings indicate robust surface area alterations in CNV carriers, with largely consistent results across analytic approaches. However, the slightly greater sensitivity of z-score models in deletion comparisons suggests potential advantages in certain contexts.

Supplementary Table 5

Summary of Group Differences in SA Across 15q11.2 BP1-BP2 CNV Carriers.
Overview of significant regional effects observed in control vs. deletion and duplication comparisons, based on both raw morphometric measures and normative z-score–standardized data.

Data Type	Comparison	Total ROIs	Sig ROIs	FDR Sig ROIs
raw	Control vs. Deletion	68	16	7
raw	Control vs. Duplication	68	26	16
z-score	Control vs. Deletion	68	17	8
z-score	Control vs. Duplication	68	25	15

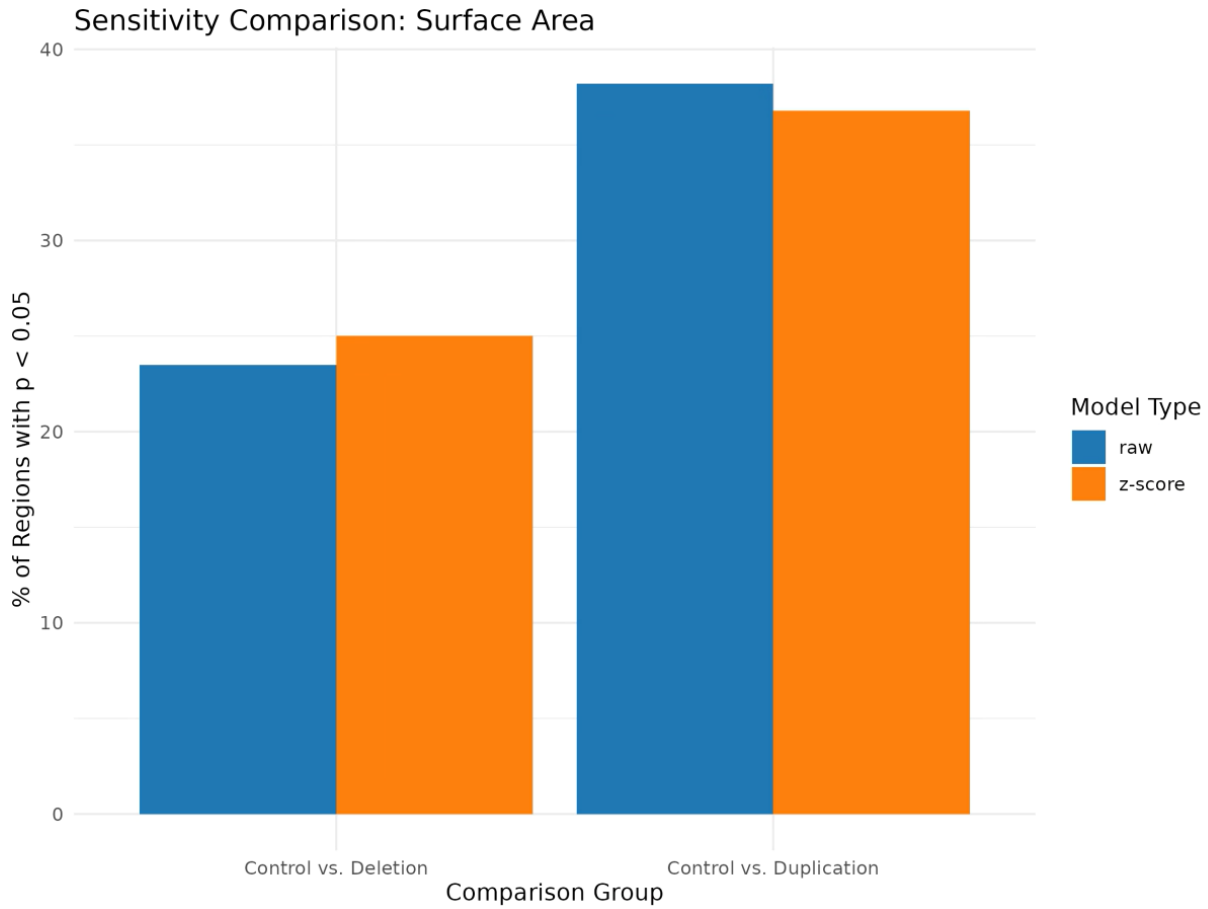

Supplementary Figure 5. Proportion of Nominally Significant Surface Area ROIs by CNV Group and Data Type. Bar plot displaying the percentage of SA ROIs with nominal significance ($p < 0.05$) across deletion and duplication comparisons. Raw morphometric values (blue) and z-score standardized models (orange) are shown separately. Z-scores yielded slightly higher sensitivity for deletions, while raw models marginally outperformed for duplications.

Developmental Trajectories

Supplementary Table 6

Summary of Nominally Significant CNV Group × Age Interaction Effects for CT.
Table showing a summary of linear mixed-effects model results of all regions with nominally significant ($p < .05$) CNV Group × Age interactions for CT. For each ROI the table displays effect estimates, standard errors, test statistics, raw and adjusted p-values.

ROI	Group	Estimate	SE	t	p.value	p_adjusted
Left Caudal Middle Frontal	Deletion	-0.081	0.03	-2.39	0.017	0.341
Left Cuneus	Duplication	-0.054	0.03	-2.12	0.034	0.408
Left Lateral Occipital	Duplication	-0.082	0.03	-2.82	0.005	0.166
Left Lateral Orbitofrontal	Deletion	0.087	0.04	2.39	0.017	0.341
Left Lingual	Duplication	-0.062	0.03	-2.38	0.017	0.341
Left Medial Orbitofrontal	Duplication	0.081	0.04	2.03	0.042	0.416
Left Pericalcarine	Duplication	-0.092	0.03	-3.05	0.002	0.138
Right Caudal Middle Frontal	Deletion	-0.079	0.03	-2.26	0.024	0.364
Right Insula	Deletion	-0.092	0.04	-2.09	0.036	0.408
Right Lateral Occipital	Duplication	-0.085	0.03	-2.97	0.003	0.138
Right Posterior Cingulate	Deletion	-0.084	0.03	-3.13	0.002	0.138
Right Precentral	Deletion	-0.077	0.04	-2.07	0.038	0.408
Right Superior Frontal	Duplication	0.073	0.03	2.27	0.023	0.364
Right Superior Parietal	Deletion	-0.071	0.03	-2.09	0.036	0.408

Supplementary Table 7

Summary of Nominally Significant CNV Group × Age Interaction Effects for SA.

Summary of linear mixed-effects model results showing all regions with nominally significant ($p < .05$) CNV Group × Age interactions for surface area. For each ROI the table displays effect estimates, standard errors, test statistics, raw and adjusted p-values.

ROI	Group	Estimate	SE	t	p.value	p_adjusted
Left Insula	Duplication	0.063	0.028	2.26	0.024	0.981
Left Lateral Orbitofrontal	Deletion	-0.038	0.019	−1,99	0.046	0.981
Left Superior Frontal	Duplication	-0.027	0.013	−2,02	0.043	0.981

Supplementary Table 8

Summary of Nominally Significant CNV Group × Age Interaction Effects for SV.

Summary of linear mixed-effects model results showing all regions with nominally significant ($p < .05$) CNV Group × Age interactions for SV. For each ROI the table displays effect estimates, standard errors, test statistics, raw and adjusted p-values.

ROI	Group	Estimate	SE	t	p.value	p_adjusted
CSF	Deletion	0.051	0.019	2.627	0.009	0.181
Left.Caudate	Duplication	-0.027	0.013	-2.034	0.042	0.375
Left.Hippocampus	Deletion	0.039	0.019	2.031	0.042	0.375
Left.Lateral.Ventricle	Deletion	0.022	0.010	2.329	0.020	0.257
Right.Lateral.Ventricle	Deletion	0.032	0.010	3.269	0.001	0.067
Right.Pallidum	Duplication	-0.087	0.033	-2.622	0.009	0.181
X4th.Ventricle	Deletion	0.031	0.014	2.313	0.021	0.257

Table Output for Repeated Measures Group Comparison Analysis

Supplementary Table 9

All Group Difference Effects in Cortical Thickness for all 15q11.2 CNV Carriers and Control Across Raw and Z-Score Models.

Sorted by FDR-corrected significance, and then by nominal significance. This table summarises all the mixed-effects model comparing cortical thickness between 15q11.2 BP1-BP2 CNV carriers and controls in all ROIs. For each mixed-effects model, the following is included: Group

(deletion/duplication), effect (Estimate), standard error (SE), degrees of freedom (df), test statistic (t), nominal significance (p.value), lowest confidence interval (ci_low), highest confidence interval (ci_high), data input to model (raw/z-score), region of interest (ROI), number of subjects (n_subjects), significance value after FDR correction (p_adjusted), nominal significance status (Yes/No), FDR corrected significance status (Yes/No).

SE	df	t	p.value	ci_low	ci_high	data_type	ROI	n_subjects	p_adjusted	Signifi
0.025	22004	4.458	0.000	0.061	0.158	raw	lh_parahippocampal	22028	0.000	Yes
0.102	22026	4.202	0.000	0.230	0.631	z-score	lh_parahippocampal	22028	0.001	Yes
0.013	22004	3.811	0.000	0.024	0.074	raw	lh_parstriangularis	22028	0.002	Yes
0.099	22026	3.702	0.000	0.173	0.561	z-score	lh_parstriangularis	22028	0.005	Yes
0.013	22004	2.757	0.006	0.010	0.062	raw	lh_postcentral	22028	0.045	Yes
0.011	22004	2.849	0.004	0.009	0.051	raw	lh_rostralmiddlefrontal	22028	0.038	Yes
0.014	22004	3.381	0.001	0.020	0.074	raw	lh_insula	22028	0.010	Yes
0.101	22026	3.179	0.001	0.123	0.519	z-score	lh_insula	22028	0.020	Yes
0.013	22004	2.943	0.003	0.013	0.066	raw	rh_cuneus	22028	0.032	Yes
0.098	22026	2.912	0.004	0.093	0.478	z-score	rh_cuneus	22028	0.041	Yes
0.021	22004	2.978	0.003	0.021	0.101	raw	rh_parahippocampal	22028	0.032	Yes
0.101	22026	2.835	0.005	0.089	0.485	z-score	rh_parahippocampal	22028	0.045	Yes
0.013	22004	5.104	0.000	0.039	0.089	raw	rh_parstriangularis	22028	0.000	Yes
0.098	22026	4.994	0.000	0.297	0.681	z-score	rh_parstriangularis	22028	0.000	Yes
0.011	22004	3.835	0.000	0.020	0.062	raw	rh_rostralmiddlefrontal	22028	0.002	Yes
0.095	22026	3.408	0.001	0.137	0.508	z-score	rh_rostralmiddlefrontal	22028	0.011	Yes
0.019	22004	-2.044	0.041	-0.077	-0.002	raw	lh_caudalanteriorcingulate	22028	0.141	Yes
0.102	22026	-2.056	0.040	-0.410	-0.010	z-score	lh_caudalanteriorcingulate	22028	0.145	Yes
0.095	22040	-2.042	0.041	-0.380	-0.008	z-score	lh_caudalanteriorcingulate	22042	0.203	Yes
0.025	22018	-3.358	0.001	-0.134	-0.035	raw	lh_entorhinal	22042	0.054	Yes

0.098	22040	-3.188	0.001	-0.503	-0.120	z-score	lh_entorhinal	22042	0.080	Yes
0.010	22018	-2.288	0.022	-0.044	-0.003	raw	lh_fusiform	22042	0.168	Yes
0.094	22040	-2.381	0.017	-0.408	-0.040	z-score	lh_fusiform	22042	0.154	Yes
0.011	22004	2.416	0.016	0.005	0.048	raw	lh_inferiorparietal	22028	0.065	Yes
0.096	22026	1.984	0.047	0.002	0.379	z-score	lh_inferiorparietal	22028	0.163	Yes
0.013	22018	-2.231	0.026	-0.056	-0.004	raw	lh_isthmuscingulate	22042	0.168	Yes
0.095	22040	-2.355	0.019	-0.410	-0.038	z-score	lh_isthmuscingulate	22042	0.154	Yes
0.091	22040	-1.989	0.047	-0.360	-0.003	z-score	lh_lateralorbitofrontal	22042	0.208	Yes
0.015	22004	2.618	0.009	0.010	0.067	raw	lh_middletemporal	22028	0.056	Yes
0.103	22026	2.168	0.030	0.022	0.427	z-score	lh_middletemporal	22028	0.119	Yes
0.012	22018	-2.608	0.009	-0.055	-0.008	raw	lh_parstriangularis	22042	0.126	Yes
0.092	22040	-2.671	0.008	-0.427	-0.066	z-score	lh_parstriangularis	22042	0.104	Yes
0.100	22026	2.559	0.011	0.060	0.454	z-score	lh_postcentral	22028	0.072	Yes
0.012	22018	-2.256	0.024	-0.051	-0.004	raw	lh_postcentral	22042	0.168	Yes
0.093	22040	-2.218	0.027	-0.390	-0.024	z-score	lh_postcentral	22042	0.167	Yes
0.010	22018	-2.243	0.025	-0.041	-0.003	raw	lh_precuneus	22042	0.168	Yes
0.087	22040	-2.325	0.020	-0.373	-0.032	z-score	lh_precuneus	22042	0.154	Yes
0.017	22004	2.457	0.014	0.008	0.075	raw	lh_rostralanteriorcingulate	22028	0.065	Yes
0.100	22026	2.411	0.016	0.045	0.438	z-score	lh_rostralanteriorcingulate	22028	0.080	Yes

0.097	22026	2.415	0.016	0.044	0.423	z-score	lh_rostralmiddlefrontal	22028	0.080	Yes
0.010	22018	-2.885	0.004	-0.048	-0.009	raw	lh_rostralmiddlefrontal	22042	0.090	Yes
0.090	22040	-2.836	0.005	-0.432	-0.079	z-score	lh_rostralmiddlefrontal	22042	0.104	Yes
0.014	22004	-2.488	0.013	-0.062	-0.007	raw	lh_superiortemporal	22028	0.065	Yes
0.104	22026	-2.709	0.007	-0.484	-0.078	z-score	lh_superiortemporal	22028	0.058	Yes
0.015	22018	-3.052	0.002	-0.076	-0.016	raw	rh_bankssts	22042	0.079	Yes
0.095	22040	-3.047	0.002	-0.474	-0.103	z-score	rh_bankssts	22042	0.080	Yes
0.012	22018	-2.722	0.006	-0.056	-0.009	raw	rh_caudalmiddlefrontal	22042	0.112	Yes
0.095	22040	-2.737	0.006	-0.448	-0.074	z-score	rh_caudalmiddlefrontal	22042	0.104	Yes
0.029	22004	2.410	0.016	0.013	0.129	raw	rh_entorhinal	22028	0.065	Yes
0.105	22026	2.405	0.016	0.047	0.457	z-score	rh_entorhinal	22028	0.080	Yes
0.010	22018	-2.283	0.022	-0.044	-0.003	raw	rh_fusiform	22042	0.168	Yes
0.094	22040	-2.391	0.017	-0.411	-0.041	z-score	rh_fusiform	22042	0.154	Yes
0.012	22004	2.654	0.008	0.008	0.056	raw	rh_lateralorbitofrontal	22028	0.055	Yes
0.099	22026	2.648	0.008	0.068	0.455	z-score	rh_lateralorbitofrontal	22028	0.062	Yes
0.014	22004	2.227	0.026	0.004	0.058	raw	rh_middletemporal	22028	0.094	Yes
0.019	22018	-2.008	0.045	-0.076	-0.001	raw	rh_parahippocampal	22042	0.237	Yes
0.094	22040	-2.143	0.032	-0.387	-0.017	z-score	rh_parahippocampal	22042	0.173	Yes

0.093	22040	-1.975	0.048	-0.364	-0.001	z-score	rh_paracentral	22042	0.208	Yes
0.013	22004	2.382	0.017	0.005	0.055	raw	rh_parsopercularis	22028	0.066	Yes
0.103	22026	2.370	0.018	0.042	0.444	z-score	rh_parsopercularis	22028	0.082	Yes
0.012	22018	-2.215	0.027	-0.049	-0.003	raw	rh_parsopercularis	22042	0.168	Yes
0.095	22040	-2.225	0.026	-0.400	-0.025	z-score	rh_parsopercularis	22042	0.167	Yes
0.017	22004	2.446	0.014	0.008	0.073	raw	rh_parsorbitalis	22028	0.065	Yes
0.099	22026	2.157	0.031	0.019	0.407	z-score	rh_parsorbitalis	22028	0.119	Yes
0.016	22018	-2.169	0.030	-0.064	-0.003	raw	rh_parsorbitalis	22042	0.173	Yes
0.092	22040	-2.137	0.033	-0.378	-0.016	z-score	rh_parsorbitalis	22042	0.173	Yes
0.010	22004	1.968	0.049	0.000	0.041	raw	rh_precuneus	22028	0.154	Yes
0.014	22004	-1.986	0.047	-0.054	0.000	raw	rh_superiortemporal	22028	0.154	Yes
0.103	22026	-2.165	0.030	-0.426	-0.021	z-score	rh_superiortemporal	22028	0.119	Yes
0.024	22004	2.541	0.011	0.014	0.108	raw	rh_frontalpole	22028	0.064	Yes
0.101	22026	2.431	0.015	0.048	0.446	z-score	rh_frontalpole	22028	0.080	Yes
0.015	22004	-0.569	0.570	-0.039	0.022	raw	lh_bankssts	22028	0.749	No
0.101	22026	-0.835	0.404	-0.282	0.113	z-score	lh_bankssts	22028	0.598	No
0.014	22018	-1.612	0.107	-0.052	0.005	raw	lh_bankssts	22042	0.321	No
0.094	22040	-1.515	0.130	-0.326	0.042	z-score	lh_bankssts	22042	0.373	No
0.018	22018	-1.926	0.054	-0.069	0.001	raw	lh_caudalanteriorcingulate	22042	0.250	No

0.013	22004	0.211	0.833	-0.022	0.028	raw	lh_caudalmiddlefrontal	22028	0.907	No
0.103	22026	-0.171	0.864	-0.220	0.184	z-score	lh_caudalmiddlefrontal	22028	0.961	No
0.012	22018	-1.275	0.202	-0.038	0.008	raw	lh_caudalmiddlefrontal	22042	0.446	No
0.096	22040	-1.455	0.146	-0.328	0.048	z-score	lh_caudalmiddlefrontal	22042	0.390	No
0.014	22004	0.278	0.781	-0.023	0.031	raw	lh_cuneus	22028	0.907	No
0.098	22026	0.241	0.809	-0.168	0.216	z-score	lh_cuneus	22028	0.931	No
0.013	22018	0.029	0.977	-0.025	0.025	raw	lh_cuneus	22042	0.991	No
0.091	22040	0.104	0.917	-0.169	0.188	z-score	lh_cuneus	22042	0.938	No
0.027	22004	1.537	0.124	-0.011	0.094	raw	lh_entorhinal	22028	0.277	No
0.105	22026	1.453	0.146	-0.053	0.359	z-score	lh_entorhinal	22028	0.319	No
0.011	22004	-0.038	0.970	-0.022	0.021	raw	lh_fusiform	22028	0.970	No
0.101	22026	-0.355	0.722	-0.234	0.162	z-score	lh_fusiform	22028	0.874	No
0.010	22018	-1.510	0.131	-0.035	0.005	raw	lh_inferiorparietal	22042	0.348	No
0.090	22040	-1.450	0.147	-0.305	0.046	z-score	lh_inferiorparietal	22042	0.390	No
0.013	22004	0.250	0.803	-0.022	0.029	raw	lh_inferiortemporal	22028	0.907	No
0.103	22026	-0.041	0.967	-0.206	0.198	z-score	lh_inferiortemporal	22028	0.986	No
0.012	22018	-0.982	0.326	-0.036	0.012	raw	lh_inferiortemporal	22042	0.563	No
0.096	22040	-1.159	0.246	-0.299	0.077	z-score	lh_inferiortemporal	22042	0.485	No
0.014	22004	-1.737	0.082	-0.053	0.003	raw	lh_isthmuscingulate	22028	0.221	No

0.102	22026	-1.613	0.107	-0.365	0.035	z-score	lh_isthmuscingulate	22028	0.273	No
0.011	22004	1.199	0.231	-0.009	0.035	raw	lh_lateraloccipital	22028	0.388	No
0.101	22026	1.055	0.291	-0.092	0.305	z-score	lh_lateraloccipital	22028	0.479	No
0.010	22018	-0.377	0.706	-0.024	0.017	raw	lh_lateraloccipital	22042	0.812	No
0.094	22040	-0.249	0.804	-0.208	0.161	z-score	lh_lateraloccipital	22042	0.866	No
0.012	22004	1.731	0.083	-0.003	0.043	raw	lh_lateralorbitofrontal	22028	0.221	No
0.098	22026	1.442	0.149	-0.051	0.333	z-score	lh_lateralorbitofrontal	22028	0.319	No
0.011	22018	-1.857	0.063	-0.042	0.001	raw	lh_lateralorbitofrontal	22042	0.258	No
0.012	22004	0.258	0.796	-0.021	0.027	raw	lh_lingual	22028	0.907	No
0.097	22026	0.288	0.773	-0.163	0.219	z-score	lh_lingual	22028	0.904	No
0.011	22018	-1.214	0.225	-0.036	0.009	raw	lh_lingual	22042	0.446	No
0.091	22040	-1.191	0.234	-0.285	0.070	z-score	lh_lingual	22042	0.480	No
0.013	22004	-0.561	0.575	-0.032	0.018	raw	lh_medialorbitofrontal	22028	0.749	No
0.098	22026	-0.625	0.532	-0.253	0.131	z-score	lh_medialorbitofrontal	22028	0.693	No
0.012	22018	-1.211	0.226	-0.038	0.009	raw	lh_medialorbitofrontal	22042	0.446	No
0.091	22040	-1.214	0.225	-0.289	0.068	z-score	lh_medialorbitofrontal	22042	0.480	No
0.014	22018	-1.211	0.226	-0.044	0.010	raw	lh_middletemporal	22042	0.446	No
0.096	22040	-1.115	0.265	-0.297	0.082	z-score	lh_middletemporal	22042	0.494	No
0.023	22018	0.439	0.660	-0.035	0.055	raw	lh_parahippocampal	22042	0.799	No

0.095	22040	0.413	0.679	-0.148	0.227	z-score	lh_parahippocampal	22042	0.806	No
0.014	22004	-0.564	0.573	-0.035	0.019	raw	lh_paracentral	22028	0.749	No
0.098	22026	-0.546	0.585	-0.246	0.139	z-score	lh_paracentral	22028	0.748	No
0.013	22018	-1.924	0.054	-0.050	0.000	raw	lh_paracentral	22042	0.250	No
0.091	22040	-1.950	0.051	-0.358	0.001	z-score	lh_paracentral	22042	0.208	No
0.012	22004	1.396	0.163	-0.007	0.041	raw	lh_parsopercularis	22028	0.312	No
0.102	22026	1.254	0.210	-0.072	0.329	z-score	lh_parsopercularis	22028	0.402	No
0.011	22018	-1.630	0.103	-0.041	0.004	raw	lh_parsopercularis	22042	0.321	No
0.095	22040	-1.795	0.073	-0.358	0.016	z-score	lh_parsopercularis	22042	0.259	No
0.017	22004	0.858	0.391	-0.019	0.048	raw	lh_parsorbitalis	22028	0.574	No
0.100	22026	0.674	0.500	-0.128	0.263	z-score	lh_parsorbitalis	22028	0.664	No
0.016	22018	-1.830	0.067	-0.060	0.002	raw	lh_parsorbitalis	22042	0.258	No
0.093	22040	-1.688	0.091	-0.338	0.025	z-score	lh_parsorbitalis	22042	0.287	No
0.014	22004	-1.145	0.252	-0.045	0.012	raw	lh_pericalcarine	22028	0.414	No
0.102	22026	-0.979	0.327	-0.299	0.100	z-score	lh_pericalcarine	22028	0.525	No
0.014	22018	-0.853	0.394	-0.038	0.015	raw	lh_pericalcarine	22042	0.623	No
0.095	22040	-0.677	0.499	-0.250	0.122	z-score	lh_pericalcarine	22042	0.675	No
0.013	22004	-0.670	0.503	-0.033	0.016	raw	lh_posteriorcingulate	22028	0.708	No

0.100	22026	-0.687	0.492	-0.266	0.128	z-score	lh_posteriorcingulate	22028	0.664	No
0.012	22018	-0.575	0.565	-0.030	0.016	raw	lh_posteriorcingulate	22042	0.730	No
0.093	22040	-0.796	0.426	-0.257	0.109	z-score	lh_posteriorcingulate	22042	0.626	No
0.013	22004	0.086	0.931	-0.024	0.026	raw	lh_precentral	22028	0.945	No
0.104	22026	0.124	0.901	-0.192	0.218	z-score	lh_precentral	22028	0.976	No
0.012	22018	-1.521	0.128	-0.041	0.005	raw	lh_precentral	22042	0.348	No
0.097	22040	-1.757	0.079	-0.361	0.020	z-score	lh_precentral	22042	0.259	No
0.010	22004	0.167	0.867	-0.019	0.022	raw	lh_precuneus	22028	0.907	No
0.093	22026	0.087	0.930	-0.175	0.191	z-score	lh_precuneus	22028	0.986	No
0.016	22018	-1.779	0.075	-0.059	0.003	raw	lh_rostralanteriorcingulate	22042	0.273	No
0.093	22040	-1.853	0.064	-0.356	0.010	z-score	lh_rostralanteriorcingulate	22042	0.245	No
0.012	22004	1.228	0.220	-0.009	0.038	raw	lh_superiorfrontal	22028	0.379	No
0.099	22026	1.062	0.288	-0.089	0.299	z-score	lh_superiorfrontal	22028	0.479	No
0.011	22018	-1.002	0.316	-0.033	0.011	raw	lh_superiorfrontal	22042	0.563	No
0.092	22040	-1.142	0.253	-0.285	0.075	z-score	lh_superiorfrontal	22042	0.485	No
0.011	22004	0.178	0.858	-0.019	0.023	raw	lh_superiorparietal	22028	0.907	No
0.096	22026	-0.062	0.950	-0.195	0.183	z-score	lh_superiorparietal	22028	0.986	No
0.010	22018	-1.250	0.211	-0.032	0.007	raw	lh_superiorparietal	22042	0.446	No
0.090	22040	-1.262	0.207	-0.288	0.063	z-score	lh_superiorparietal	22042	0.461	No

0.013	22018	-0.246	0.806	-0.029	0.022	raw	lh_superiortemporal	22042	0.870	No
0.097	22040	-0.337	0.736	-0.222	0.157	z-score	lh_superiortemporal	22042	0.806	No
0.013	22004	-0.682	0.495	-0.033	0.016	raw	lh_supramarginal	22028	0.708	No
0.100	22026	-1.192	0.233	-0.314	0.077	z-score	lh_supramarginal	22028	0.424	No
0.012	22018	-1.408	0.159	-0.039	0.006	raw	lh_supramarginal	22042	0.407	No
0.093	22040	-1.184	0.237	-0.292	0.072	z-score	lh_supramarginal	22042	0.480	No
0.025	22004	0.258	0.796	-0.042	0.054	raw	lh_frontalpole	22028	0.907	No
0.101	22026	-0.018	0.986	-0.200	0.197	z-score	lh_frontalpole	22028	0.986	No
0.023	22018	1.703	0.089	-0.006	0.084	raw	lh_frontalpole	22042	0.302	No
0.094	22040	1.566	0.117	-0.037	0.333	z-score	lh_frontalpole	22042	0.352	No
0.027	22004	0.505	0.614	-0.040	0.067	raw	lh_temporalpole	22028	0.784	No
0.105	22026	0.369	0.712	-0.167	0.245	z-score	lh_temporalpole	22028	0.874	No
0.025	22018	-0.968	0.333	-0.074	0.025	raw	lh_temporalpole	22042	0.563	No
0.098	22040	-0.837	0.403	-0.274	0.110	z-score	lh_temporalpole	22042	0.618	No
0.018	22004	1.238	0.216	-0.013	0.059	raw	lh_transversetemporal	22028	0.379	No
0.102	22026	1.143	0.253	-0.083	0.316	z-score	lh_transversetemporal	22028	0.448	No
0.017	22018	-0.590	0.555	-0.044	0.024	raw	lh_transversetemporal	22042	0.730	No
0.095	22040	-0.549	0.583	-0.238	0.134	z-score	lh_transversetemporal	22042	0.745	No
0.013	22018	-0.461	0.645	-0.031	0.019	raw	lh_insula	22042	0.795	No

0.094	22040	-0.433	0.665	-0.225	0.144	z-score	lh_insula	22042	0.806	No
0.016	22004	-1.598	0.110	-0.058	0.006	raw	rh_bankssts	22028	0.253	No
0.102	22026	-1.673	0.094	-0.369	0.029	z-score	rh_bankssts	22028	0.261	No
0.018	22004	-1.485	0.138	-0.062	0.009	raw	rh_caudalanteriorcingulate	22028	0.288	No
0.102	22026	-1.431	0.152	-0.346	0.054	z-score	rh_caudalanteriorcingulate	22028	0.319	No
0.017	22018	-0.210	0.834	-0.036	0.029	raw	rh_caudalanteriorcingulate	22042	0.885	No
0.095	22040	-0.426	0.670	-0.227	0.146	z-score	rh_caudalanteriorcingulate	22042	0.806	No
0.013	22004	0.868	0.386	-0.014	0.036	raw	rh_caudalmiddlefrontal	22028	0.574	No
0.102	22026	0.686	0.493	-0.130	0.271	z-score	rh_caudalmiddlefrontal	22028	0.664	No
0.012	22018	-0.566	0.571	-0.031	0.017	raw	rh_cuneus	22042	0.730	No
0.091	22040	-0.470	0.638	-0.222	0.136	z-score	rh_cuneus	22042	0.801	No
0.027	22018	-0.831	0.406	-0.077	0.031	raw	rh_entorhinal	22042	0.623	No
0.098	22040	-0.773	0.440	-0.267	0.116	z-score	rh_entorhinal	22042	0.632	No
0.011	22004	-0.613	0.540	-0.029	0.015	raw	rh_fusiform	22028	0.745	No
0.101	22026	-0.806	0.420	-0.280	0.117	z-score	rh_fusiform	22028	0.604	No
0.011	22004	0.116	0.908	-0.020	0.023	raw	rh_inferiorparietal	22028	0.935	No
0.097	22026	-0.301	0.763	-0.220	0.161	z-score	rh_inferiorparietal	22028	0.904	No

0.010	22018	0.162	0.872	-0.018	0.021	raw	rh_inferiorparietal	22042	0.911	No
0.091	22040	0.348	0.728	-0.146	0.209	z-score	rh_inferiorparietal	22042	0.806	No
0.013	22004	-0.170	0.865	-0.028	0.023	raw	rh_inferiortemporal	22028	0.907	No
0.103	22026	-0.434	0.664	-0.247	0.157	z-score	rh_inferiortemporal	22028	0.833	No
0.012	22018	0.775	0.438	-0.014	0.033	raw	rh_inferiortemporal	22042	0.644	No
0.096	22040	0.736	0.461	-0.118	0.259	z-score	rh_inferiortemporal	22042	0.646	No
0.015	22004	-1.063	0.288	-0.045	0.013	raw	rh_isthmuscingulate	22028	0.462	No
0.102	22026	-0.828	0.407	-0.284	0.115	z-score	rh_isthmuscingulate	22028	0.598	No
0.014	22018	0.080	0.936	-0.026	0.028	raw	rh_isthmuscingulate	22042	0.964	No
0.095	22040	0.019	0.985	-0.184	0.188	z-score	rh_isthmuscingulate	22042	0.985	No
0.012	22004	0.864	0.387	-0.013	0.033	raw	rh_lateraloccipital	22028	0.574	No
0.102	22026	0.762	0.446	-0.122	0.276	z-score	rh_lateraloccipital	22028	0.629	No
0.011	22018	-0.707	0.479	-0.029	0.014	raw	rh_lateraloccipital	22042	0.663	No
0.095	22040	-0.625	0.532	-0.244	0.126	z-score	rh_lateraloccipital	22042	0.692	No
0.011	22018	-1.345	0.179	-0.037	0.007	raw	rh_lateralorbitofrontal	22042	0.440	No
0.092	22040	-1.414	0.157	-0.310	0.050	z-score	rh_lateralorbitofrontal	22042	0.402	No
0.012	22004	-0.209	0.834	-0.026	0.021	raw	rh_lingual	22028	0.907	No
0.096	22026	-0.026	0.980	-0.192	0.187	z-score	rh_lingual	22028	0.986	No
0.011	22018	-1.147	0.252	-0.035	0.009	raw	rh_lingual	22042	0.482	No

0.090	22040	-1.078	0.281	-0.273	0.079	z-score	rh_lingual	22042	0.510	No
0.012	22004	1.699	0.089	-0.003	0.044	raw	rh_medialorbitofrontal	22028	0.228	No
0.096	22026	1.720	0.085	-0.023	0.352	z-score	rh_medialorbitofrontal	22028	0.246	No
0.011	22018	-1.299	0.194	-0.037	0.007	raw	rh_medialorbitofrontal	22042	0.446	No
0.089	22040	-1.394	0.163	-0.298	0.050	z-score	rh_medialorbitofrontal	22042	0.403	No
0.102	22026	1.796	0.073	-0.017	0.385	z-score	rh_middletemporal	22028	0.228	No
0.013	22018	-0.008	0.993	-0.026	0.025	raw	rh_middletemporal	22042	0.993	No
0.095	22040	0.095	0.925	-0.178	0.196	z-score	rh_middletemporal	22042	0.938	No
0.013	22004	1.426	0.154	-0.007	0.045	raw	rh_paracentral	22028	0.304	No
0.099	22026	1.233	0.218	-0.072	0.317	z-score	rh_paracentral	22028	0.406	No
0.012	22018	-1.832	0.067	-0.047	0.002	raw	rh_paracentral	22042	0.258	No
0.012	22018	-0.836	0.403	-0.033	0.013	raw	rh_parstriangularis	22042	0.623	No
0.091	22040	-0.847	0.397	-0.256	0.102	z-score	rh_parstriangularis	22042	0.618	No
0.015	22004	1.341	0.180	-0.009	0.049	raw	rh_pericalcarine	22028	0.335	No
0.102	22026	1.513	0.130	-0.046	0.355	z-score	rh_pericalcarine	22028	0.310	No
0.014	22018	-0.299	0.765	-0.031	0.023	raw	rh_pericalcarine	22042	0.851	No
0.095	22040	-0.225	0.822	-0.208	0.165	z-score	rh_pericalcarine	22042	0.872	No
0.014	22004	0.206	0.837	-0.024	0.030	raw	rh_postcentral	22028	0.907	No
0.100	22026	0.189	0.850	-0.178	0.216	z-score	rh_postcentral	22028	0.961	No
0.013	22018	-0.965	0.335	-0.038	0.013	raw	rh_postcentral	22042	0.563	No

0.093	22040	-1.054	0.292	-0.281	0.085	z-score	rh_postcentral	22042	0.516	No
0.012	22004	1.617	0.106	-0.004	0.042	raw	rh_posteriorcingulate	22028	0.252	No
0.100	22026	1.581	0.114	-0.038	0.355	z-score	rh_posteriorcingulate	22028	0.281	No
0.011	22018	-0.706	0.480	-0.029	0.014	raw	rh_posteriorcingulate	22042	0.663	No
0.093	22040	-0.897	0.370	-0.267	0.099	z-score	rh_posteriorcingulate	22042	0.608	No
0.014	22004	1.822	0.068	-0.002	0.052	raw	rh_precentral	22028	0.197	No
0.104	22026	1.743	0.081	-0.023	0.386	z-score	rh_precentral	22028	0.244	No
0.013	22018	-0.543	0.587	-0.032	0.018	raw	rh_precentral	22042	0.737	No
0.097	22040	-0.634	0.526	-0.252	0.129	z-score	rh_precentral	22042	0.692	No
0.093	22026	1.826	0.068	-0.012	0.353	z-score	rh_precuneus	22028	0.223	No
0.010	22018	-0.792	0.428	-0.027	0.011	raw	rh_precuneus	22042	0.643	No
0.087	22040	-0.900	0.368	-0.249	0.092	z-score	rh_precuneus	22042	0.608	No
0.018	22004	-1.425	0.154	-0.062	0.010	raw	rh_rostralanteriorcingulate	22028	0.304	No
0.102	22026	-1.454	0.146	-0.348	0.052	z-score	rh_rostralanteriorcingulate	22028	0.319	No
0.017	22018	-0.421	0.674	-0.040	0.026	raw	rh_rostralanteriorcingulate	22042	0.802	No
0.095	22040	-0.341	0.733	-0.218	0.154	z-score	rh_rostralanteriorcingulate	22042	0.806	No
0.010	22018	-1.557	0.119	-0.035	0.004	raw	rh_rostralmiddlefrontal	22042	0.343	No
0.088	22040	-1.326	0.185	-0.290	0.056	z-score	rh_rostralmiddlefrontal	22042	0.440	No

0.012	22004	1.497	0.135	-0.005	0.040	raw	rh_superiorfrontal	22028	0.288	No
0.098	22026	1.275	0.202	-0.067	0.318	z-score	rh_superiorfrontal	22028	0.399	No
0.011	22018	-0.599	0.549	-0.028	0.015	raw	rh_superiorfrontal	22042	0.730	No
0.092	22040	-0.725	0.468	-0.246	0.113	z-score	rh_superiorfrontal	22042	0.646	No
0.011	22004	1.300	0.194	-0.007	0.035	raw	rh_superiorparietal	22028	0.352	No
0.096	22026	1.062	0.288	-0.087	0.291	z-score	rh_superiorparietal	22028	0.479	No
0.010	22018	-0.317	0.751	-0.023	0.017	raw	rh_superiorparietal	22042	0.849	No
0.090	22040	-0.342	0.732	-0.207	0.145	z-score	rh_superiorparietal	22042	0.806	No
0.013	22018	-1.213	0.225	-0.040	0.009	raw	rh_superiortemporal	22042	0.446	No
0.096	22040	-1.282	0.200	-0.312	0.065	z-score	rh_superiortemporal	22042	0.459	No
0.012	22004	-0.489	0.625	-0.030	0.018	raw	rh_supramarginal	22028	0.784	No
0.101	22026	-0.898	0.369	-0.288	0.107	z-score	rh_supramarginal	22028	0.576	No
0.012	22018	-0.245	0.807	-0.025	0.020	raw	rh_supramarginal	22042	0.870	No
0.094	22040	-0.178	0.859	-0.201	0.167	z-score	rh_supramarginal	22042	0.898	No
0.022	22018	0.831	0.406	-0.025	0.062	raw	rh_frontalpole	22042	0.623	No
0.094	22040	0.802	0.423	-0.109	0.261	z-score	rh_frontalpole	22042	0.626	No
0.028	22004	0.991	0.322	-0.027	0.082	raw	rh_temporalpole	22028	0.504	No
0.105	22026	0.886	0.375	-0.113	0.299	z-score	rh_temporalpole	22028	0.576	No
0.026	22018	-0.395	0.693	-0.061	0.040	raw	rh_temporalpole	22042	0.811	No

0.098	22040	-0.358	0.720	-0.227	0.157	z-score	rh_temporalpole	22042	0.806	No
0.019	22004	0.245	0.807	-0.032	0.041	raw	rh_transversetemporal	22028	0.907	No
0.102	22026	0.120	0.905	-0.188	0.213	z-score	rh_transversetemporal	22028	0.976	No
0.017	22018	-1.099	0.272	-0.053	0.015	raw	rh_transversetemporal	22042	0.506	No
0.095	22040	-0.960	0.337	-0.278	0.095	z-score	rh_transversetemporal	22042	0.581	No
0.014	22004	1.925	0.054	0.000	0.056	raw	rh_insula	22028	0.163	No
0.102	22026	1.629	0.103	-0.034	0.367	z-score	rh_insula	22028	0.273	No
0.013	22018	-0.753	0.452	-0.036	0.016	raw	rh_insula	22042	0.649	No
0.095	22040	-0.851	0.395	-0.268	0.106	z-score	rh_insula	22042	0.618	No
0.008	22004	1.659	0.097	-0.002	0.029	raw	Mean	22028	0.240	No
0.096	22026	1.344	0.179	-0.059	0.316	z-score	Mean	22028	0.363	No
0.007	22018	-1.685	0.092	-0.027	0.002	raw	Mean	22042	0.302	No
0.089	22040	-1.767	0.077	-0.332	0.017	z-score	Mean	22042	0.259	No

Supplementary Table 10

All Group Difference Effects in Cortical Surface Area for all 15q11.2 CNV Carriers and Control Across Raw and Z-Score Models.

Sorted by FDR-corrected significance, and then by nominal significance. This table summarises all the mixed-effects model comparing cortical surface area between 15q11.2 BP1-BP2 CNV carriers and controls in all ROIs. For each mixed-effects model, the following is included: Group (deletion/duplication), effect (Estimate), standard error (SE), degrees of freedom (df), test

statistic (t), nominal significance (p.value), lowest confidence interval (ci_low), highest confidence interval (ci_high), data input to model (raw/z-score), region of interest (ROI), number of subjects (n_subjects), significance value after FDR correction (p_adjusted), nominal significance status (Yes/No), FDR corrected significance status (Yes/No).

SE	df	t	p.value	ci_low	ci_high	data_type	ROI	n_subjects	p_adjusted	Sign
20.236	22004	-2.900	0.004	-98.355	-19.027	raw	lh_bankssts	22028	0.036	Y
0.098	22026	-2.941	0.003	-0.482	-0.096	z-score	lh_bankssts	22028	0.032	Y
16.489	22004	-2.968	0.003	-81.258	-16.620	raw	lh_caudalanteriorcingulate	22028	0.034	Y
0.102	22026	-2.880	0.004	-0.494	-0.094	z-score	lh_caudalanteriorcingulate	22028	0.034	Y
15.365	22018	-4.150	0.000	-93.882	-33.649	raw	lh_caudalanteriorcingulate	22042	0.001	Y
0.095	22040	-4.222	0.000	-0.587	-0.215	z-score	lh_caudalanteriorcingulate	22042	0.001	Y
9.302	22018	4.371	0.000	22.422	58.888	raw	lh_entorhinal	22042	0.001	Y
0.093	22040	4.397	0.000	0.226	0.590	z-score	lh_entorhinal	22042	0.001	Y
39.580	22004	-3.195	0.001	-204.016	-48.858	raw	lh_fusiform	22028	0.020	Y
0.088	22026	-3.244	0.001	-0.460	-0.114	z-score	lh_fusiform	22028	0.017	Y
74.463	22004	-3.423	0.001	-400.807	-108.902	raw	lh_inferiorparietal	22028	0.014	Y
0.096	22026	-3.321	0.001	-0.505	-0.130	z-score	lh_inferiorparietal	22028	0.017	Y
69.367	22018	-2.612	0.009	-317.165	-45.237	raw	lh_inferiorparietal	22042	0.041	Y
43.292	22018	-2.628	0.009	-198.635	-28.922	raw	lh_middletemporal	22042	0.041	Y

0.085	22040	-2.596	0.009	-0.386	-0.054	z-score	lh_middletemporal	22042	0.046	Y
9.076	22004	-3.175	0.001	-46.607	-11.029	raw	lh_parahippocampal	22028	0.020	Y
0.098	22026	-3.219	0.001	-0.509	-0.124	z-score	lh_parahippocampal	22028	0.017	Y
15.795	22018	-3.639	0.000	-88.434	-26.514	raw	lh_rostralanteriorcingulate	22042	0.006	Y
0.088	22040	-3.616	0.000	-0.490	-0.146	z-score	lh_rostralanteriorcingulate	22042	0.007	Y
75.935	22018	-2.831	0.005	-363.833	-66.158	raw	lh_rostralmiddlefrontal	22042	0.029	Y
0.083	22040	-2.724	0.006	-0.387	-0.063	z-score	lh_rostralmiddlefrontal	22042	0.040	Y
49.535	22018	-2.568	0.010	-224.304	-30.118	raw	lh_superiortemporal	22042	0.043	Y
0.083	22040	-2.610	0.009	-0.380	-0.054	z-score	lh_superiortemporal	22042	0.046	Y
0.092	22026	-3.012	0.003	-0.457	-0.097	z-score	lh_supramarginal	22028	0.029	Y
24.792	22018	-3.494	0.000	-135.207	-38.019	raw	lh_insula	22042	0.008	Y
0.084	22040	-3.442	0.001	-0.455	-0.125	z-score	lh_insula	22042	0.010	Y
14.839	22018	-3.112	0.002	-75.258	-17.087	raw	rh_bankssts	22042	0.016	Y
0.091	22040	-3.093	0.002	-0.462	-0.104	z-score	rh_bankssts	22042	0.019	Y
87.118	22004	-3.823	0.000	-503.832	-162.318	raw	rh_inferiorparietal	22028	0.009	Y

0.090	22026	-3.853	0.000	-0.525	-0.171	z-score	rh_inferiorparietal	22028	0.008	Y
43.124	22018	-3.199	0.001	-222.461	-53.408	raw	rh_lingual	22042	0.016	Y
0.092	22040	-3.250	0.001	-0.479	-0.119	z-score	rh_lingual	22042	0.013	Y
45.491	22018	-3.311	0.001	-239.775	-61.445	raw	rh_middletemporal	22042	0.013	Y
0.084	22040	-3.372	0.001	-0.449	-0.119	z-score	rh_middletemporal	22042	0.010	Y
8.906	22004	-3.524	0.000	-48.840	-13.928	raw	rh_parahippocampal	22028	0.014	Y
0.096	22026	-3.568	0.000	-0.532	-0.155	z-score	rh_parahippocampal	22028	0.012	Y
26.963	22018	-3.144	0.002	-137.627	-31.928	raw	rh_parstriangularis	22042	0.016	Y
0.089	22040	-3.046	0.002	-0.445	-0.097	z-score	rh_parstriangularis	22042	0.020	Y
49.756	22018	-2.885	0.004	-241.075	-46.023	raw	rh_postcentral	22042	0.027	Y
0.086	22040	-2.729	0.006	-0.404	-0.066	z-score	rh_postcentral	22042	0.040	Y
82.708	22018	-2.652	0.008	-381.466	-57.238	raw	rh_rostralmiddlefrontal	22042	0.041	Y
0.084	22040	-2.549	0.011	-0.377	-0.049	z-score	rh_rostralmiddlefrontal	22042	0.049	Y
59.265	22018	-2.629	0.009	-271.971	-39.644	raw	rh_supramarginal	22042	0.041	Y
0.088	22040	-2.608	0.009	-0.403	-0.057	z-score	rh_supramarginal	22042	0.046	Y

23.945	22018	-2.923	0.003	-116.913	-23.046	raw	rh_insula	22042	0.026	Y
0.081	22040	-2.885	0.004	-0.395	-0.075	z-score	rh_insula	22042	0.030	Y
18.864	22018	-2.247	0.025	-79.356	-5.407	raw	lh_bankssts	22042	0.076	Y
0.092	22040	-2.429	0.015	-0.402	-0.043	z-score	lh_bankssts	22042	0.061	Y
0.089	22040	-2.497	0.013	-0.397	-0.048	z-score	lh_inferiorparietal	22042	0.053	Y
40.595	22018	-2.261	0.024	-171.343	-12.207	raw	lh_lingual	22042	0.076	Y
0.091	22040	-2.187	0.029	-0.378	-0.021	z-score	lh_lingual	22042	0.081	Y
18.554	22004	-2.246	0.025	-78.033	-5.298	raw	lh_paracentral	22028	0.120	Y
0.097	22026	-2.441	0.015	-0.428	-0.047	z-score	lh_paracentral	22028	0.091	Y
49.725	22018	-2.410	0.016	-217.292	-22.364	raw	lh_postcentral	22042	0.060	Y
0.085	22040	-2.340	0.019	-0.364	-0.032	z-score	lh_postcentral	22042	0.066	Y
16.951	22004	-2.163	0.031	-69.897	-3.445	raw	lh_rostralanteriorcingulate	22028	0.138	Y
0.094	22026	-2.117	0.034	-0.385	-0.015	z-score	lh_rostralanteriorcingulate	22028	0.155	Y
53.181	22004	-2.043	0.041	-212.906	-4.430	raw	lh_superiortemporal	22028	0.174	Y
0.089	22026	-2.004	0.045	-0.354	-0.004	z-score	lh_superiortemporal	22028	0.182	Y

78.592	22004	-2.753	0.006	-370.423	-62.333	raw	lh_supramarginal	22028	0.050	Y
73.193	22018	-2.205	0.027	-304.877	-17.952	raw	lh_supramarginal	22042	0.077	Y
0.086	22040	-2.319	0.020	-0.366	-0.031	z-score	lh_supramarginal	22042	0.066	Y
7.050	22018	-1.997	0.046	-27.895	-0.258	raw	lh_transversetemporal	22042	0.120	Y
0.100	22026	-2.001	0.045	-0.398	-0.004	z-score	rh_caudalanteriorcingulate	22028	0.182	Y
21.779	22018	-2.192	0.028	-90.432	-5.055	raw	rh_cuneus	22042	0.077	Y
0.088	22040	-2.121	0.034	-0.359	-0.014	z-score	rh_cuneus	22042	0.092	Y
38.171	22004	-2.534	0.011	-171.540	-21.905	raw	rh_fusiform	22028	0.077	Y
0.086	22026	-2.645	0.008	-0.394	-0.059	z-score	rh_fusiform	22028	0.062	Y
81.155	22018	-2.473	0.013	-359.759	-41.620	raw	rh_inferiorparietal	22042	0.054	Y
0.084	22040	-2.374	0.018	-0.364	-0.035	z-score	rh_inferiorparietal	22042	0.063	Y
42.759	22018	-2.376	0.018	-185.409	-17.789	raw	rh_inferiortemporal	22042	0.062	Y
0.082	22040	-2.374	0.018	-0.357	-0.034	z-score	rh_inferiortemporal	22042	0.063	Y
21.509	22018	-2.193	0.028	-89.324	-5.006	raw	rh_medialorbitofrontal	22042	0.077	Y
0.084	22040	-2.193	0.028	-0.347	-0.019	z-score	rh_medialorbitofrontal	22042	0.081	Y

11.627	22018	-2.358	0.018	-50.210	-4.632	raw	rh_parsorbitalis	22042	0.062	Y
0.084	22040	-2.237	0.025	-0.355	-0.023	z-score	rh_parsorbitalis	22042	0.078	Y
20.762	22004	-2.255	0.024	-87.516	-6.124	raw	rh_posteriorcingulate	22028	0.120	Y
0.096	22026	-2.341	0.019	-0.413	-0.037	z-score	rh_posteriorcingulate	22028	0.109	Y
13.175	22004	-2.350	0.019	-56.790	-5.142	raw	rh_rostralanteriorcingulate	22028	0.106	Y
0.097	22026	-2.231	0.026	-0.407	-0.026	z-score	rh_rostralanteriorcingulate	22028	0.125	Y
4.899	22004	-2.563	0.010	-22.159	-2.955	raw	rh_frontalpole	22028	0.077	Y
0.095	22026	-2.575	0.010	-0.432	-0.059	z-score	rh_frontalpole	22028	0.068	Y
25.737	22004	2.365	0.018	10.419	111.311	raw	rh_insula	22028	0.106	Y
0.088	22026	2.278	0.023	0.028	0.371	z-score	rh_insula	22028	0.119	Y
43.565	22004	1.114	0.265	-36.859	133.923	raw	lh_caudalmiddlefrontal	22028	0.582	I
0.098	22026	1.023	0.306	-0.092	0.293	z-score	lh_caudalmiddlefrontal	22028	0.631	I
40.577	22018	-0.325	0.745	-92.736	66.330	raw	lh_caudalmiddlefrontal	22042	0.779	I
0.091	22040	-0.160	0.873	-0.194	0.165	z-score	lh_caudalmiddlefrontal	22042	0.892	I
22.990	22004	0.400	0.689	-35.876	54.247	raw	lh_cuneus	22028	0.945	I
0.096	22026	0.379	0.705	-0.152	0.225	z-score	lh_cuneus	22028	0.933	I
21.421	22018	-1.890	0.059	-82.462	1.511	raw	lh_cuneus	22042	0.138	I
0.090	22040	-1.815	0.070	-0.338	0.013	z-score	lh_cuneus	22042	0.163	I

9.981	22004	-0.011	0.991	-19.678	19.451	raw	lh_entorhinal	22028	0.991	
0.100	22026	-0.001	0.999	-0.196	0.195	z-score	lh_entorhinal	22028	0.999	
36.868	22018	-1.443	0.149	-125.483	19.046	raw	lh_fusiform	22042	0.247	
0.082	22040	-1.322	0.186	-0.270	0.053	z-score	lh_fusiform	22042	0.302	
50.481	22004	-0.063	0.950	-102.142	95.752	raw	lh_inferiortemporal	22028	0.991	
0.091	22026	0.006	0.995	-0.178	0.179	z-score	lh_inferiortemporal	22028	0.999	
47.025	22018	-1.038	0.299	-141.008	43.337	raw	lh_inferiortemporal	22042	0.407	
0.085	22040	-0.900	0.368	-0.242	0.090	z-score	lh_inferiortemporal	22042	0.479	
17.429	22004	-0.890	0.374	-49.667	18.657	raw	lh_isthmuscingulate	22028	0.677	
0.091	22026	-0.734	0.463	-0.246	0.112	z-score	lh_isthmuscingulate	22028	0.768	
16.240	22018	-0.402	0.688	-38.358	25.304	raw	lh_isthmuscingulate	22042	0.742	
0.085	22040	-0.235	0.814	-0.186	0.146	z-score	lh_isthmuscingulate	22042	0.879	
67.555	22004	-1.354	0.176	-223.878	40.946	raw	lh_lateraloccipital	22028	0.467	
0.090	22026	-1.370	0.171	-0.298	0.053	z-score	lh_lateraloccipital	22028	0.449	
62.862	22018	-1.899	0.058	-242.602	3.826	raw	lh_lateraloccipital	22042	0.138	
0.083	22040	-1.719	0.086	-0.306	0.020	z-score	lh_lateraloccipital	22042	0.176	

31.625	22004	-0.930	0.352	-91.404	32.571	raw	lh_lateralorbitofrontal	22028	0.665	
0.092	22026	-0.931	0.352	-0.267	0.095	z-score	lh_lateralorbitofrontal	22028	0.684	
29.460	22018	-1.274	0.203	-95.268	20.219	raw	lh_lateralorbitofrontal	22042	0.300	
0.086	22040	-1.231	0.218	-0.275	0.063	z-score	lh_lateralorbitofrontal	22042	0.325	
43.569	22004	-1.204	0.229	-137.864	32.934	raw	lh_lingual	22028	0.518	
0.098	22026	-1.287	0.198	-0.318	0.066	z-score	lh_lingual	22028	0.481	
23.501	22004	0.096	0.924	-43.811	48.317	raw	lh_medialorbitofrontal	22028	0.991	
0.090	22026	0.092	0.926	-0.169	0.186	z-score	lh_medialorbitofrontal	22028	0.999	
21.899	22018	-0.849	0.396	-61.525	24.323	raw	lh_medialorbitofrontal	22042	0.498	
0.084	22040	-0.713	0.476	-0.225	0.105	z-score	lh_medialorbitofrontal	22042	0.578	
46.453	22004	0.353	0.724	-74.663	107.441	raw	lh_middletemporal	22028	0.945	
0.091	22026	0.494	0.621	-0.133	0.223	z-score	lh_middletemporal	22028	0.862	
8.461	22018	0.221	0.825	-14.712	18.456	raw	lh_parahippocampal	22042	0.837	
0.092	22040	0.206	0.837	-0.161	0.198	z-score	lh_parahippocampal	22042	0.889	
17.279	22018	-1.423	0.155	-58.448	9.288	raw	lh_paracentral	22042	0.251	
0.090	22040	-1.295	0.195	-0.295	0.060	z-score	lh_paracentral	22042	0.303	
31.543	22004	0.717	0.473	-39.209	84.445	raw	lh_parsopercularis	22028	0.775	
0.100	22026	0.821	0.412	-0.114	0.278	z-score	lh_parsopercularis	22028	0.737	
29.388	22018	-0.305	0.760	-66.564	48.642	raw	lh_parsopercularis	22042	0.783	

0.093	22040	-0.136	0.892	-0.195	0.170	z-score	lh_parsopercularis	22042	0.892	
10.354	22004	-0.230	0.818	-22.680	17.908	raw	lh_parsorbitalis	22028	0.991	
0.091	22026	-0.045	0.964	-0.183	0.175	z-score	lh_parsorbitalis	22028	0.999	
9.646	22018	-1.494	0.135	-33.315	4.499	raw	lh_parsorbitalis	22042	0.230	
0.085	22040	-1.373	0.170	-0.283	0.050	z-score	lh_parsorbitalis	22042	0.288	
24.628	22004	-0.147	0.883	-51.893	44.653	raw	lh_parstriangularis	22028	0.991	
0.096	22026	-0.070	0.944	-0.195	0.181	z-score	lh_parstriangularis	22028	0.999	
22.960	22018	-0.607	0.544	-58.948	31.059	raw	lh_parstriangularis	22042	0.648	
0.089	22040	-0.594	0.552	-0.228	0.122	z-score	lh_parstriangularis	22042	0.647	
26.321	22004	-0.421	0.674	-62.663	40.517	raw	lh_pericalcarine	22028	0.945	
0.102	22026	-0.592	0.554	-0.259	0.139	z-score	lh_pericalcarine	22028	0.837	
24.530	22018	-1.295	0.195	-79.848	16.315	raw	lh_pericalcarine	22042	0.295	
0.095	22040	-1.338	0.181	-0.312	0.059	z-score	lh_pericalcarine	22042	0.300	
53.391	22004	-0.747	0.455	-144.544	64.755	raw	lh_postcentral	22028	0.773	
0.091	22026	-0.791	0.429	-0.250	0.106	z-score	lh_postcentral	22028	0.748	

20.253	22004	-1.304	0.192	-66.102	13.291	raw	lh_posteriorcingulate	22028	0.467	
0.096	22026	-1.367	0.172	-0.318	0.057	z-score	lh_posteriorcingulate	22028	0.449	
18.874	22018	-0.594	0.552	-48.212	25.779	raw	lh_posteriorcingulate	22042	0.648	
0.089	22040	-0.576	0.565	-0.226	0.123	z-score	lh_posteriorcingulate	22042	0.647	
56.385	22004	0.954	0.340	-56.751	164.287	raw	lh_precentral	22028	0.665	
0.089	22026	1.074	0.283	-0.079	0.270	z-score	lh_precentral	22028	0.621	
52.532	22018	-0.344	0.731	-121.060	84.873	raw	lh_precentral	22042	0.776	
0.083	22040	-0.177	0.859	-0.177	0.148	z-score	lh_precentral	22042	0.892	
54.417	22004	0.460	0.645	-81.619	131.702	raw	lh_precuneus	22028	0.934	
0.092	22026	0.235	0.814	-0.159	0.202	z-score	lh_precuneus	22028	0.984	
50.708	22018	-0.511	0.609	-125.317	73.466	raw	lh_precuneus	22042	0.688	
0.086	22040	-0.678	0.498	-0.226	0.110	z-score	lh_precuneus	22042	0.594	
81.502	22004	-0.881	0.378	-231.531	87.968	raw	lh_rostralmiddlefrontal	22028	0.677	
0.089	22026	-0.833	0.405	-0.248	0.100	z-score	lh_rostralmiddlefrontal	22028	0.737	
99.581	22004	1.914	0.056	-4.552	385.821	raw	lh_superiorfrontal	22028	0.219	
0.089	22026	1.927	0.054	-0.003	0.348	z-score	lh_superiorfrontal	22028	0.204	
92.727	22018	-1.127	0.260	-286.240	77.264	raw	lh_superiorfrontal	22042	0.361	
0.083	22040	-1.003	0.316	-0.247	0.080	z-score	lh_superiorfrontal	22042	0.438	

80.992	22004	0.019	0.985	-157.236	160.264	raw	lh_superiorparietal	22028	0.991	
0.098	22026	0.007	0.994	-0.191	0.192	z-score	lh_superiorparietal	22028	0.999	
75.458	22018	-1.785	0.074	-282.599	13.207	raw	lh_superiorparietal	22042	0.153	
0.091	22040	-1.707	0.088	-0.333	0.023	z-score	lh_superiorparietal	22042	0.176	
3.912	22004	-0.760	0.447	-10.643	4.694	raw	lh_frontalpole	22028	0.773	
0.096	22026	-0.632	0.527	-0.248	0.127	z-score	lh_frontalpole	22028	0.820	
3.646	22018	-1.659	0.097	-13.194	1.099	raw	lh_frontalpole	22042	0.185	
0.089	22040	-1.617	0.106	-0.318	0.031	z-score	lh_frontalpole	22042	0.195	
6.643	22004	-0.690	0.490	-17.600	8.439	raw	lh_temporalpole	22028	0.776	
0.093	22026	-0.767	0.443	-0.253	0.111	z-score	lh_temporalpole	22028	0.753	
6.185	22018	-1.137	0.256	-19.154	5.092	raw	lh_temporalpole	22042	0.361	
0.086	22040	-1.065	0.287	-0.262	0.077	z-score	lh_temporalpole	22042	0.406	
7.569	22004	0.017	0.986	-14.707	14.964	raw	lh_transversetemporal	22028	0.991	
0.099	22026	0.052	0.958	-0.188	0.198	z-score	lh_transversetemporal	22028	0.999	
0.092	22040	-1.924	0.054	-0.356	0.003	z-score	lh_transversetemporal	22042	0.142	
26.625	22004	1.505	0.132	-12.115	92.261	raw	lh_insula	22028	0.391	
0.091	22026	1.425	0.154	-0.049	0.307	z-score	lh_insula	22028	0.437	
15.920	22004	-1.587	0.112	-56.478	5.932	raw	rh_bankssts	22028	0.364	

0.098	22026	-1.467	0.142	-0.336	0.048	z-score	rh_bankssts	22028	0.428	
17.103	22004	-1.897	0.058	-65.957	1.087	raw	rh_caudalanteriorcingulate	22028	0.219	
15.943	22018	-0.823	0.411	-44.365	18.136	raw	rh_caudalanteriorcingulate	22042	0.499	
0.094	22040	-0.948	0.343	-0.272	0.095	z-score	rh_caudalanteriorcingulate	22042	0.467	
44.343	22004	-1.308	0.191	-144.920	28.909	raw	rh_caudalmiddlefrontal	22028	0.467	
0.099	22026	-1.212	0.225	-0.314	0.074	z-score	rh_caudalmiddlefrontal	22028	0.511	
41.336	22018	-1.154	0.249	-128.721	33.321	raw	rh_caudalmiddlefrontal	22042	0.360	
0.092	22040	-1.228	0.220	-0.294	0.068	z-score	rh_caudalmiddlefrontal	22042	0.325	
23.391	22004	1.341	0.180	-14.484	77.212	raw	rh_cuneus	22028	0.467	
0.095	22026	1.214	0.225	-0.071	0.300	z-score	rh_cuneus	22028	0.511	
8.774	22004	-0.129	0.897	-18.331	16.065	raw	rh_entorhinal	22028	0.991	
0.098	22026	-0.463	0.644	-0.238	0.147	z-score	rh_entorhinal	22028	0.875	
8.171	22018	0.183	0.855	-14.522	17.510	raw	rh_entorhinal	22042	0.855	
0.091	22040	0.143	0.886	-0.166	0.192	z-score	rh_entorhinal	22042	0.892	
35.554	22018	-1.500	0.134	-123.027	16.348	raw	rh_fusiform	22042	0.230	
0.080	22040	-1.292	0.196	-0.259	0.053	z-score	rh_fusiform	22042	0.303	
45.882	22004	-0.368	0.713	-106.826	73.037	raw	rh_inferiortemporal	22028	0.945	

0.089	22026	-0.239	0.811	-0.195	0.152	z-score	rh_inferiortemporal	22028	0.984	
15.592	22004	-1.692	0.091	-56.943	4.181	raw	rh_isthmuscingulate	22028	0.324	
0.094	22026	-1.653	0.098	-0.339	0.029	z-score	rh_isthmuscingulate	22028	0.346	
14.532	22018	1.371	0.170	-8.558	48.407	raw	rh_isthmuscingulate	22042	0.269	
0.087	22040	1.492	0.136	-0.041	0.302	z-score	rh_isthmuscingulate	22042	0.237	
69.531	22004	-0.011	0.991	-137.080	135.491	raw	rh_lateraloccipital	22028	0.991	
0.088	22026	-0.123	0.902	-0.184	0.162	z-score	rh_lateraloccipital	22028	0.999	
64.686	22018	-1.295	0.195	-210.553	43.025	raw	rh_lateraloccipital	22042	0.295	
0.082	22040	-1.108	0.268	-0.252	0.070	z-score	rh_lateraloccipital	22042	0.388	
33.722	22004	-1.231	0.218	-107.597	24.599	raw	rh_lateralorbitofrontal	22028	0.512	
0.092	22026	-1.336	0.181	-0.304	0.057	z-score	rh_lateralorbitofrontal	22028	0.457	
31.411	22018	-1.575	0.115	-111.049	12.088	raw	rh_lateralorbitofrontal	22042	0.212	
0.086	22040	-1.540	0.123	-0.300	0.036	z-score	rh_lateralorbitofrontal	22042	0.221	
46.267	22004	0.284	0.776	-77.536	103.837	raw	rh_lingual	22028	0.960	
0.099	22026	0.342	0.733	-0.160	0.227	z-score	rh_lingual	22028	0.940	
23.071	22004	-0.946	0.344	-67.055	23.386	raw	rh_medialorbitofrontal	22028	0.665	
0.090	22026	-1.033	0.301	-0.269	0.083	z-score	rh_medialorbitofrontal	22028	0.631	

48.797	22004	-1.024	0.306	-145.616	45.675	raw	rh_middletemporal	22028	0.650	
0.090	22026	-0.867	0.386	-0.255	0.099	z-score	rh_middletemporal	22028	0.729	
8.303	22018	-0.500	0.617	-20.422	12.126	raw	rh_parahippocampal	22042	0.688	
0.090	22040	-0.567	0.571	-0.227	0.125	z-score	rh_parahippocampal	22042	0.647	
21.783	22004	-0.331	0.741	-49.902	35.491	raw	rh_paracentral	22028	0.945	
0.097	22026	-0.367	0.714	-0.225	0.154	z-score	rh_paracentral	22028	0.933	
20.296	22018	-0.516	0.606	-50.263	29.301	raw	rh_paracentral	22042	0.688	
0.090	22040	-0.500	0.617	-0.221	0.131	z-score	rh_paracentral	22042	0.688	
25.307	22004	-0.561	0.575	-63.789	35.419	raw	rh_parsopercularis	22028	0.869	
0.099	22026	-0.652	0.515	-0.258	0.129	z-score	rh_parsopercularis	22028	0.820	
23.565	22018	-1.818	0.069	-89.027	3.350	raw	rh_parsopercularis	22042	0.147	
0.092	22040	-1.690	0.091	-0.336	0.025	z-score	rh_parsopercularis	22042	0.177	
12.481	22004	-1.598	0.110	-44.404	4.522	raw	rh_parsorbitalis	22028	0.364	
0.091	22026	-1.505	0.132	-0.315	0.041	z-score	rh_parsorbitalis	22028	0.428	
28.966	22004	-0.074	0.941	-58.928	54.624	raw	rh_parstriangularis	22028	0.991	

0.096	22026	-0.130	0.897	-0.200	0.175	z-score	rh_parstriangularis	22028	0.999	
27.319	22004	-0.341	0.733	-62.874	44.220	raw	rh_pericalcarine	22028	0.945	
0.101	22026	-0.520	0.603	-0.250	0.145	z-score	rh_pericalcarine	22028	0.854	
25.458	22018	-1.655	0.098	-92.025	7.774	raw	rh_pericalcarine	22042	0.185	
0.094	22040	-1.745	0.081	-0.347	0.020	z-score	rh_pericalcarine	22042	0.176	
53.409	22004	-0.940	0.347	-154.887	54.485	raw	rh_postcentral	22028	0.665	
0.093	22026	-0.995	0.320	-0.274	0.089	z-score	rh_postcentral	22028	0.639	
19.349	22018	-1.909	0.056	-74.863	0.988	raw	rh_posteriorcingulate	22042	0.138	
0.089	22040	-1.789	0.074	-0.336	0.015	z-score	rh_posteriorcingulate	22042	0.167	
57.638	22004	1.337	0.181	-35.913	190.036	raw	rh_precentral	22028	0.467	
0.090	22026	1.458	0.145	-0.045	0.307	z-score	rh_precentral	22028	0.428	
53.727	22018	-0.413	0.680	-127.491	83.125	raw	rh_precentral	22042	0.742	
0.084	22040	-0.309	0.757	-0.190	0.138	z-score	rh_precentral	22042	0.831	
57.027	22004	0.709	0.479	-71.373	152.183	raw	rh_precuneus	22028	0.775	
0.091	22026	0.540	0.589	-0.129	0.228	z-score	rh_precuneus	22028	0.852	
53.122	22018	-1.710	0.087	-194.943	13.303	raw	rh_precuneus	22042	0.175	
0.085	22040	-1.712	0.087	-0.311	0.021	z-score	rh_precuneus	22042	0.176	

12.281	22018	-1.827	0.068	-46.505	1.638	raw	rh_rostralanteriorcingulate	22042	0.147	
0.090	22040	-1.861	0.063	-0.346	0.009	z-score	rh_rostralanteriorcingulate	22042	0.152	
88.819	22004	-1.562	0.118	-312.869	35.314	raw	rh_rostralmiddlefrontal	22028	0.365	
0.090	22026	-1.636	0.102	-0.323	0.029	z-score	rh_rostralmiddlefrontal	22028	0.346	
00.346	22004	0.139	0.890	-182.771	210.600	raw	rh_superiorfrontal	22028	0.991	
0.090	22026	0.221	0.825	-0.157	0.197	z-score	rh_superiorfrontal	22028	0.984	
93.472	22018	-1.003	0.316	-276.922	89.504	raw	rh_superiorfrontal	22042	0.416	
0.084	22040	-0.915	0.360	-0.242	0.088	z-score	rh_superiorfrontal	22042	0.479	
78.543	22004	0.318	0.750	-128.974	178.925	raw	rh_superiorparietal	22028	0.945	
0.096	22026	0.255	0.799	-0.164	0.213	z-score	rh_superiorparietal	22028	0.984	
73.223	22018	-0.827	0.408	-204.096	82.947	raw	rh_superiorparietal	22042	0.499	
0.090	22040	-0.726	0.468	-0.240	0.110	z-score	rh_superiorparietal	22042	0.578	
46.047	22004	0.467	0.640	-68.742	111.769	raw	rh_superiortemporal	22028	0.934	
0.093	22026	0.627	0.531	-0.124	0.241	z-score	rh_superiortemporal	22028	0.820	
42.895	22018	-1.835	0.066	-162.806	5.349	raw	rh_superiortemporal	22042	0.147	
0.087	22040	-1.894	0.058	-0.334	0.006	z-score	rh_superiortemporal	22042	0.147	
63.603	22004	0.650	0.516	-83.339	165.996	raw	rh_supramarginal	22028	0.797	
0.095	22026	0.569	0.569	-0.132	0.240	z-score	rh_supramarginal	22028	0.841	

4.566	22018	-0.998	0.318	-13.507	4.393	raw	rh_frontalpole	22042	0.416	
0.089	22040	-0.890	0.374	-0.253	0.095	z-score	rh_frontalpole	22042	0.479	
6.787	22004	0.203	0.840	-11.929	14.679	raw	rh_temporalpole	22028	0.991	
0.096	22026	0.186	0.852	-0.170	0.206	z-score	rh_temporalpole	22028	0.999	
6.322	22018	-0.856	0.392	-17.802	6.979	raw	rh_temporalpole	22042	0.498	
0.089	22040	-0.850	0.396	-0.251	0.099	z-score	rh_temporalpole	22042	0.498	
5.001	22004	-0.133	0.894	-10.465	9.138	raw	rh_transversetemporal	22028	0.991	
0.097	22026	-0.083	0.934	-0.199	0.183	z-score	rh_transversetemporal	22028	0.999	
4.663	22018	-1.544	0.123	-16.341	1.941	raw	rh_transversetemporal	22042	0.219	
0.091	22040	-1.628	0.103	-0.326	0.030	z-score	rh_transversetemporal	22042	0.195	

Supplementary Table 11

All Group Difference Effects in Subcortical and Cerebellar Volume for all 15q11.2 CNV Carriers and Control Across Raw and Z-Score Models.

Sorted by FDR-corrected significance, and then by nominal significance. This table summarises all the mixed-effects model comparing subcortical and cerebellar volumes between 15q11.2 BP1-BP2 CNV carriers and controls in all ROIs. For each mixed-effects model, the following is included: Group (deletion/duplication), effect (Estimate), standard error (SE), degrees of

freedom (df), test statistic (t), nominal significance (p.value), lowest confidence interval (ci_low), highest confidence interval (ci_high), data input to model (raw/z-score), region of interest (ROI), number of subjects (n_subjects), significance value after FDR correction (p_adjusted), nominal significance status (Yes/No), FDR corrected significance status (Yes/No).

E	df	t	p.value	ci_low	ci_high	data_type	ROI	n_subjects	p_adjusted
92	22026	-2.551	0.011	-0.417	-0.055	z-score	Left.Cerebellum.White.Matter	22028	0.042
470	22004	-2.960	0.003	-2688.525	-546.285	raw	Left.Cerebellum.Cortex	22028	0.020
03	22026	-2.649	0.008	-0.473	-0.071	z-score	Left.Cerebellum.Cortex	22028	0.042
395	22018	-3.127	0.002	-2591.356	-594.454	raw	Left.Cerebellum.Cortex	22042	0.018
95	22040	-3.313	0.001	-0.504	-0.129	z-score	Left.Cerebellum.Cortex	22042	0.010
64	22004	-3.746	0.000	-321.609	-100.652	raw	Left.Putamen	22028	0.003
00	22026	-3.765	0.000	-0.574	-0.181	z-score	Left.Putamen	22028	0.003
87	22004	2.953	0.003	22.632	111.962	raw	X3rd.Ventricle	22028	0.020
83	22026	3.452	0.001	0.124	0.449	z-score	X3rd.Ventricle	22028	0.004
70	22004	3.020	0.003	22.647	106.419	raw	CSF	22028	0.020
08	22026	2.937	0.003	0.105	0.526	z-score	CSF	22028	0.021
42	22018	-2.735	0.006	-46.204	-7.622	raw	Left.Accumbens.area	22042	0.048
344	22004	2.657	0.008	205.244	1359.116	raw	Right.Lateral.Ventricle	22028	0.035
95	22026	3.482	0.000	0.145	0.518	z-score	Right.Lateral.Ventricle	22028	0.004
944	22004	-2.546	0.011	-2509.352	-326.051	raw	Right.Cerebellum.Cortex	22028	0.042

150	22018	-3.152	0.002	-2653.986	-618.843	raw	Right.Cerebellum.Cortex	22042	0.018
96	22040	-3.390	0.001	-0.512	-0.137	z-score	Right.Cerebellum.Cortex	22042	0.010
89	22004	-3.828	0.000	-323.468	-104.376	raw	Right.Putamen	22028	0.003
98	22026	-3.920	0.000	-0.578	-0.193	z-score	Right.Putamen	22028	0.003
42	22004	-2.734	0.006	-194.521	-32.061	raw	Right.Hippocampus	22028	0.032
03	22026	-2.569	0.010	-0.468	-0.063	z-score	Right.Hippocampus	22028	0.042
94	22018	-3.176	0.001	-46.704	-11.056	raw	Right.Accumbens.area	22042	0.018
98	22040	-3.658	0.000	-0.549	-0.166	z-score	Right.Accumbens.area	22042	0.008
92	22026	1.990	0.047	0.003	0.362	z-score	Left.Lateral.Ventricle	22028	0.123
545	22004	-2.330	0.020	-804.592	-69.390	raw	Left.Cerebellum.White.Matter	22028	0.061
61	22004	-2.037	0.042	-42.209	-0.810	raw	Left.Accumbens.area	22028	0.117
03	22026	-1.981	0.048	-0.406	-0.002	z-score	Left.Accumbens.area	22028	0.123
96	22040	-2.616	0.009	-0.439	-0.063	z-score	Left.Accumbens.area	22042	0.069
98	22018	-2.249	0.025	-58.072	-3.983	raw	Right.Inf.Lat.Vent	22042	0.109
75	22040	-2.085	0.037	-0.305	-0.009	z-score	Right.Inf.Lat.Vent	22042	0.164
87	22026	-2.005	0.045	-0.344	-0.004	z-score	Right.Cerebellum.White.Matter	22028	0.123

03	22026	-2.216	0.027	-0.430	-0.026	z-score	Right.Cerebellum.Cortex	22028	0.092
29	22004	-2.373	0.018	-96.763	-9.228	raw	Right.Pallidum	22028	0.061
.173	22018	-2.319	0.020	-51310.824	-4303.705	raw	EstimatedTotalIntraCranialVol	22042	0.105
93	22040	-2.156	0.031	-0.382	-0.018	z-score	EstimatedTotalIntraCranialVol	22042	0.161
994	22018	-2.440	0.015	-39891.012	-4347.093	raw	SupraTentorialVol	22042	0.091
98	22040	-2.264	0.024	-0.412	-0.030	z-score	SupraTentorialVol	22042	0.146
431	22004	1.317	0.188	-204.659	1043.638	raw	Left.Lateral.Ventricle	22028	0.323
486	22018	-1.839	0.066	-1126.406	35.861	raw	Left.Lateral.Ventricle	22042	0.255
85	22040	-1.429	0.153	-0.289	0.045	z-score	Left.Lateral.Ventricle	22042	0.474
24	22004	-1.571	0.116	-52.347	5.767	raw	Left.Inf.Lat.Vent	22028	0.227
83	22026	-1.290	0.197	-0.270	0.056	z-score	Left.Inf.Lat.Vent	22028	0.359
14	22018	0.136	0.892	-25.200	28.952	raw	Left.Inf.Lat.Vent	22042	0.927
77	22040	0.580	0.562	-0.107	0.197	z-score	Left.Inf.Lat.Vent	22042	0.881
007	22018	0.479	0.632	-259.163	426.890	raw	Left.Cerebellum.White.Matter	22042	0.927
86	22040	0.154	0.878	-0.156	0.182	z-score	Left.Cerebellum.White.Matter	22042	0.907
16	22004	0.612	0.541	-103.990	198.317	raw	Left.Thalamus.Proper	22028	0.645
33	22026	0.750	0.453	-0.160	0.359	z-score	Left.Thalamus.Proper	22028	0.561
36	22018	-1.438	0.151	-244.073	37.532	raw	Left.Thalamus.Proper	22042	0.467
23	22040	0.332	0.740	-0.201	0.283	z-score	Left.Thalamus.Proper	22042	0.881

77	22004	-1.020	0.308	-143.271	45.197	raw	Left.Caudate	22028	0.434
03	22026	-0.727	0.467	-0.277	0.127	z-score	Left.Caudate	22028	0.561
98	22018	-0.472	0.637	-108.950	66.665	raw	Left.Caudate	22042	0.927
96	22040	-0.380	0.704	-0.225	0.152	z-score	Left.Caudate	22042	0.881
93	22018	-1.041	0.298	-157.523	48.258	raw	Left.Putamen	22042	0.718
93	22040	-0.718	0.472	-0.250	0.116	z-score	Left.Putamen	22042	0.881
31	22004	-1.936	0.053	-91.678	0.567	raw	Left.Pallidum	22028	0.137
03	22026	-1.801	0.072	-0.386	0.016	z-score	Left.Pallidum	22028	0.159
06	22018	0.027	0.979	-42.351	43.522	raw	Left.Pallidum	22042	0.979
95	22040	0.275	0.783	-0.161	0.213	z-score	Left.Pallidum	22042	0.881
49	22018	-0.154	0.878	-44.920	38.380	raw	X3rd.Ventricle	22042	0.927
77	22040	0.298	0.766	-0.128	0.174	z-score	X3rd.Ventricle	22042	0.881
25	22004	0.462	0.644	-78.372	126.749	raw	X4th.Ventricle	22028	0.688
04	22026	0.721	0.471	-0.129	0.278	z-score	X4th.Ventricle	22028	0.561
78	22018	-0.540	0.589	-121.939	69.277	raw	X4th.Ventricle	22042	0.927
97	22040	-0.259	0.796	-0.215	0.165	z-score	X4th.Ventricle	22042	0.881
452	22004	-0.489	0.625	-468.800	281.719	raw	Brain.Stem	22028	0.688
96	22026	-0.346	0.729	-0.222	0.155	z-score	Brain.Stem	22028	0.754

498	22018	1.034	0.301	-165.328	534.409	raw	Brain.Stem	22042	0.718
90	22040	1.608	0.108	-0.032	0.320	z-score	Brain.Stem	22042	0.372
68	22004	-1.567	0.117	-140.270	15.626	raw	Left.Hippocampus	22028	0.227
02	22026	-1.418	0.156	-0.345	0.055	z-score	Left.Hippocampus	22028	0.304
60	22018	-0.350	0.727	-85.594	59.687	raw	Left.Hippocampus	22042	0.927
95	22040	-0.469	0.639	-0.231	0.142	z-score	Left.Hippocampus	22042	0.881
02	22004	-1.189	0.234	-68.351	16.725	raw	Left.Amygdala	22028	0.346
03	22026	-1.224	0.221	-0.329	0.076	z-score	Left.Amygdala	22028	0.367
08	22018	0.596	0.551	-27.559	51.659	raw	Left.Amygdala	22042	0.927
96	22040	0.273	0.785	-0.162	0.215	z-score	Left.Amygdala	22042	0.881
08	22018	-0.773	0.439	-54.416	23.626	raw	CSF	22042	0.908
00	22040	0.189	0.850	-0.177	0.215	z-score	CSF	22042	0.907
29	22004	-0.726	0.468	-102.678	47.185	raw	Left.VentralDC	22028	0.602
98	22026	-0.503	0.615	-0.240	0.142	z-score	Left.VentralDC	22028	0.706
34	22018	0.129	0.897	-65.241	74.450	raw	Left.VentralDC	22042	0.927
91	22040	0.281	0.779	-0.153	0.204	z-score	Left.VentralDC	22042	0.881
004	22018	-1.225	0.220	-872.847	201.288	raw	Right.Lateral.Ventricle	22042	0.621
88	22040	-0.670	0.503	-0.233	0.114	z-score	Right.Lateral.Ventricle	22042	0.881
19	22004	0.015	0.988	-28.827	29.264	raw	Right.Inf.Lat.Vent	22028	0.988

81	22026	-0.030	0.976	-0.161	0.156	z-score	Right.Inf.Lat.Vent	22028	0.976
469	22004	-1.731	0.083	-688.248	42.738	raw	Right.Cerebellum.White.Matter	22028	0.185
893	22018	0.193	0.847	-307.202	374.482	raw	Right.Cerebellum.White.Matter	22042	0.927
81	22040	-0.561	0.575	-0.204	0.113	z-score	Right.Cerebellum.White.Matter	22042	0.881
82	22004	0.579	0.563	-94.735	174.117	raw	Right.Thalamus.Proper	22028	0.646
29	22026	0.837	0.402	-0.145	0.360	z-score	Right.Thalamus.Proper	22028	0.542
16	22018	-0.317	0.752	-145.510	105.050	raw	Right.Thalamus.Proper	22042	0.927
20	22040	0.980	0.327	-0.118	0.352	z-score	Right.Thalamus.Proper	22042	0.869
63	22004	-1.222	0.222	-153.906	35.685	raw	Right.Caudate	22028	0.344
02	22026	-0.918	0.359	-0.293	0.106	z-score	Right.Caudate	22028	0.528
52	22018	-0.229	0.819	-98.610	78.000	raw	Right.Caudate	22042	0.927
95	22040	-0.015	0.988	-0.187	0.184	z-score	Right.Caudate	22042	0.988
44	22018	-1.760	0.078	-193.591	10.427	raw	Right.Putamen	22042	0.270
91	22040	-1.697	0.090	-0.334	0.024	z-score	Right.Putamen	22042	0.347
02	22026	-1.914	0.056	-0.396	0.005	z-score	Right.Pallidum	22028	0.133
91	22018	0.680	0.497	-26.621	54.885	raw	Right.Pallidum	22042	0.927
95	22040	0.962	0.336	-0.095	0.278	z-score	Right.Pallidum	22042	0.869
04	22018	-0.373	0.709	-90.061	61.271	raw	Right.Hippocampus	22042	0.927

96	22040	-0.625	0.532	-0.248	0.128	z-score	Right.Hippocampus	22042	0.881
92	22004	-1.467	0.142	-72.290	10.393	raw	Right.Amygdala	22028	0.260
96	22026	-1.213	0.225	-0.306	0.072	z-score	Right.Amygdala	22028	0.367
65	22018	-0.380	0.704	-46.011	31.078	raw	Right.Amygdala	22042	0.927
90	22040	-0.576	0.565	-0.227	0.124	z-score	Right.Amygdala	22042	0.881
53	22004	-1.282	0.200	-31.616	6.617	raw	Right.Accumbens.area	22028	0.326
05	22026	-1.075	0.282	-0.318	0.093	z-score	Right.Accumbens.area	22028	0.438
63	22004	-0.698	0.485	-100.106	47.539	raw	Right.VentralDC	22028	0.602
98	22026	-0.447	0.655	-0.235	0.148	z-score	Right.VentralDC	22028	0.725
86	22018	-0.651	0.515	-91.597	45.947	raw	Right.VentralDC	22042	0.927
91	22040	-0.521	0.602	-0.226	0.131	z-score	Right.VentralDC	22042	0.881
.059	22004	-0.098	0.922	-26486.420	23969.980	raw	EstimatedTotalIntraCranialVol	22028	0.953
00	22026	0.373	0.709	-0.158	0.233	z-score	EstimatedTotalIntraCranialVol	22028	0.754
309	22004	0.745	0.456	-11826.295	26341.435	raw	SupraTentorialVol	22028	0.602
05	22026	0.887	0.375	-0.112	0.298	z-score	SupraTentorialVol	22028	0.528
933	22004	-1.832	0.067	-1755.553	59.210	raw	SubCortGrayVol	22028	0.160

10	22026	-1.416	0.157	-0.372	0.060	z-score	SubCortGrayVol	22028	0.304
172	22018	-0.960	0.337	-1258.960	431.295	raw	SubCortGrayVol	22042	0.747
02	22040	-0.321	0.748	-0.234	0.168	z-score	SubCortGrayVol	22042	0.881

Table Output for Longitudinal Analysis

Supplementary Table 12

All Nominally Significant CNV Group × Age Interaction Effects for Cortical Thickness.

Summary of linear mixed-effects model results showing all regions with nominally significant ($p < .05$) CNV Group × Age interactions for cortical thickness. For each ROI the table displays a an interaction term (Group x age), estimate (Estimate) standard error (SE), test statistic (t), significance value (p.value), FDR-corrected significance value, nominal significance status (Yes/No), FDR corrected significance status (Yes/No)effect estimates, standard errors, test statistics, degrees of freedom, raw and adjusted p-values, and FDR significance status.

ROI	Group x age	Estimate	SE	df	t	p.value	p_adjusted	Significant	Significant_
eraloccipital	Duplication:age_c	-0.085	0.029	10509	-2.968	0.003	0.138	Yes	No
steriorcingulate	Deletion:age_c	-0.084	0.027	10509	-3.129	0.002	0.138	Yes	No
ricalcarine	Duplication:age_c	-0.092	0.030	10509	-3.046	0.002	0.138	Yes	No

eraloccipital	Duplication:age_c	-0.082	0.029	10509	-2.821	0.005	0.166	Yes	No
gual	Duplication:age_c	-0.062	0.026	10509	-2.380	0.017	0.341	Yes	No
udalmiddlefrontal	Deletion:age_c	-0.081	0.034	10509	-2.387	0.017	0.341	Yes	No
eralorbitofrontal	Deletion:age_c	0.087	0.037	10509	2.386	0.017	0.341	Yes	No
periorfrontal	Duplication:age_c	0.073	0.032	10509	2.275	0.023	0.364	Yes	No
udalmiddlefrontal	Deletion:age_c	-0.079	0.035	10509	-2.262	0.024	0.364	Yes	No
ecentral	Deletion:age_c	-0.077	0.037	10509	-2.071	0.038	0.408	Yes	No
periorparietal	Deletion:age_c	-0.071	0.034	10509	-2.095	0.036	0.408	Yes	No
neus	Duplication:age_c	-0.054	0.026	10509	-2.118	0.034	0.408	Yes	No
sula	Deletion:age_c	-0.092	0.044	10509	-2.094	0.036	0.408	Yes	No
edialorbitofrontal	Duplication:age_c	0.081	0.040	10509	2.032	0.042	0.416	Yes	No
periorparietal	Duplication:age_c	-0.064	0.034	10509	-1.878	0.060	0.556	No	No
ricalcarine	Duplication:age_c	-0.056	0.031	10509	-1.810	0.070	0.558	No	No
hmuscingulate	Deletion:age_c	-0.045	0.025	10509	-1.794	0.073	0.558	No	No
racentral	Deletion:age_c	-0.055	0.030	10509	-1.845	0.065	0.558	No	No
steriorcingulate	Duplication:age_c	-0.045	0.026	10509	-1.717	0.086	0.624	No	No
mporalpole	Duplication:age_c	-0.079	0.047	10509	-1.671	0.095	0.654	No	No

racentral	Duplication:age_c	-0.050	0.031	10509	-1.634	0.102	0.672	No	No
feriortemporal	Deletion:age_c	-0.046	0.031	10509	-1.513	0.130	0.681	No	No
ecentral	Deletion:age_c	-0.054	0.035	10509	-1.517	0.129	0.681	No	No
ecuneus	Deletion:age_c	-0.041	0.027	10509	-1.515	0.130	0.681	No	No
	Deletion:age_c	-0.042	0.027	10509	-1.545	0.122	0.681	No	No
mporalpole	Deletion:age_c	-0.067	0.046	10509	-1.465	0.143	0.681	No	No
periorfrontal	Duplication:age_c	0.046	0.031	10509	1.477	0.140	0.681	No	No
neus	Deletion:age_c	-0.038	0.026	10509	-1.469	0.142	0.681	No	No
nkssts	Duplication:age_c	-0.036	0.024	10509	-1.516	0.129	0.681	No	No
steriorcingulate	Duplication:age_c	0.039	0.027	10509	1.431	0.153	0.702	No	No
siform	Duplication:age_c	-0.032	0.031	10509	-1.024	0.306	0.705	No	No
udalanteriorcingulate	Duplication:age_c	-0.030	0.028	10509	-1.087	0.277	0.705	No	No
feriorparietal	Duplication:age_c	-0.033	0.032	10509	-1.024	0.306	0.705	No	No
feriortemporal	Duplication:age_c	-0.039	0.031	10509	-1.241	0.214	0.705	No	No
siform	Deletion:age_c	-0.037	0.031	10509	-1.186	0.235	0.705	No	No
siform	Duplication:age_c	-0.032	0.032	10509	-1.021	0.307	0.705	No	No

ecentral	Duplication:age_c	-0.037	0.036	10509	-1.038	0.299	0.705	No	No
periorparietal	Deletion:age_c	-0.040	0.034	10509	-1.197	0.231	0.705	No	No
torhinal	Duplication:age_c	-0.041	0.042	10509	-0.990	0.322	0.705	No	No
nsversetemporal	Duplication:age_c	-0.033	0.029	10509	-1.112	0.266	0.705	No	No
stralmiddlefrontal	Duplication:age_c	0.040	0.035	10509	1.145	0.252	0.705	No	No
racentral	Deletion:age_c	-0.042	0.031	10509	-1.349	0.178	0.705	No	No
rsopercularis	Deletion:age_c	-0.037	0.029	10509	-1.272	0.204	0.705	No	No
udalanteriorcingulate	Deletion:age_c	-0.034	0.025	10509	-1.370	0.171	0.705	No	No
udalanteriorcingulate	Duplication:age_c	-0.031	0.025	10509	-1.210	0.226	0.705	No	No
ecentral	Duplication:age_c	-0.039	0.038	10509	-1.026	0.305	0.705	No	No
gual	Deletion:age_c	-0.030	0.026	10509	-1.160	0.246	0.705	No	No
periortemporal	Deletion:age_c	-0.029	0.029	10509	-1.001	0.317	0.705	No	No
periortemporal	Duplication:age_c	-0.029	0.029	10509	-1.013	0.311	0.705	No	No
mporalpole	Duplication:age_c	0.051	0.047	10509	1.090	0.276	0.705	No	No
rahippocampal	Duplication:age_c	0.026	0.022	10509	1.186	0.236	0.705	No	No
eraloccipital	Deletion:age_c	-0.031	0.028	10509	-1.102	0.270	0.705	No	No
periorparietal	Duplication:age_c	-0.034	0.035	10509	-0.994	0.320	0.705	No	No

rahippocampal	Duplication:age_c	-0.025	0.026	10509	-0.980	0.327	0.705	No	No
ddletemporal	Deletion:age_c	-0.034	0.029	10509	-1.181	0.238	0.705	No	No
periorfrontal	Deletion:age_c	-0.035	0.031	10509	-1.123	0.261	0.705	No	No
pramarginal	Deletion:age_c	-0.044	0.033	10509	-1.333	0.183	0.705	No	No
pramarginal	Duplication:age_c	-0.045	0.033	10509	-1.351	0.177	0.705	No	No
stcentral	Deletion:age_c	-0.041	0.031	10509	-1.302	0.193	0.705	No	No
sula	Deletion:age_c	-0.044	0.044	10509	-0.996	0.319	0.705	No	No
periortemporal	Deletion:age_c	-0.031	0.029	10509	-1.102	0.271	0.705	No	No
periortemporal	Duplication:age_c	-0.034	0.029	10509	-1.169	0.242	0.705	No	No
neus	Duplication:age_c	-0.030	0.026	10509	-1.155	0.248	0.705	No	No
nkssts	Deletion:age_c	-0.029	0.023	10509	-1.253	0.210	0.705	No	No
racentral	Duplication:age_c	-0.030	0.031	10509	-0.955	0.340	0.708	No	No
	Duplication:age_c	-0.026	0.028	10509	-0.947	0.344	0.708	No	No
nsversetemporal	Duplication:age_c	-0.029	0.031	10509	-0.962	0.336	0.708	No	No
rstriangularis	Duplication:age_c	0.030	0.033	10509	0.918	0.359	0.724	No	No
hmuscingulate	Deletion:age_c	-0.022	0.024	10509	-0.902	0.367	0.724	No	No

pramarginal	Duplication:age_c	-0.030	0.033	10509	-0.903	0.367	0.724	No	No
stralanteriorcingulate	Deletion:age_c	-0.032	0.036	10509	-0.885	0.376	0.731	No	No
torhinal	Duplication:age_c	-0.035	0.042	10509	-0.843	0.399	0.731	No	No
ecuneus	Deletion:age_c	-0.022	0.027	10509	-0.818	0.413	0.731	No	No
ecuneus	Duplication:age_c	-0.022	0.027	10509	-0.819	0.413	0.731	No	No
mporalpole	Deletion:age_c	0.039	0.046	10509	0.848	0.396	0.731	No	No
rsorbitalis	Duplication:age_c	-0.027	0.030	10509	-0.875	0.382	0.731	No	No
nkssts	Duplication:age_c	-0.022	0.025	10509	-0.859	0.390	0.731	No	No
sula	Duplication:age_c	-0.037	0.045	10509	-0.826	0.409	0.731	No	No
ntalpole	Duplication:age_c	0.028	0.034	10509	0.806	0.420	0.734	No	No
rstriangularis	Deletion:age_c	-0.025	0.032	10509	-0.793	0.428	0.738	No	No
rstriangularis	Duplication:age_c	-0.025	0.032	10509	-0.766	0.444	0.749	No	No
edialorbitofrontal	Deletion:age_c	-0.029	0.038	10509	-0.764	0.445	0.749	No	No
feriorparietal	Duplication:age_c	-0.023	0.032	10509	-0.731	0.465	0.765	No	No
stralmiddlefrontal	Deletion:age_c	-0.025	0.034	10509	-0.730	0.466	0.765	No	No
rsorbitalis	Duplication:age_c	-0.021	0.030	10509	-0.719	0.472	0.766	No	No
eraloccipital	Deletion:age_c	0.020	0.029	10509	0.694	0.487	0.782	No	No

pramarginal	Deletion:age_c	-0.022	0.033	10509	-0.685	0.493	0.782	No	No
edialorbitofrontal	Duplication:age_c	0.026	0.038	10509	0.670	0.503	0.788	No	No
udalmiddlefrontal	Duplication:age_c	-0.023	0.035	10509	-0.662	0.508	0.788	No	No
eralorbitofrontal	Duplication:age_c	0.026	0.041	10509	0.642	0.521	0.793	No	No
stcentral	Duplication:age_c	-0.019	0.030	10509	-0.639	0.523	0.793	No	No
hmuscingulate	Duplication:age_c	0.015	0.025	10509	0.629	0.529	0.794	No	No
rahippocampal	Deletion:age_c	0.013	0.022	10509	0.601	0.548	0.812	No	No
rsorbitalis	Deletion:age_c	0.017	0.030	10509	0.579	0.563	0.826	No	No
feriorparietal	Deletion:age_c	-0.017	0.032	10509	-0.543	0.587	0.831	No	No
periorfrontal	Deletion:age_c	-0.018	0.032	10509	-0.560	0.575	0.831	No	No
feriortemporal	Deletion:age_c	-0.017	0.032	10509	-0.539	0.590	0.831	No	No
stralmiddlefrontal	Duplication:age_c	0.019	0.035	10509	0.545	0.586	0.831	No	No
torhinal	Deletion:age_c	-0.022	0.041	10509	-0.529	0.597	0.832	No	No
rsopercularis	Deletion:age_c	-0.016	0.031	10509	-0.509	0.611	0.834	No	No
ecuneus	Duplication:age_c	-0.014	0.028	10509	-0.517	0.605	0.834	No	No
eralorbitofrontal	Duplication:age_c	-0.018	0.037	10509	-0.495	0.621	0.840	No	No
eralorbitofrontal	Deletion:age_c	0.019	0.040	10509	0.466	0.641	0.859	No	No
torhinal	Deletion:age_c	0.018	0.041	10509	0.436	0.663	0.863	No	No
nsversetemporal	Deletion:age_c	0.013	0.029	10509	0.451	0.652	0.863	No	No
ricalcarine	Deletion:age_c	-0.014	0.031	10509	-0.442	0.658	0.863	No	No

steriorcingulate	Deletion:age_c	-0.010	0.026	10509	-0.394	0.694	0.866	No	No
stralanteriorcingulate	Duplication:age_c	0.015	0.036	10509	0.399	0.690	0.866	No	No
rahippocampal	Deletion:age_c	-0.010	0.025	10509	-0.397	0.691	0.866	No	No
ddletemporal	Duplication:age_c	-0.011	0.029	10509	-0.381	0.703	0.866	No	No
stcentral	Duplication:age_c	0.012	0.032	10509	0.382	0.702	0.866	No	No
feriortemporal	Duplication:age_c	-0.013	0.032	10509	-0.396	0.692	0.866	No	No
neus	Deletion:age_c	-0.009	0.025	10509	-0.360	0.719	0.878	No	No
gual	Deletion:age_c	0.009	0.026	10509	0.342	0.732	0.879	No	No
rsopercularis	Duplication:age_c	-0.010	0.030	10509	-0.350	0.727	0.879	No	No
stralmiddlefrontal	Deletion:age_c	0.011	0.034	10509	0.329	0.742	0.882	No	No
rsopercularis	Duplication:age_c	0.010	0.032	10509	0.310	0.756	0.884	No	No
gual	Duplication:age_c	-0.008	0.026	10509	-0.299	0.765	0.884	No	No
stralanteriorcingulate	Duplication:age_c	-0.013	0.041	10509	-0.319	0.750	0.884	No	No
nkssts	Deletion:age_c	0.007	0.025	10509	0.294	0.769	0.884	No	No
nsversetemporal	Deletion:age_c	-0.008	0.030	10509	-0.278	0.781	0.891	No	No
ddletemporal	Deletion:age_c	0.007	0.030	10509	0.249	0.804	0.909	No	No
feriorparietal	Deletion:age_c	-0.007	0.031	10509	-0.210	0.833	0.935	No	No
udalanteriorcingulate	Deletion:age_c	-0.005	0.027	10509	-0.187	0.852	0.941	No	No
udalmiddlefrontal	Duplication:age_c	0.007	0.035	10509	0.193	0.847	0.941	No	No
stcentral	Deletion:age_c	0.004	0.029	10509	0.148	0.882	0.958	No	No

sula	Duplication:age_c	0.007	0.045	10509	0.149	0.882	0.958	No	No
siform	Deletion:age_c	-0.001	0.031	10509	-0.021	0.983	0.983	No	No
stralanteriorcingulate	Deletion:age_c	0.001	0.040	10509	0.024	0.981	0.983	No	No
rstriangularis	Deletion:age_c	-0.001	0.032	10509	-0.027	0.978	0.983	No	No
ntalpole	Deletion:age_c	0.002	0.034	10509	0.045	0.964	0.983	No	No
ntalpole	Duplication:age_c	-0.003	0.035	10509	-0.091	0.927	0.983	No	No
ddletemporal	Duplication:age_c	-0.001	0.030	10509	-0.045	0.964	0.983	No	No
edialorbitofrontal	Deletion:age_c	0.003	0.039	10509	0.088	0.930	0.983	No	No
hmuscingulate	Duplication:age_c	0.003	0.025	10509	0.102	0.918	0.983	No	No
rsorbitalis	Deletion:age_c	0.002	0.029	10509	0.054	0.957	0.983	No	No
ntalpole	Deletion:age_c	0.002	0.034	10509	0.051	0.959	0.983	No	No
ricalcarine	Deletion:age_c	0.002	0.030	10509	0.062	0.951	0.983	No	No

Supplementary Table 13

All Nominally Significant CNV Group × Age Interaction Effects for Cortical Surface Area.

Summary of linear mixed-effects model results showing all regions with nominally significant ($p < .05$) CNV Group × Age interactions for cortical surface area. For each ROI the table displays a an interaction term (Group x age), estimate (Estimate) standard error (SE), test statistic (t), significance value (p.value), FDR-corrected significance value, nominal significance status

(Yes/No), FDR corrected significance status (Yes/No)effect estimates, standard errors, test statistics, degrees of freedom, raw and adjusted p-values, and FDR significance status.

ROI	Group x age	Estimate	SE	df	t	p.value	p_adjusted	Significant	Significant_FDR
lh_insula	Duplication:age_c	0.063	0.028	10509	2.258	0.024	0.981	Yes	No
lh_superiorfrontal	Duplication:age_c	-0.027	0.013	10509	-2.022	0.043	0.981	Yes	No
lh_lateralorbitofrontal	Deletion:age_c	-0.038	0.019	10509	-1.994	0.046	0.981	Yes	No
rh_temporalpole	Duplication:age_c	0.048	0.027	10509	1.747	0.081	0.981	No	No
lh_inferiortemporal	Deletion:age_c	0.020	0.012	10509	1.681	0.093	0.981	No	No
lh_bankssts	Deletion:age_c	-0.025	0.015	10509	-1.610	0.107	0.981	No	No
lh_paracentral	Deletion:age_c	0.026	0.016	10509	1.604	0.109	0.981	No	No
rh_rostralanteriorcingulate	Duplication:age_c	-0.028	0.017	10509	-1.596	0.111	0.981	No	No
rh_isthmuscingulate	Duplication:age_c	-0.027	0.017	10509	-1.595	0.111	0.981	No	No
lh_parsorbitalis	Duplication:age_c	-0.024	0.016	10509	-1.573	0.116	0.981	No	No

lh_lateraloccipital	Duplication:age_c	0.016	0.010	10509	1.562	0.118	0.981	No	No
lh_lateralorbitofrontal	Duplication:age_c	-0.030	0.019	10509	-1.549	0.121	0.981	No	No
lh_pericalcarine	Duplication:age_c	0.019	0.013	10509	1.542	0.123	0.981	No	No
rh_pericalcarine	Duplication:age_c	0.019	0.013	10509	1.432	0.152	0.981	No	No
lh_frontalpole	Duplication:age_c	-0.040	0.028	10509	-1.410	0.159	0.981	No	No
rh_posteriorcingulate	Duplication:age_c	-0.016	0.012	10509	-1.404	0.160	0.981	No	No
lh_precuneus	Duplication:age_c	-0.016	0.012	10509	-1.384	0.166	0.981	No	No
rh_lingual	Deletion:age_c	-0.015	0.011	10509	-1.382	0.167	0.981	No	No
rh_caudalmiddlefrontal	Deletion:age_c	0.026	0.019	10509	1.366	0.172	0.981	No	No
rh_lateralorbitofrontal	Duplication:age_c	-0.037	0.027	10509	-1.352	0.176	0.981	No	No
lh_parahippocampal	Duplication:age_c	-0.030	0.023	10509	-1.324	0.186	0.981	No	No

lh_middletemporal	Duplication:age_c	-0.018	0.014	10509	-1.322	0.186	0.981	No	No
rh_superiorfrontal	Duplication:age_c	-0.022	0.016	10509	-1.312	0.189	0.981	No	No
lh_medialorbitofrontal	Duplication:age_c	-0.035	0.028	10509	-1.250	0.211	0.981	No	No
lh_caudalanteriorcingulate	Deletion:age_c	-0.015	0.012	10509	-1.208	0.227	0.981	No	No
lh_caudalmiddlefrontal	Duplication:age_c	-0.019	0.016	10509	-1.186	0.236	0.981	No	No
lh_inferiorparietal	Deletion:age_c	0.014	0.012	10509	1.170	0.242	0.981	No	No
lh_parahippocampal	Deletion:age_c	-0.026	0.023	10509	-1.162	0.245	0.981	No	No
rh_inferiorparietal	Duplication:age_c	-0.013	0.012	10509	-1.085	0.278	0.981	No	No
lh_medialorbitofrontal	Deletion:age_c	-0.030	0.027	10509	-1.077	0.281	0.981	No	No
rh_parahippocampal	Duplication:age_c	0.024	0.022	10509	1.050	0.294	0.981	No	No
rh_entorhinal	Deletion:age_c	-0.025	0.025	10509	-1.017	0.309	0.981	No	No

lh_entorhinal	Deletion:age_c	0.025	0.025	10509	0.971	0.332	0.981	No	No
rh_posteriorcingulate	Deletion:age_c	0.011	0.012	10509	0.968	0.333	0.981	No	No
lh_precuneus	Deletion:age_c	-0.011	0.012	10509	-0.955	0.340	0.981	No	No
lh_isthmuscingulate	Deletion:age_c	-0.013	0.013	10509	-0.941	0.347	0.981	No	No
lh_rostralanteriorcingulate	Deletion:age_c	-0.016	0.018	10509	-0.917	0.359	0.981	No	No
lh_transversetemporal	Duplication:age_c	-0.014	0.016	10509	-0.891	0.373	0.981	No	No
rh_caudalanteriorcingulate	Duplication:age_c	0.012	0.014	10509	0.885	0.376	0.981	No	No
rh_precentral	Deletion:age_c	0.017	0.019	10509	0.873	0.383	0.981	No	No
lh_inferiortemporal	Duplication:age_c	-0.010	0.012	10509	-0.869	0.385	0.981	No	No
rh_precuneus	Duplication:age_c	-0.011	0.012	10509	-0.861	0.390	0.981	No	No
rh_insula	Deletion:age_c	0.024	0.028	10509	0.855	0.393	0.981	No	No
lh_fusiform	Duplication:age_c	0.009	0.011	10509	0.841	0.400	0.981	No	No

lh_frontalpole	Deletion:age_c	0.023	0.028	10509	0.837	0.403	0.981	No	No
rh_inferiortemporal	Deletion:age_c	-0.009	0.011	10509	-0.834	0.404	0.981	No	No
lh_postcentral	Duplication:age_c	-0.013	0.016	10509	-0.810	0.418	0.981	No	No
lh_lingual	Duplication:age_c	0.009	0.011	10509	0.809	0.419	0.981	No	No
rh_supramarginal	Duplication:age_c	0.015	0.019	10509	0.762	0.446	0.981	No	No
lh_rostralmiddlefrontal	Deletion:age_c	0.012	0.015	10509	0.758	0.448	0.981	No	No
rh_lateraloccipital	Deletion:age_c	-0.007	0.010	10509	-0.741	0.459	0.981	No	No
rh_parsopercularis	Duplication:age_c	0.012	0.017	10509	0.731	0.465	0.981	No	No
lh_posteriorcingulate	Deletion:age_c	-0.008	0.011	10509	-0.701	0.483	0.981	No	No
rh_parstriangularis	Duplication:age_c	0.012	0.017	10509	0.696	0.486	0.981	No	No
lh_postcentral	Deletion:age_c	-0.011	0.015	10509	-0.695	0.487	0.981	No	No
lh_parstriangularis	Duplication:age_c	-0.009	0.013	10509	-0.668	0.504	0.981	No	No

rh_bankssts	Duplication:age_c	-0.010	0.015	10509	-0.663	0.508	0.981	No	No
lh_insula	Deletion:age_c	-0.018	0.027	10509	-0.652	0.515	0.981	No	No
rh_rostralanteriorcingulate	Deletion:age_c	-0.011	0.017	10509	-0.648	0.517	0.981	No	No
rh_superiortemporal	Deletion:age_c	0.008	0.012	10509	0.643	0.520	0.981	No	No
rh_medialorbitofrontal	Duplication:age_c	-0.016	0.024	10509	-0.639	0.523	0.981	No	No
rh_paracentral	Deletion:age_c	0.010	0.016	10509	0.632	0.527	0.981	No	No
rh_paracentral	Duplication:age_c	-0.010	0.016	10509	-0.611	0.542	0.981	No	No
lh_rostralmiddlefrontal	Duplication:age_c	-0.009	0.015	10509	-0.577	0.564	0.981	No	No
rh_superiorfrontal	Deletion:age_c	0.009	0.016	10509	0.571	0.568	0.981	No	No
rh_postcentral	Duplication:age_c	-0.011	0.019	10509	-0.559	0.576	0.981	No	No
lh_supramarginal	Duplication:age_c	-0.008	0.015	10509	-0.556	0.578	0.981	No	No

lh_lateraloccipital	Deletion:age_c	-0.005	0.010	10509	-0.541	0.588	0.981	No	No
rh_caudalanteriorcingulate	Deletion:age_c	-0.007	0.013	10509	-0.541	0.588	0.981	No	No
rh_isthmuscingulate	Deletion:age_c	0.009	0.017	10509	0.530	0.596	0.981	No	No
rh_lateralorbitofrontal	Deletion:age_c	-0.014	0.027	10509	-0.527	0.598	0.981	No	No
rh_superiortemporal	Duplication:age_c	0.006	0.012	10509	0.524	0.600	0.981	No	No
rh_cuneus	Duplication:age_c	-0.007	0.014	10509	-0.511	0.609	0.981	No	No
lh_bankssts	Duplication:age_c	-0.008	0.016	10509	-0.492	0.622	0.981	No	No
lh_inferiorparietal	Duplication:age_c	-0.006	0.012	10509	-0.489	0.625	0.981	No	No
rh_middletemporal	Deletion:age_c	-0.006	0.012	10509	-0.485	0.627	0.981	No	No
rh_precuneus	Deletion:age_c	0.006	0.012	10509	0.474	0.636	0.981	No	No
rh_cuneus	Deletion:age_c	0.006	0.014	10509	0.457	0.648	0.981	No	No

lh_temporalpole	Duplication:age_c	-0.013	0.028	10509	-0.457	0.648	0.981	No	No
lh_superiorfrontal	Deletion:age_c	0.006	0.013	10509	0.432	0.666	0.981	No	No
rh_rostralmiddlefrontal	Deletion:age_c	-0.007	0.017	10509	-0.418	0.676	0.981	No	No
rh_superiorparietal	Deletion:age_c	0.008	0.020	10509	0.418	0.676	0.981	No	No
lh_parsopercularis	Deletion:age_c	0.006	0.015	10509	0.418	0.676	0.981	No	No
rh_supramarginal	Deletion:age_c	-0.008	0.019	10509	-0.415	0.678	0.981	No	No
lh_cuneus	Duplication:age_c	0.005	0.013	10509	0.408	0.683	0.981	No	No
rh_pericalcarine	Deletion:age_c	0.005	0.013	10509	0.408	0.684	0.981	No	No
rh_parahippocampal	Deletion:age_c	0.009	0.022	10509	0.394	0.694	0.981	No	No
rh_entorhinal	Duplication:age_c	0.009	0.025	10509	0.375	0.708	0.981	No	No
lh_superiorparietal	Duplication:age_c	-0.007	0.018	10509	-0.375	0.708	0.981	No	No
rh_parsorbitalis	Duplication:age_c	-0.006	0.015	10509	-0.373	0.709	0.981	No	No

rh_inferiorparietal	Deletion:age_c	-0.005	0.012	10509	-0.372	0.710	0.981	No	No
lh_temporalpole	Deletion:age_c	-0.010	0.028	10509	-0.371	0.711	0.981	No	No
lh_parsopercularis	Duplication:age_c	-0.005	0.015	10509	-0.361	0.718	0.981	No	No
lh_superiorparietal	Deletion:age_c	0.006	0.017	10509	0.334	0.738	0.981	No	No
lh_parsorbitalis	Deletion:age_c	-0.005	0.015	10509	-0.333	0.739	0.981	No	No
lh_rostralanteriorcingulate	Duplication:age_c	0.006	0.018	10509	0.306	0.760	0.981	No	No
rh_postcentral	Deletion:age_c	0.006	0.019	10509	0.304	0.761	0.981	No	No
rh_inferiortemporal	Duplication:age_c	-0.003	0.012	10509	-0.278	0.781	0.981	No	No
lh_precentral	Deletion:age_c	-0.004	0.016	10509	-0.274	0.784	0.981	No	No
lh_supramarginal	Deletion:age_c	-0.004	0.014	10509	-0.271	0.786	0.981	No	No
rh_frontalpole	Deletion:age_c	0.008	0.029	10509	0.263	0.792	0.981	No	No

lh_lingual	Deletion:age_c	-0.003	0.011	10509	-0.234	0.815	0.981	No	No
rh_middletemporal	Duplication:age_c	0.003	0.013	10509	0.229	0.819	0.981	No	No
lh_entorhinal	Duplication:age_c	-0.006	0.026	10509	-0.222	0.825	0.981	No	No
lh_superiortemporal	Duplication:age_c	-0.003	0.012	10509	-0.216	0.829	0.981	No	No
lh_cuneus	Deletion:age_c	-0.003	0.012	10509	-0.212	0.832	0.981	No	No
rh_fusiform	Duplication:age_c	0.002	0.011	10509	0.210	0.834	0.981	No	No
lh_isthmuscingulate	Duplication:age_c	0.003	0.014	10509	0.198	0.843	0.981	No	No
lh_transversetemporal	Deletion:age_c	-0.003	0.016	10509	-0.186	0.852	0.981	No	No
lh_fusiform	Deletion:age_c	0.002	0.011	10509	0.180	0.857	0.981	No	No
rh_transversetemporal	Duplication:age_c	0.003	0.018	10509	0.166	0.868	0.981	No	No
rh_lingual	Duplication:age_c	-0.002	0.011	10509	-0.161	0.872	0.981	No	No
lh_parstriangularis	Deletion:age_c	-0.002	0.013	10509	-0.156	0.876	0.981	No	No

rh_temporalpole	Deletion:age_c	-0.004	0.027	10509	-0.150	0.880	0.981	No	No
rh_frontalpole	Duplication:age_c	0.004	0.029	10509	0.149	0.882	0.981	No	No
rh_lateraloccipital	Duplication:age_c	0.001	0.010	10509	0.140	0.888	0.981	No	No
rh_parsorbitalis	Deletion:age_c	-0.002	0.015	10509	-0.116	0.908	0.981	No	No
lh_middletemporal	Deletion:age_c	0.002	0.013	10509	0.115	0.909	0.981	No	No
lh_posteriorcingulate	Duplication:age_c	-0.001	0.011	10509	-0.112	0.911	0.981	No	No
lh_paracentral	Duplication:age_c	-0.002	0.016	10509	-0.104	0.917	0.981	No	No
lh_superiortemporal	Deletion:age_c	0.001	0.012	10509	0.100	0.921	0.981	No	No
rh_caudalmiddlefrontal	Duplication:age_c	0.002	0.019	10509	0.093	0.926	0.981	No	No
rh_rostralmiddlefrontal	Duplication:age_c	0.002	0.017	10509	0.090	0.928	0.981	No	No
lh_pericalcarine	Deletion:age_c	0.001	0.012	10509	0.080	0.936	0.981	No	No
rh_fusiform	Deletion:age_c	0.001	0.010	10509	0.075	0.940	0.981	No	No
rh_superiorparietal	Duplication:age_c	-0.001	0.020	10509	-0.069	0.945	0.981	No	No

lh_caudalanteriorcingulate	Duplication:age_c	0.001	0.013	10509	0.055	0.956	0.981	No	No
lh_precentral	Duplication:age_c	-0.001	0.017	10509	-0.054	0.957	0.981	No	No
rh_transversetemporal	Deletion:age_c	0.001	0.018	10509	0.053	0.958	0.981	No	No
rh_parsopercularis	Deletion:age_c	-0.001	0.017	10509	-0.051	0.959	0.981	No	No
lh_caudalmiddlefrontal	Deletion:age_c	0.001	0.016	10509	0.047	0.962	0.981	No	No
rh_bankssts	Deletion:age_c	0.001	0.015	10509	0.046	0.963	0.981	No	No
rh_precentral	Duplication:age_c	0.001	0.019	10509	0.046	0.963	0.981	No	No
rh_medialorbitofrontal	Deletion:age_c	-0.001	0.024	10509	-0.030	0.976	0.981	No	No
rh_parstriangularis	Deletion:age_c	0.000	0.016	10509	0.028	0.978	0.981	No	No
rh_insula	Duplication:age_c	0.001	0.029	10509	0.024	0.981	0.981	No	No

Supplementary Table 14

All Nominally Significant CNV Group × Age Interaction Effects for Subcortical and Cerebellar Volume.

Summary of linear mixed-effects model results showing all regions with nominally significant ($p < .05$) CNV Group × Age interactions for subcortical and cerebellar volume. For each ROI the

table displays a an interaction term (Group x age), estimate (Estimate) standard error (SE), test statistic (t), significance value (p.value), FDR-corrected significance value, nominal significance status (Yes/No), FDR corrected significance status (Yes/No) effect estimates, standard errors, test statistics, degrees of freedom, raw and adjusted p-values, and FDR significance status.

ROI	Group x age	Estimate	SE	df	t	p.value	p_adjusted	Significant	Sign
.Ventricle_Z_predict	Deletion:age_c	0.032	0.010	10509	3.269	0.001	0.067	Yes	
ict	Deletion:age_c	0.051	0.019	10509	2.627	0.009	0.181	Yes	
m_Z_predict	Duplication:age_c	-0.087	0.033	10509	-2.622	0.009	0.181	Yes	
Ventricle_Z_predict	Deletion:age_c	0.022	0.010	10509	2.329	0.020	0.257	Yes	
le_Z_predict	Deletion:age_c	0.031	0.014	10509	2.313	0.021	0.257	Yes	
_Z_predict	Duplication:age_c	-0.027	0.013	10509	-2.034	0.042	0.375	Yes	
mpus_Z_predict	Deletion:age_c	0.039	0.019	10509	2.031	0.042	0.375	Yes	
le_Z_predict	Duplication:age_c	0.025	0.014	10509	1.709	0.088	0.679	No	
en_Z_predict	Duplication:age_c	0.030	0.019	10509	1.588	0.112	0.722	No	
nus.Proper_Z_predict	Duplication:age_c	-0.038	0.024	10509	-1.570	0.116	0.722	No	
um.White.Matter_Z_predict	Duplication:age_c	-0.041	0.027	10509	-1.501	0.133	0.752	No	
la_Z_predict	Deletion:age_c	-0.036	0.030	10509	-1.217	0.223	0.922	No	
_Z_predict	Deletion:age_c	0.025	0.020	10509	1.207	0.227	0.922	No	
_Z_predict	Deletion:age_c	-0.044	0.037	10509	-1.189	0.234	0.922	No	
campus_Z_predict	Duplication:age_c	0.020	0.017	10509	1.180	0.238	0.922	No	
Z_predict	Duplication:age_c	-0.012	0.011	10509	-1.123	0.261	0.922	No	
dala_Z_predict	Duplication:age_c	0.028	0.025	10509	1.105	0.269	0.922	No	
alVol_Z_predict	Duplication:age_c	-0.010	0.009	10509	-1.081	0.280	0.922	No	

_Z_predict	Deletion:age_c	-0.013	0.013	10509	-1.009	0.313	0.922	No
.Vent_Z_predict	Duplication:age_c	0.021	0.021	10509	1.001	0.317	0.922	No
.Vent_Z_predict	Deletion:age_c	0.018	0.020	10509	0.911	0.362	0.922	No
campus_Z_predict	Deletion:age_c	0.015	0.017	10509	0.870	0.384	0.922	No
talIntraCranialVol_Z_predict	Duplication:age_c	0.019	0.022	10509	0.860	0.390	0.922	No
ict	Duplication:age_c	0.017	0.020	10509	0.853	0.394	0.922	No
Ventricle_Z_predict	Duplication:age_c	0.008	0.010	10509	0.850	0.395	0.922	No
ens.area_Z_predict	Duplication:age_c	0.029	0.035	10509	0.812	0.417	0.922	No
bens.area_Z_predict	Deletion:age_c	0.024	0.031	10509	0.768	0.442	0.922	No
en_Z_predict	Deletion:age_c	0.014	0.018	10509	0.767	0.443	0.922	No
lDC_Z_predict	Duplication:age_c	0.017	0.023	10509	0.766	0.444	0.922	No
mpus_Z_predict	Duplication:age_c	-0.014	0.019	10509	-0.720	0.472	0.922	No
DC_Z_predict	Duplication:age_c	-0.016	0.023	10509	-0.715	0.475	0.922	No
talIntraCranialVol_Z_predict	Deletion:age_c	0.015	0.022	10509	0.694	0.488	0.922	No
llum.White.Matter_Z_predict	Duplication:age_c	-0.019	0.029	10509	-0.676	0.499	0.922	No
le_Z_predict	Deletion:age_c	0.010	0.014	10509	0.666	0.506	0.922	No
um.Cortex_Z_predict	Deletion:age_c	0.009	0.014	10509	0.637	0.524	0.929	No
llum.Cortex_Z_predict	Duplication:age_c	-0.008	0.015	10509	-0.559	0.576	0.933	No
dala_Z_predict	Deletion:age_c	-0.013	0.025	10509	-0.541	0.588	0.933	No
Vent_Z_predict	Duplication:age_c	0.012	0.022	10509	0.537	0.591	0.933	No
_Z_predict	Duplication:age_c	0.011	0.021	10509	0.525	0.600	0.933	No
us.Proper_Z_predict	Deletion:age_c	0.012	0.027	10509	0.445	0.656	0.933	No
um.Cortex_Z_predict	Duplication:age_c	-0.006	0.014	10509	-0.433	0.665	0.933	No

us.Proper_Z_predict	Duplication:age_c	-0.012	0.027	10509	-0.430	0.668	0.933	No
alVol_Z_predict	Deletion:age_c	-0.004	0.009	10509	-0.420	0.675	0.933	No
n_Z_predict	Duplication:age_c	0.016	0.038	10509	0.415	0.678	0.933	No
.Ventricle_Z_predict	Duplication:age_c	0.004	0.010	10509	0.403	0.687	0.933	No
Vol_Z_predict	Deletion:age_c	0.005	0.011	10509	0.396	0.692	0.933	No
e_Z_predict	Deletion:age_c	-0.005	0.013	10509	-0.375	0.708	0.934	No
m_Z_predict	Deletion:age_c	-0.011	0.033	10509	-0.336	0.737	0.942	No
Z_predict	Deletion:age_c	0.003	0.011	10509	0.305	0.760	0.942	No
Vol_Z_predict	Duplication:age_c	-0.003	0.011	10509	-0.303	0.762	0.942	No
e_Z_predict	Duplication:age_c	-0.004	0.013	10509	-0.286	0.775	0.942	No
bens.area_Z_predict	Duplication:age_c	0.008	0.032	10509	0.243	0.808	0.964	No
la_Z_predict	Duplication:age_c	0.006	0.030	10509	0.201	0.840	0.983	No
um.White.Matter_Z_predict	Deletion:age_c	0.005	0.027	10509	0.176	0.861	0.988	No
lDC_Z_predict	Deletion:age_c	0.002	0.022	10509	0.111	0.911	0.997	No
DC_Z_predict	Deletion:age_c	0.002	0.023	10509	0.085	0.932	0.997	No
llum.White.Matter_Z_predict	Deletion:age_c	-0.002	0.028	10509	-0.084	0.933	0.997	No
nus.Proper_Z_predict	Deletion:age_c	0.002	0.024	10509	0.069	0.945	0.997	No
Vent_Z_predict	Deletion:age_c	-0.001	0.022	10509	-0.035	0.972	0.997	No
llum.Cortex_Z_predict	Deletion:age_c	0.000	0.015	10509	-0.026	0.979	0.997	No
ens.area_Z_predict	Deletion:age_c	0.000	0.035	10509	0.013	0.989	0.997	No
le_Z_predict	Duplication:age_c	0.000	0.014	10509	0.004	0.997	0.997	No